DISSECTING MOLECULAR MECHANISMS OF RADIORESISTANCE USING *IN VITRO* AND *IN VIVO* BRAIN TUMOR MODEL SYSTEMS

APPROVED BY SUPERVISORY COMMITTEE

Sandeep Burma, Ph.D.

Robert Bachoo, M.D. Ph.D.

James Amatruda, M.D. Ph.D.

Steven Kernie, M.D.

Jenny Hsieh, Ph.D.

DEDICATION

I would like to dedicate this to my parents, for all of their continuous support and encouragement.

DISSECTING MOLECULAR MECHANISMS OF RADIORESISTANCE USING *IN VITRO* AND *IN VIVO* BRAIN TUMOR MODEL SYSTEMS

by

BRIAN MATTHEW MCELLIN

DISSERTATION

Presented to the Faculty of the Graduate School of Biomedical Sciences

The University of Texas Southwestern Medical Center at Dallas

In Partial Fulfillment of the Requirements

For the Degree of

DOCTOR OF PHILOSOPHY

The University of Texas Southwestern Medical Center at Dallas

Dallas, Texas

March, 2012

ACKNOWLEDGEMENTS

First and foremost, I would like to thank both of my mentors, Sandeep Burma, Ph.D. and Robert Bachoo, M.D., Ph.D. for all of their efforts in training me to think and to work as a scientist.

I would also like to thank all members of my committee – James Amatruda, M.D., Ph.D., Jenny Hsieh, Ph.D., Steve Kernie, M.D. and Matthew Porteus, M.D., Ph.D. (former member) for their continued input.

I would also like to thank all the current and former lab members of the Burma and Bachoo laboratories for their help at all stages of my scientific career.

Finally, I would like to thank my family for all of their support.

DISSECTING MOLECULAR MECHANISMS OF RADIORESISTANCE USING *IN VITRO* AND *IN VIVO* BRAIN TUMOR MODEL SYSTEMS

BRIAN MATTHEW MCELLIN, B.S.

The University of Texas Southwestern Medical Center at Dallas, GRADUATION YEAR

SANDEEP BURMA, PH.D.
ROBERT BACHOO, M.D. PH.D.

Glioblastoma multiforme (GBM) are deadly brain tumors that are refractory to radiation and chemotherapy. Despite decades of work, little progress has been made in improving patient outcomes. Recent mapping of the GBM genome by the Cancer Genome Atlas Network revealed that these cancers commonly exhibit several signature mutations that promote gliomagenesis (e.g. EGFR amplification/activation, PTEN loss, p53 loss, Ink4a/Arf loss). How these genetic changes may modulate responses to radiation and chemotherapy is not well understood. To elucidate this relationship, genetically defined mouse models have been used for both *in vitro* and *in vivo a*nalysis.

Work has uncovered novel links between oncogenic signaling and DNA repair pathways. First, activation of the Akt pathway by EGFRvIII, a constitutively active form of EGFR, promotes DNA double strand break repair by non-homologous end joining in astrocytes and glioma cell lines. This results in faster repair and increased radioresistance, both *in vitro* and in orthotopic GBM models. While activation of Akt by the loss of PTEN has similar results, data shows that PTEN loss reduces resistance to agents that induce replication-associated DSBs. This phenotype is due to reduced levels of homologous recombination, as astrocytes show increased radial chromosome aberrations and decreased sister chromatid exchanges after PTEN loss. These results have exciting implications, as it has identified two potential new therapeutic strategies for improving treatment in subsets of GBM patients.

The cancer stem cell hypothesis postulates that cancers are organized similar to endogenous stem cell compartments, composed of a self-renewing cancer stem cell and other more "differentiated", non-stem progeny. To determine how key GBM mutations affect the different cell types in GBM, I used the adult neural stem cell compartment as a reductionist model of a tumor. Surprisingly, data demonstrated that quiescent stem cells showed inherent resistance, even in a wild type mouse. In addition, stem cell-specific p53 loss increases radioresistance only in a subset of non-dividing progenitors, while proliferating progenitors remain sensitive to radiation. This model has offered novel insight into the effect of key pathways deregulated in GBM and how they impact different cell types.

TABLE OF CONTENTS

PRIOR PUBLICATIONS

McEllin B, Camacho CV, Mukherjee B, Hahm B, Tomimatsu N, Bachoo RM, Burma S. PTEN loss compromises homologous recombination repair in astrocytes: implications for glioblastoma therapy with Temozolomide or poly (ADP-ribose) polymerase inhibitors. *Cancer Research*, 2010 Jul 1;70(13):5457-64.

Mukherjee B, **McEllin B**, Camacho CV, Tomimatsu N, Sirasanagandala S, Nannepaga S, Hatanpaa KJ, Mickey B, Madden C, Maher E, Boothman DA, Furnari F, Cavenee WK, Bachoo RM, Burma S. "EGFRvIII and DNA double-strand break repair: a molecular mechanism for radioresistance in glioblastoma". *Cancer Research*, 2009 May 15;69(10):4252-9.

Camacho C, Mukherjee B, **McEllin B**, Ding L-H, Hu B, Habib A, Xie X. J., Nirodi C, Saha D, Story M, Balajee A, Bachoo R. M., Boothman D. A., Burma S. Loss of p15/Ink4b accompanies tumorigenesis triggered by complex DNA double-strand breaks. *Carcinogenesis* 31(10):1889-96 (2010).

Marian CO, Cho SK, **McEllin B**, Maher EA, Hatanpaa KJ, Madden CJ, Mickey BE, Wright WE, Shay JW, Bachoo RM. "The telomerase antagonist, imetelstat, efficiently targets glioblastoma tumor-initiating cells leading to decreased proliferation and tumor growth" *Clin Can Res*, 2010. Jan 1;16(1): 154-63.

LIST OF FIGURES

TABLES

LIST OF ABBREVIATIONS

2-HG	2-hydroxyglutarate
AGT	O^6-alkylguanine DNA alkyltransferase
BrdU	Bromodeoxyuridine
Cdk	Cyclin-dependent kinase
CSC	Cancer stem cell
CstC	Cystatin C
DCX	Doublecortin
DDR	DNA damage response
DG	Dentate gyrus
DNA	Deoxyribonucleic acid
DSB	Double strand break
EGF	Epidermal growth factor
EGFR	Epidermal growth factor receptor
EGFRkd	Kinase dead epidermal growth factor receptor
EGFRvIII	Epidermal growth factor receptor, variant III
EGFRwt	Wild type epidermal growth factor receptor
GBM	Glioblastoma multiforme
GFAP	Glial fibrillary acidic protein
Gy	Gray
hGFAP	human GFAP promoter
HOT line	Human orthotopic tumor (derived from primary human GBM)
HR	Homologous recombination

hTERT	Human telomerase catalytic component
IDH1	Isocitrate dehydrogenase 1
IR	Ionizing radiation
MAPK	Mitogen activated protein kinase
Mdm2	Murine double minute 2
Mdm4	Murine double minute 4
MEF	Mouse embryonic fibroblast
MGMT	O^6-methyl guanine methyl transferase
MMR	Mismatch repair
MNNG	N-methyl-n'-nitro-n-nitrosoguanidine
NHA	Normal human astrocytes
NHEJ	Nom-homologous end joining
NOD-SCID	Non-obese diabetic severe combined immunodeficient mouse
NSC	Neural stem cell
O^6meG	O^6methylguanine
PARP	Poly (ADP) ribose polymerase
PFA	Paraformaldehyde
PI3K	Phosphatidylinositol 3–kinase
PIP_2	Phosphatidylinositol-4,5 bisphosphate
PIP_3	Phosphatidylinositol-3,4,5 trisphosphate
PTEN	Phosphatase and tensin homolog deleted on chromosome 10
RNA	Ribonucleic acid
RT-PCR	Reverse transcription polymerase chain reaction

RTK	Receptor tyrosine kinase
SCE	Sister chromatid exchange
SGZ	Subgranular zone
Sox2	SRY-related HMG-box gene 2
SV40-LT	Simian Vacuolating Virus 40 Tag
SVZ	Subventricular zone
TCGA	The Cancer Genome Atlas
TMZ	Temozolomide
WBRT	Whole brain radiotherapy
α-KG	α-ketoglutarate

Chapter 1

Introduction

1.1 Introduction to Glioblastoma Multiforme

Glioblastoma multiforme (GBM) is the most common and aggressive type of primary brain tumor found in adults, accounting for ~54% of all gliomas. These tumors are classified as grade IV astrocytoma by the WHO criteria, and are marked by several key features. These include diffuse infiltration, high proliferation, regions of necrosis with palisading nuclei, microvascular proliferation, and rampant genomic instability (Maher et al., 2001; Furnari et al., 2007). These tumors are universally fatal, and the median survival for patients with this disease is currently ~14.6 months, with less than 5% of all patients surviving 5 years after diagnosis. Glioblastoma has two distinct classifications based upon clinical history (Kleihues and Ohgaki, 1999; Maher et al., 2001). Primary GBM are defined as spontaneous Grade IV astrocytomas without prior history of any brain tumor lesion. These are primarily found in older patients. Secondary GBM are defined as GBM arising from a pre-existing low grade lesion, which gradually progresses to a high grade tumor over an extended time frame (Kleihues and Ohgaki, 1999; Maher et al., 2001). Molecular analysis of key genomic alterations in primary and secondary glioblastoma shows differences between each of these subtypes. It has long been known that primary GBM is enriched for *phosphatase and tensin homolog deleted on chromosome 10 (PTEN*) deletions and epidermal growth factor receptor (EGFR) amplifications, while secondary GBM more frequently shows mutations in the p53 gene

(Watanabe et al., 1996; Watanabe et al., 1997). Several recent studies have also compared overall gene expression signatures between primary and secondary GBM and noted significant differences in these GBM subtypes (Maher et al., 2006). Despite the difference, these subtypes are indistinguishable when it comes to histology, overall survival, and resistance to radiation and chemotherapy.

1.2 Current Treatment Regimens for GBM

Relatively little progress has been made in patient outcomes over the past few decades, despite a vast increase in knowledge about the basic biology of glioblastoma. Current treatment regimens begin with surgical resection of the primary tumor mass, followed by a combination of fractionated radiation therapy and treatment with the DNA alkylating agent temozolomide (Stupp et al., 2009). The benefit of radiation therapy for glioblastoma patients was first identified over 30 years ago (Walker et al., 1979; Walker et al., 1980). Randomized clinical trials were performed comparing the efficacy of nitrosourea and/or radiation therapy in combination with surgical resection, and found that the overall median survival was increased about 6 months by radiation therapy, with little additional benefit of nitrosourea treatment. Since that time, there has been minimal additional progress. The most successful therapeutic regimen in recent years has been the addition of temozolomide (TMZ), a Sn1 type alkylating agent, to radiation therapy. The efficacy of temozolomide in combination with radiation therapy was first identified in the landmark EORTC-NCIC study (Stupp et al., 2005 initial results; Stupp et al 2009 final results). In this study, TMZ was given both concurrently with radiation doses and as an adjuvant treatment for 6 months following the completion of radiation therapy (with a 4

week break between concomitant and adjuvant treatment). Dosing for temozolomide was 75mg/m^2 concurrently with radiation and 150-200mg/m^2/d for 5 out of every 28 days in the adjuvant setting. The data showed an increase in overall survival of ~2.5 months for all patients, with a significant benefit seen for a small number of long term survivors, as evidence by increases in the two and five year survival rates (10.4% to 26.5% and 1.9% to 9.8%, respectively). As a result of this clinical trial, temozolomide has now been incorporated into the standard treatment regimens for GBM. Despite these improvements, the prognosis for patients with GBM remains grim.

Both ionizing radiation and alkylating agents such as temozolomide induce the most cytotoxic type of DNA lesion, the DNA double strand break. However, the mechanism of action for this DSB induction differs between each type of treatment, ultimately resulting in the use of two different DNA repair pathways to resolve each type of damage. Ionizing radiation creates breaks either by directly breaking bonds between DNA bases or indirectly through the ionization of water, creating OH radicals. These radicals will interact with DNA, creating several types of DNA base modifications and DSBs (Hall and Giaccia, 2006). Because radiation relies on physical events to cause damage, it creates breaks immediately after exposure in all cells, regardless of cell cycle phase.

Temozolomide is a pro-drug that spontaneously converts to its active form 5-(3-methyl-1-triazen-1-yl) imidazole-4-carboxamide (MTIC) at physiological pH, which can methylate DNA (Omar and Mason, 2009). Mechanistic studies *in vitro* have linked sensitivity to Sn1 alkylating agents to two basic requirements – cells must be actively replicating and have functional mismatch repair (MMR) (Roos et al., 2004; Kaina et al.,

2007). This drug functions by interacting with DNA to transfer a methyl group to several DNA bases, creating common lesions such as N^7-methylguanine, N^3-methyladenine, and O^6methylguanine (O^6meG). The majority of these lesions are recognized and repaired by base excision repair pathways and do not contribute extensively to toxicity (Kaina et al., 2007). Although it comprises less than 10% of all methylations, O^6meG is thought to be the critical methylation that promotes toxicity. Normally, this damage can only be reversed by O^6-alkylguanine DNA alkyltransferase (AGT), a protein encoded by the MGMT gene. This enzyme is a suicide enzyme that functions by transferring the methyl group from DNA to an internal cysteine residue, thereby inactivating the protein and targeting it for degradation (Gerson, 2004). Levels of AGT show strong correlation *in vitro* with sensitivity to DNA alkylating agents; increased expression enhances resistance to alkylating agents (Kaina et al., 1991, Allay et al., 1995), whereas MGMT knockout mice are extremely sensitive to these agents (Glassner et al., 1999). In the absence of AGT, O^6meG forms a mispair with thymine during DNA replication. This is recognized by the MMR machinery, which then attempts to repair the lesion by removing the thymine base pair. However, this does not fix the lesion, creating a "futile cycle" that results in aborted processing and the formation of replication-associated DNA double strand breaks (Kaina et al., 2007).

1.3 DNA Repair pathways required for repair of treatment-induced DNA double strand breaks

Therefore, while both ionizing radiation and temozolomide treatment ultimately create double strand breaks, these breaks occur in different phases of the cell cycle. DSB

repair can occur through two major pathways that also show cell cycle dependence – non-homologous end joining (NHEJ) and homologous recombination (HR). NHEJ is active in all phases of the cell cycle (Branzei and Foiani, 2008; Lieber, 2010). It requires several components, including Ku70/80, the catalytic enzyme DNA-PKcs, and Ligase IV. This pathway is considered to be error prone, as it is not homology-directed and processing of DSB ends can result in sequence loss. As depicted in Figure 1.1, the catalytic enzyme DNA-PKcs is recruited to the sites of DSBs by the Ku70/Ku80 complex, where it is thought to stabilize the DNA ends and facilitate recruitment of other key DNA repair proteins to the strand break. After end processing, the DNA break is ultimately ligated by Ligase IV without regard for homology (Weterings and Chen, 2008; Lieber 2010). On the other hand, homologous recombination (HR) is a relatively error-free repair pathway that utilizes the sister chromatid as a template for high-fidelity repair (San Filippo et al., 2008). This process can only occur in S and G2 phases when a sister chromatid is available, and is thought to be the dominant pathway during these two cell cycle stages (Branzei and Foiani, 2008; Weterings and Chen 2008; San Filippo et al., 2008). There are several basic steps in this pathway, as reviewed extensively in San Filippo et al., 2008. First proper resection of the break is performed, creating a single-stranded 3' overhang that is immediately coated with RPA. With the help of BRCA2, Rad51 is loaded onto the overhang, displacing RPA. This Rad51 coated filament then invades into the sister chromatid and initiates the repair process. After repair is complete, the complex is then resolved, sometimes resulting in a crossover event between the two sister chromatids (sister chromatid exchange, or SCE). Both Rad51loading and SCE formation (Wilson and Thompson, 2007) can be used for surrogate markers of homologous recombination, with

Figure 1.1

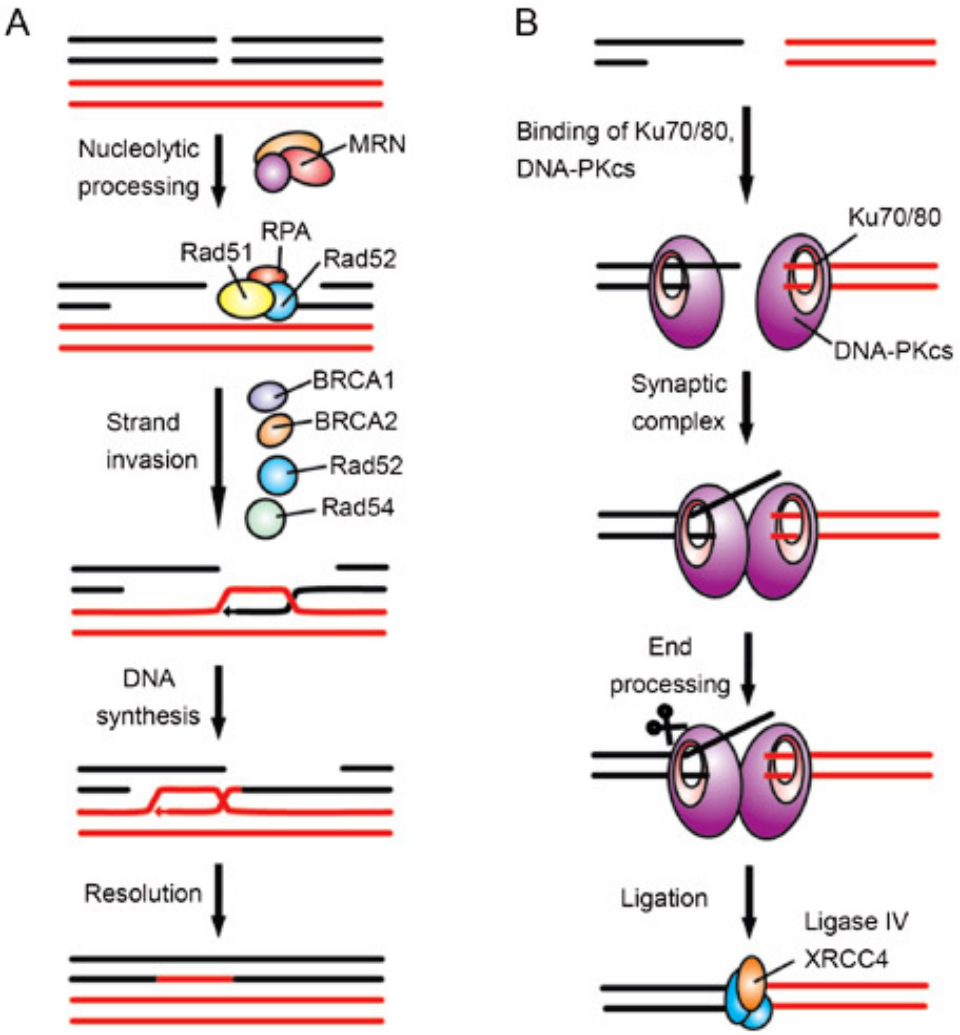

Figure 1.1 Basic schematic of HR and NHEJ Pathways (from Weterings and Chen, 2008). (A) Repair of DNA double strand breaks by homologous recombination requires that the sister chromatid (red) be used to copy sequence information, ensuring proper repair. This process can therefore only occur in S and G2 phases of the cell cycle when the sister chromatid is present. This pathway has multiple steps of DNA resection at the sites of breaks, invasion into the sister chromatid, and subsequent copying of relevant genetic information. **(B)** For breaks that occur in G1, non-homologous end-joining takes place. This repair pathway involves end processing and ligation without regard to homology.

reduction of SCEs and impairment in Rad51 focus formation reflecting a reduction in HR events.

Thus, ionizing radiation induced breaks are primarily repaired by NHEJ, while secondary DSBs caused by temozolomide require homologous recombination (Roos et al., 2009). This is a critical point to take into consideration. One possible mechanism for enhanced resistance in GBM involves an increased capacity to deal with DNA damage induced by therapy. This may be due to increased repair rates and/or inhibition of normal signaling events that promote cell arrest and apoptosis in response to DNA damage. Without considering how the damage occurs, one may not investigate the proper repair pathways and signaling events. Thus, identifying potential links between the signature genetic changes in GBM and repair pathways would become much more difficult.

1.4 Signaling pathways deregulated in GBM

For a long time, it has been known that GBM are marked by several key signature mutations – loss/mutation of p53, loss of the CDKN2A locus ($p16^{Ink4a}$/ARF), loss of PTEN, activation of EGFR, and activation of PDGFR (reviewed in Maher et al., 2001; Furnari et al., 2007). However, to date no clear prognostic value for any of these specific mutations alone has been identified (Newcomb et al., 1998). In order to gain a more complete understanding of the vast network of genetic changes found in GBM, two landmark studies were conducted with the goal of performing multivariate analysis on a large number of patient tumors to fully and completely annotate the GBM genome. Overall, these two studies offered an unprecedented look into the vast array of mutations in GBM. The Cancer Genome Atlas (TCGA) Project screened a large cohort of 206

primary GBM samples for copy number variations, mutations, gene expression changes, and DNA methylation changes (TCGA, 2008). The majority of these (185) samples were collected prior to treatment, and the remainder were collected after treatment regimens. Analysis of the study uncovered several novel findings. In contrast to the traditional classification of p53 mutations as marking secondary GBM, the TCGA study revealed TP53 mutations in 27/72 untreated GBM and 11/19 treated GBM samples, indicating that p53 mutations do happen at significant frequencies in primary GBM. The study also validated previous studies showing cooperation of NF1 and p53 deletion to generate *de novo* mouse models of glioblastoma (Zhu et al., 2005; Kwon et al., 2008; Alcantara Llaguno et al., 2009) by identifying NF1 as a tumor suppressor gene frequently mutated in GBM (47/206 samples showed either mutations or single allelic deletions).

In a similar manner, another study focused on analyzing changes in copy number, expression patterns, and DNA sequences in clinical samples (Parsons et al., 2008). Similar to the TCGA study, this work also identified less frequent mutations in PIK3CA, PIK3R1, and NF1. In addition, one of the major novel findings was the identification of isocitrate dehydrogenase 1 (IDH1), a gene mutated in 12% of the overall tumors and significantly enriched in young patients and those with secondary GBM. This finding was notable, as the overall survival of patient with this mutation was significantly enhanced (3.8 years vs. 1.1 years, $p<0.001$). Mutations in IDH1 have been the subject of intense study in the past few years. Reports have indicated that IDH1 mutations alter metabolism through increased production of 2-hydroxyglutarate (2-HG) at the expense of α-ketoglutarate (α-KG) (Dang et al., 2009; Xu et al., 2011), which can have significant disruptions on the entire metabolome (Reitman et al., 2012). In addition, IDH1 and 2

Figure 1.2

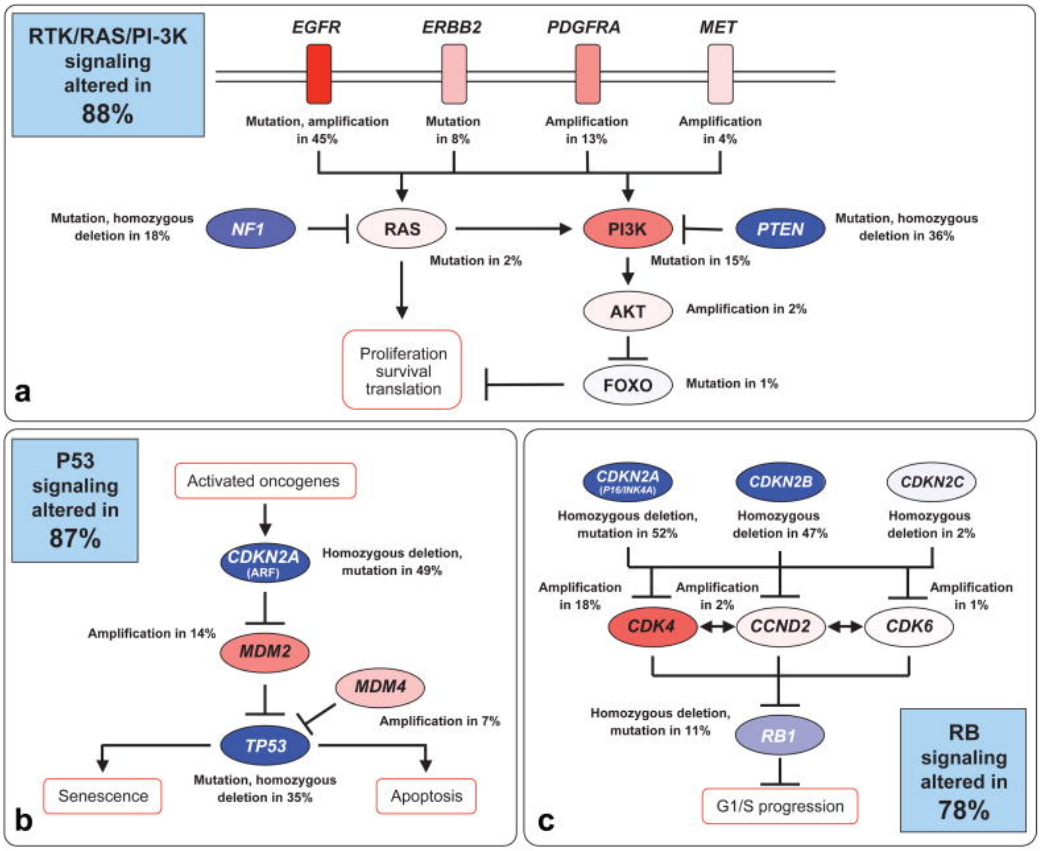

Figure 1.2 Core pathways altered in GBM – Summary of the TCGA results (from TCGA, 2008). Multivariate analysis of the GBM genome for copy number variations, transcriptional changes, and somatic mutations revealed that 3 core pathways are mutated in the majority of GBMs – inactivation of p53 signaling, inactivation of Rb signaling, and activation of receptor tyrosine kinase pathway(s). Red refers to amplifications/activating mutations, blue is deletions/inactivations.

mutations have been linked to increased histone methylation that can prevent differentiation (Turcan et al., 2012; Lu et al., 2012). This is an exciting new area of research that may both uncover novel therapeutic strategies and provide new insights into altered metabolism and gliomagenesis. While this comprehensive screen did identify a few novel mutations, the results confirmed the previously identified subset of GBM associated mutations – the major hits in both studies were EGFR, CDKN2A, p53, PTEN, and PDGFRA. However, the full characterization of all the mutations in each tumor allowed the interpretations to shift from a mutation-centric view to a more pathway-centric view. As shown in the Figure 1.2, the p53 pathway (87%), Rb pathway (78%), and receptor tyrosine kinase (RTK) pathway (88%) were all deregulated either by copy number changes or mutations (TCGA, 2008). Thus, while there the commonly signature alleles are independently verified (p53 35%, CDKN2A 52%, PTEN 36%, EGFR 45%), many other mutations can feed into these same three pathways to generate the same end result of a highly deadly glioblastoma. Additionally, it appears that dysfunction in all three pathways may represent a minimal requirement for gliomagenesis, as 74% of GBMs harbored at least 1 mutation/copy number alteration in all three pathways (TCGA). One would also expect to see minimal cases in which two mutations with similar functions were observed in each pathway, as this would be functionally redundant and not provide any advantage for transformation. Consistent with this expectation, both studies reported minimal redundancy from a tumor to tumor basis; however, there were several cases in the TCGA data set of multiple RTK amplifications/activating mutations in the same tumor. This has particular significance, since human glioma lines can exhibit multiple active RTK pathways (Stommel et al., 2007). This phenotype renders these cells

resistant to single agent therapy against RTK members (e.g. EGFR inhibitors). It is only when multiple RTK pathways are targeted via inhibitors or knockdowns that the U87s show any changes in survival and anchorage independent growth (Stommel et al., 2007).

The p53 Pathway

P53 is mutated in a large variety of cancers (Hollstein et al., 1991). Mutations in this gene were first identified in brain cancer over 20 years ago, and it was noted at the time that these mutations occurred in the four most highly conserved domains of p53 across different species (Nigro et al., 1989). It is now known that these regions are the main DNA binding domains of p53 and are critical for its activity (TCGA, 2008). Stabilization of p53 is generally induced following oxidative stress and DNA damage, resulting in a large network of transcriptional changes that initiate cell arrest and/or promote apoptosis (Levine et al., 2006). Under normal conditions, p53 is sequestered by the Mdm2 gene, a key negative regulator of p53 (Momand et al., 1992; Haupt et al., 1997). Mdm4 also serves some redundant functions as Mdm2 to inhibit p53 (Shvarts et al., 1996). During times of stress, the $p14^{ARF}$ ($p19^{ARF}$ in mouse) gene (encoded by the CDKN2A locus) is induced, and this protein can directly bind and inhibit Mdm2, thus stabilizing p53 (Kamijo et al., 1998; Honda and Yasuda, 1999; Zhang et al., 1998). After stabilization, p53 is subjected to several post-translational modifications, including phosphorylation at serine 15, marker of DNA double strand breaks (Siciliano JD et al., 1997) and acetylation at numerous lysines (Brooks and Gu, 2011). This acetylation can occur in response to both genotoxic and oncogenic stress, with acetylation at lysine 20 promoted by $p19^{ARF}$ stabilization (Mellert et al., 2007). These modifications can help

prevent Mdm2 ubiquitination of p53, preventing degradation (Li, Luo et al., 2002). Acetylation can also promote DNA binding, where p53 can act as a transcription factor to initiate gene expression changes (Brooks and Gu, 2011).

Inactivation of the p53 pathway is a key event in gliomagenesis, and it can occur through a variety of mechanisms. As shown in the TCGA results, p53 is mutated or deleted in 35% of cases, and Mdm2 and Mdm4 are amplified in 14% and 7% of cases, respectively, and the most common event is loss of the CDKN2A locus, which encodes for $p14^{ARF}$ (TCGA, 2008). Loss or mutation of p53 occurs primarily in secondary GBM, and is thought to represent an early event in the process of gliomagenesis (Maher et al., 2001). Interestingly, a recent publication has identified an alternate mechanism for suppression of p53 by Olig2, a stem/progenitor marker found in almost all gliomas (Ligon et al., 2004). The authors showed that Olig2 prevents acetylation of p53 in response to DNA damage, thereby promoting radiation resistance in primary neural stem cells and glioblastoma cell lines (Mehta et al., 2010). This mechanism highlights the diverse ways in which p53 gene function can be inactivated, aside from copy number changes/mutations in key regulators.

The Rb pathway

Mutations in Rb were first identified in astrocytoma almost 20 years ago (Henson et al., 1994). As evidenced by the recent TCGA, this is a pathway that is frequently altered at several different places in GBM, with the majority of inactivations in the CDKN2A/B loci (52 and 47%) and Rb protein (11%), while Cdk4 is amplified in 18% of cases (TCGA, 2008). The Rb pathway is a critical pathway that controls cell cycle

progression. The basic pathway has been extensively studied. In non-dividing cells, Rb functions to block cell cycle progression by phosphorylating and inactivating the E2F family of transcription factors, a class of proteins known to promote cell division. In response to Ras signaling, the D cyclins are actively transcribed, and subsequently form a complex with Cdk4 and Cdk6, two cyclin dependent kinases. This active complex phosphorylates Rb, relieving the inhibition on the E2F family of transcription factors and promoting cell cycle progression. A key negative regulator of this process is the p16/INK4a tumor suppressor, which functions to block the formation of cyclin-cdk complexes (reviewed by Sherr and McCormick, 2002). While this pathway is initially identified as a cell cycle regulatory pathway, emerging evidence suggests that deregulation of the Rb pathway may have more diverse roles depending on cellular context, including preventing senescence, promoting angiogenesis, increased metastatic potential and decreased DNA repair (reviewed by Burkhart and Sage, 2008). Thus, inactivating this pathway may have many cancer promoting phenotypes.

The RTK Pathway

In addition to inactivating pathways that constrain growth, GBMs almost universally activate one or more receptor tyrosine kinase (RTK) signaling pathways in order to drive progression through the cell cycle. The most common RTK activated in GBM is the epidermal growth receptor (EGFR), either by copy number amplification or by expression of the constitutively active mutant, EGFRvIII, which lacks the extracellular ligand binding domain (McLendon et al., 2007). While EGFR amplification is commonly found in GBM, it is rarely seen in low grade lesions (Wong et al., 1987) or in secondary

GBM (Watanabe et al., 1996). Aside from EGFR, amplification in the platelet derived growth factor receptor alpha (PDGFRA), MET, and ERBB2 have also been reported in GBM (TCGA, 2008). These RTKs primarily signal through either the phosphatidylinositol 3–kinase (PI3K) or Ras/mitogen activated protein kinase (MAPK) pathways, which promote proliferation and survival (Maher et al., 2001).

Of particular interest is the PI3K pathway, which is commonly mutated in a large number of different cancers (reviewed in Chalhoub and Baker, 2009). PI3K is composed of a regulatory and catalytic subunit. Generally, upon activation of the receptor tyrosine kinases, the catalytic subunit (p110) is recruited to the RTK by the regulatory subunit, where PI3K phosphorylates phosphatidylinositol-4,5 bisphosphate (PIP2) to generate phosphatidylinositol-3,4,5 trisphosphate(PIP3). This is a key step in the pathway, as PIP3 serves to recruit key proteins (e.g. Akt) to the membrane, ultimately resulting in phosphorylation and activation of Akt isoforms. A key point of negative regulation on this pathway is the PTEN tumor suppressor gene, which functions as a lipid phosphatase to convert PIP3 to PIP2 (Chalhoub and Baker, 2009). Loss of PTEN is well known as a common event in GBM, occurring about 36% of the time (Maher et al., 2001; Furnari et al., 2007; TCGA, 2008), but activations of other components, e.g. PIK3CA (encodes p85, a regulatory subunit) and PIK3R1 (p110α, a catalytic subunit), were not appreciated until the recent genome-wide analyses showed recurrent alterations in these two genes (TCGA, 2008; Parsons et al., 2008). EGFR and EGFRvIII are well known to signal through the PI3K pathway (Huang et al., 2009).

Due to the high percentage of GBM that show amplifications in EGFR, several clinical trials have investigated the utility of EGFR inhibitors as a monotherapy for GBM.

The results have been mixed, but there are some hints that subgrouping patients using more than one key mutation may provide more successful results. In 2005, a retrospective study was published describing a clinical trial using either targeted EGFR inhibitors (gefitinib or erlotinib) in recurrent GBM patients (Mellinghoff et al., 2005). Tumor specimens from thirty-seven patients were analyzed for various molecular markers, with 7 showing a clinical response (>25% tumor shrinkage) and 19 showing progression. Analysis of the individual genotypes of each patient's tumor showed that 6/7 patients had both EGFRvIII overexpression and an intact PTEN gene, while only two patients with this combination were found in the non-responders. Thus, co-expression of EGFRvIII and PTEN showed predictive value, with $p<.001$. This finding was also replicated in another set of 33 patients from UCSF (relying solely on immunohistochemistry), in which 5/8 responsive patients exhibited co-expression of EGFR and PTEN, compared to only 1/25 non-responders ($p=.001$). In addition, another retrospective study showed correlations between Akt phosphorylation levels and response to EGFR inhibitors (Haas-Kogan et al., 2005). However, as discussed in Brandes et al., 2008, data from other prospective studies has failed to show any benefit for EGFR inhibitors as single agents, even among EGFR expressing tumors (Rich et al., 2004; Franceschi et al., 2007; van den Bent et al 2009; Raizer et al., 2010). One possible reason for failure of these trials may be that multiple RTK pathways can be co-activated in GBM, thus targeting just one pathway is insufficient to produce a viable response. Therefore, the lack of clear utility of EGFR inhibitors in GBM may be due to incomplete responses of treatment, with an intact PTEN gene potentially contributing to limiting RTK signaling enough to provide modest

therapeutic benefit. Future combinations of treatments that target both the receptor and other vulnerable nodes in the signaling pathway may prove to have more success.

1.5 Insights into the cell of origin of GBM from mouse models

Prior to the identification of adult stem cell compartments, it was widely assumed that astrocytes were the presumptive cells of origin for GBM. This was based on morphological criteria and high levels of expression of the astrocyte marker glial fibrillary acidic protein (GFAP) (Maher et al., 2001). In experimental model systems, there are several reports suggesting that astrocytes have the potential to be transformed in a multistep process to produce tumors with the clinical phenotype of GBM (Bachoo et al., 2002; Dai et al., 2001; Sonoda et al., 2001a,b). Astrocytes carrying mutations in the Ink4a/Arf locus (p16/p19) undergo a process of de-differentiation, allowing these cells to grow as neurospheres similar to cultured neural stem cells (Bachoo et al., 2002). Furthermore, overexpression of EGFRvIII in both Ink4a/Arf-/- astrocytes and stem cells was sufficient to transform both sets of cell lines, causing them to readily form tumors when injected intra-cranially in the brains of immunocompromised mice. Histological examination showed poorly differentiated, high grade tumors in both cases with the classic diffuse, infiltrative morphology seen clinically in GBM patients, also characterized by expression of multiple lineage markers, such as GFAP, nestin, Olig2, and Sox10 (Bachoo et al., 2002). Work from Pieper's group also focused on generating multistep models of transformation using normal human astroctytes. In a series of papers, this group demonstrated that E6/E7 and hTERT expression were sufficient to immortalized human astrocytes, but not render them tumorigenic when injected intra-

cranially into immunocompromised mice (Sonoda et al., 2001b). Subsequent expression of H-ras alone or in combination with myristoylated Akt-1 transformed this cell line, forming Grade III anaplastic astrocytoma and Grade IV astrocytoma, respectively, in orthotopic models (Sonoda et al., 2001b; Sonoda et al., 2001a). Thus, it is possible to transform astrocytes into glioblastoma using specific combinations of mutations.

However, the description of an active adult stem cell population in the adult brain capable of self-renewal and differentiation has opened the possibility that neural stem cells may also be capable of forming GBM. This was further supported by the identification of glioma cancer stem cells (Singh et al. 2003; Singh et al. 2004; Galli et al., 2004) that were shown to exhibit the classic stem cell properties of self-renewal and multipotency, in addition to tumor initiation properties. Transgenic mouse models of glioblastoma have further supported a role for neural stem cells and/or early multipotent progenitors as targets for transformation. These models have also provided solid evidence that the signature mutations found in human GBM play significant roles in the gliomagenesis – deletion of key tumor suppressor genes such as p53, PTEN, Ink4a/Arf, NF1 and Rb have all help to promote transformation *in vivo* to generate *de novo* tumors.

There have been multiple methods used to generate mouse models of gliomagenesis. Early studies by Holland et al. used the RCAS/tv-a system to investigate the relative susceptibility of neural stem cells (nestin promoter) and astrocytes (GFAP promoter) to transformation by activated Ras and Akt isoforms. This group noted that the combination was necessary to induce gliomagenesis, and this only occurred in the nestin compartment (Holland et al., 2000). There is known to be overlaps between GFAP and nestin in the adult stem cell compartments (Suh et al., 2009), so it is unclear why there is

a discrepancy between these two models. Nonetheless, this approach has shown the ability of activated RTK signaling to induce gliomas in mice. Further publications also showed that an Ink4a/Arf deletion combined with activated RTK signaling generated similar results (Uhrbom et al., 2002).

More recently, several cancer models have used the human GFAP promoter (hGFAP) to drive cre expression (Zhuo et al., 2001). Although GFAP is primarily and astrocyte and stem cell marker, characterization of this model showed that the hGFAP-cre caused recombination in multipotent progenitors in embryonic development. As a result, recombination occurs in nearly all neurons, astrocytes and oligodendrocytes in the adult brain (Zhuo et al. 2001). Despite the multitude of cell types targeted, introducing GBM-specific mutations has consistently developed astrocytoma. Parada's group first used an hGFAP promoter to generate *de novo* gliomas using combined inactivation of p53 and NF1, showing a high penetrance and range of tumor grades (Zhu et al., 2005). This phenotype was further enhanced by the addition of heterozygous PTEN deletion, decreasing tumor latency and increasing the occurrence of Grade IV astrocytoma (GBM) (Kwon et al., 2008). DePinho's group reported that homozygous deletion of p53 and heterozygous deletion of PTEN in an hGFAP-cre cooperated to induce high grade gliomas *de novo* in mice. This phenotype was linked to d suppression of differentiation, as dual inactivation of these proteins was shown to activate Myc, increase self-renewal and prevent differentiation (Zheng et al., 2008). Other models by van Dyke's group have implicated the Rb pathway in combination with PTEN loss (Xiao et al., 2002; Xiao et al., 2005).

Using mouse models that drive cre expression early in development may not be representative of clinical disease, which commonly occurs late in life. Therefore, some studies have focused on using inducible cre recombinase systems to introduce mutations in a temporally and spatially controlled manner. Using the NF1/p53 combination, Parada's group demonstrated that deletion of combinations of p53, NF1, and PTEN specifically in the adult neural stem cell compartments resulted in the formation of malignant astrocytoma, including GBM (Alcantara Llaguna et al., 2009). Recent reports also demonstrate that conditional deletions of p53, PTEN, and Rb using a GFAP-CreER mouse model are sufficient to promote gliomagenesis (Chow et al., 2011).

Together, these *in vivo* studies are important to establish two very critical concepts – first, they provide definitive links between key genes often mutated in gliomas and the process of gliomagenesis; second, they show that the adult neural stem cell compartments are relevant cell types to study for radiation and drug resistance, as these are the likely candidates for origins of glioblastoma. However, this does not rule out the possibility of transformation by astrocytes in the adult mouse; it may be that astrocytes require an additional step to promote de-differentiation prior to transformation.

1.6 Strategies for understanding therapy resistance in GBM

The molecular mechanisms of radiation and drug resistance in GBM remain poorly understood. In order to address this problem, one can take one of two approaches. First, one can start with data from patient samples and work backwards to identify commonalities between responders and non-responders to generate candidate genes, and then validate these targets using experimental approaches in various model systems (e.g.,

TCGA database). There are many positives to this methodology. Data can be easily correlated to patient outcomes after therapy, and global patterns of expression/clinical subtyping may provide more prognostic value than single mutations alone. However, the high rates of genomic instability in GBM can generate large amounts of noise, and generation of statistically powered data sets can be expensive and time consuming. In addition, one cannot assess the contributions of certain genes/gene signatures to resistance to single agents, as all patients are now given both ionizing radiation and DNA alkylating agents as standard chemotherapy.

Alternatively, one can attempt to reconstruct the development of GBM using genetically defined, mouse and/or human cell culture based system. This paradigm allows one to assess individual steps along the transformation process, to assay how specific combinations of mutations may be influencing both the process of gliomagenesis and subsequent acquired radiation and drug resistance. The isogenic nature of cell lines and mouse models used in this approach minimizes the contribution of any random genetic changes due to inherent genomic instability. For this approach to work, there are a couple of key components that need to be present in a faithful model of glioblastoma. First, it must recapitulate the morphology and molecular profile of this disease. Next, the model must introduce relevant genetic alterations in the proper cell(s) or origin at the correct developmental stage. Once these conditions are met, then one can begin to dissect how the relevant genes/pathways that promote gliomagenesis may contribute to the highly radioresistant and drug resistant phenotype seen in GBM. Importantly, this defined system allows multiple factors to be investigated in a systematic manner. This includes elucidation of any additive or synergistic phenotypes with different gene combinations

and with different treatments. By identifying the relevant targets/combinations of targets, improved strategies for treatment can be designed to improve survival based on the patient's specific genomic profile. As previously discussed, both astrocytes and neural stem cells have been shown to be targets of transformation into GBM. Therefore, I have used primary astrocytes in cell culture and a novel Cre-ER^{T2} mouse model that targets both relevant compartments (astrocytes/stem cells) and also allows for appropriate temporal specification of deletion of key GBM genes. These model systems provide an ideal approach to assess the role of GBM signature mutations, alone and in combination, to modulate radiation and drug resistance both *in vitro* and *in vivo*.

Chapter 2
Novel Links Between Oncogenic Signaling and DNA Repair

2.1 Introduction

Despite considerable work in recent years elucidating the molecular underpinnings of GBM, the most deadly of brain cancers, little progress has been made in improving clinical outcomes. The most significant breakthrough in patient response to date emerged from the use of the DNA alkylating agent temozolomide in combination with ionizing radiation (IR) that increased the overall median survival from approximately 12 to 15 months (Friedman et al., 2000; Stupp et al. 2005; Stupp et al. 2009). Recent multivariate whole genome characterizations have given unprecedented insight into the genetics of adult GBM tumors, revealing that these tumors have radically altered genomes with many mutations, gene copy number gains and losses, and methylation changes (TCGA, 2008; Parsons et al., 2008; Verhaak et al., 2010). Amongst the large spectrum of genetic alterations that populate the GBM genomic landscape, five genetic changes dominate: loss of *Ink4a*, *Arf*, *p53*, or *PTEN* and amplification of *EGFR*. How these genetic aberrations contribute to conferring therapeutic resistance remains unclear. Understanding the contribution of these lesions, singly and in combination, to GBM therapy resistance along with the underlying mechanism(s) will be of paramount importance in developing more effective therapeutic modalities.

As a first step towards understanding the genetic basis of GBM radioresistance, studies were focused on two of the most commonly mutated genes that serve to activate oncogenic pathways in GBM – EGFR and PTEN. *EGFR is* the most commonly

amplified/mutated gene in GBMs (Furnari et al., 2007; TCGA, 2008; Parsons et al., 2008). EGFR is a transmembrane receptor tyrosine kinase (RTK) whose ligands include epidermal growth factor (EGF) and transforming growth factor-alpha (TGFα) (Bublil et al., 2007; Sergina NV et al., 2007). The *EGFR* gene is amplified in approximately 50% of GBMs and, of these, about half express a truncated version of the receptor, EGFRvIII (Furnari et al., 2007; TCGA, 2008; Parsons DW et al., 2008). Although EGFRvIII lacks the ligand-binding domain (McLendon et al., 2007), it is constitutively active (Huang et al., 1997), stimulating downstream signaling effectors that include PI3K, Akt-1, Ras, and MAPK. It has been demonstrated that EGFRvIII promotes malignant growth (Nagane et al., 1996). Previous *in vitro* studies using established glioma cell lines have shown that EGFRvIII confers resistance to IR (Lammering et al., 2001; Lammering et al., 2003; Stea et al., 2003). Xenograft studies have demonstrated that EGFR-specific inhibitors (small molecule as well as α-EGFR antibodies) significantly enhance the efficacy of radiotherapy (Huang et al., 2000; Chakravarti et al., 2004). However, the signaling pathways directly involved in EGFRvIII-mediated radiation resistance have not been completely elucidated.

Loss of PTEN is a very prominent event during gliomagenesis, occurring in about 36% of GBMs (Furnari et al., 2007; TCGA, 2008; Parsons et al., 2008). PTEN is a lipid phosphatase with a canonical role in dampening the PI3K-Akt-1 signaling pathway; hence, loss of PTEN has oncogenic consequences during gliomagenesis (Salmena et al., 2008). In addition, it is becoming increasingly clear that PTEN has novel nuclear functions (Baker, 2007), including potentially regulating the transcription of the *Rad51* gene, whose product is essential for homologous recombination (HR) repair of DNA

breaks (Shen et al., 2007; Yin et al., 2008). Both ionizing radiation and DNA alkylating agents are known to induce cell death by induction of DNA double strand breaks after exposure. This fact combined with previous links between EGFR signaling and radiation resistance prompted investigation into the mechanism(s) by which the activation of the Akt pathway may affect DNA repair to change sensitivity to DNA damage agents.

2.2 Results

A. Role of EGFRvIII in radioresistance

EGFRvIII, in cooperation with glioma-relevant tumor suppressor loss, confers IR resistance to primary murine astrocytes

In the first project, I began working with a senior postdoctoral researcher, Dr. Bipasha Mukherjee, on an *in vitro* project examining the contribution of EGFRvIII to radioresistance in primary astrocytes (Mukherjee B, McEllin B et al., 2008), the presumptive cells of origin of GBMs (Bachoo et al., 2002). For analyses of IR resistance, we used either Ink4a/Arf-null primary mouse astrocytes (Ink4a/Arf−/− astrocytes) or astrocytes in which p53/Rb tumor suppressors were inactivated by retroviral expression of SV40-LT (SV40-LT-astrocytes). Ink4a/Arf (p16/p19) and p53/Rb tumor suppressors are frequently lost in GBM (Furnari et al., 2007; TCGA, 2008; Parsons et al., 2008). Therefore, these two cell lines, with two distinct, GBM-relevant tumor suppressor backgrounds, are most appropriate for this study. To assess the impact of EGFRvIII on IR resistance, we compared EGFRvIII to equivalently expressed levels of wild type EGFR (EGFRwt) or kinase-dead EGFR (EGFRkd) **(**Fig 2.1a). Resistance to IR was quantified by standard colony formation assays. Expression of EGFRvIII, but not EGFRwt or

EGFRkd, resulted in dramatically increased survival of both Ink4a/Arf−/− astrocytes and SV40-LT-astrocytes (Fig 2.1b). Radioresistance conferred by EGFRvIII was abrogated by the small-molecule inhibitor Gefitinib (Iressa) that binds to the ATP-binding pocket of EGFR (Sergina et al., 2007) (Figs 2.1c). These data suggest that EGFRvIII signaling is involved in the increased resistance to IR irrespective of the tumor suppressor background.

EGFRvIII-induced IR resistance correlates with proficient DSB repair in primary murine astrocytes

The major mechanism by which IR induces lethality is by introducing DSBs. We examined whether the increased resistance to IR conferred by EGFRvIII expression might be due to enhanced DSB repair. SV40-LT and Ink4a/Arf−/− parental and EGFRvIII-expressing lines were irradiated with a total dose of 1Gy and induction and rate of DSB repair were visualized by immunofluorescence staining for 53BP1 foci as described (Mukherjee et al., 2008) **(**Fig 2.2a). Compared to parental lines, the EGFRvIII-expressing lines displayed significantly faster DSB repair kinetics, completing repair by 4 hours (Fig 2.2b). Pre-treatment of these cells with Gefitinib (Iressa), which inhibits EGFRvIII signaling (Sergina et al., 2007), slowed down repair to the extent observed in parental lines. These data clearly link improved repair kinetics with signaling from the EGFRvIII receptor.

Figure 2.1

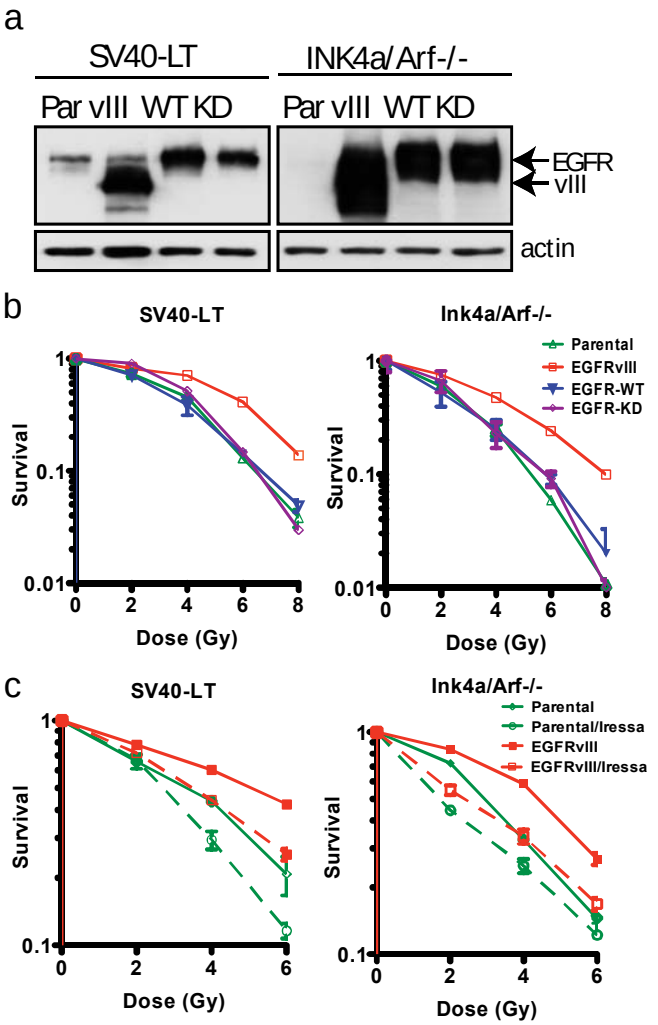

Figure 2.1 EGFRvIII expression renders astrocytes radioresistant irrespective of tumor-suppressor background (A) Expression of EGFRvIII (vIII), wild type EGFR (WT), or kinase-dead EGFR (KD) in SV40-LT-expressing mouse astrocytes or in Ink4a/Arf−/− primary mouse astrocytes was assayed by Western blotting with α-EGFR and α-actin (loading control) antibodies. "Par" denotes parental cells. **(B)** Radiation survival of astrocyte lines was quantified by colony formation assays. The fraction of surviving colonies (*y*-axis) was plotted against corresponding radiation dose (*x*-axis). Error bars represent standard error of the mean of experiments performed three or more times. Please note increased survival after EGFRvIII expression (red lines). **(C)** Radiation survival of astrocytes pre-treated with Gefitinib (Iressa) was quantified as above. Note reduced survival after Iressa pre-treatment (dashed lines).

Small-molecule inhibition of DNA-PKcs counters improved repair and survival exhibited by EGFRvIII-expressing cells

DNA-PKcs is a critical component of the predominant DSB repair pathway in mammalian cells – non-homologous end joining (NHEJ) (Burma and Chen, 2004; Burma et al., 2006). We tested the hypothesis that EGFR signaling promotes DSB repair *via* efficient activation of DNA-PKcs (Dittmann et al., 2005; Friedmann et al., 2006; Nyati et al., 2006). To investigate a possible link between EGFRvIII and DNA-PKcs activity in glioblastomas, we pre-treated EGFRvIII-expressing astrocytes with NU7026, a potent and specific DNA-PKcs inhibitor (Veuger et al., 2003). Pre-treatment with NU7026 blocked fast repair kinetics observed in EGFRvIII-expressing astrocytes (Figure 2.2b). The slower kinetics of DSB repair, in turn, correlated with increased radiation sensitivity in survival assays (Figure 2.2c), underscoring the potential usefulness of small-molecule inhibitors of DNA-PKcs as radiosensitizers for GBM treatment. Results from this figure were also repeated using DNA-PKcs WT and -/- mouse embryonic fibroblasts (MEFs). EGFRvIII overexpression was sufficient to increase radiation resistance in DNA-PKcs WT MEFs, but had no effect in DNA-PKcs-/- MEFs (Mukherjee, McEllin et al., 2009). Thus, DNA-PKcs is required for EGFRvIII-mediated radiation resistance.

Activation of Akt-1 in mouse astrocytes mimics the effects of EGFRvIII expression on DSB repair

EGFRvIII preferentially signals through the PI3K-Akt-1 pathway (Learn et al., 2004; Li et al., 2004). Pharmacological inhibition of this pathway can block DSB repair and radiosensitize mammalian cells (Friedmann et al., 2004; Toulany et al., 2006).

Figure 2.2

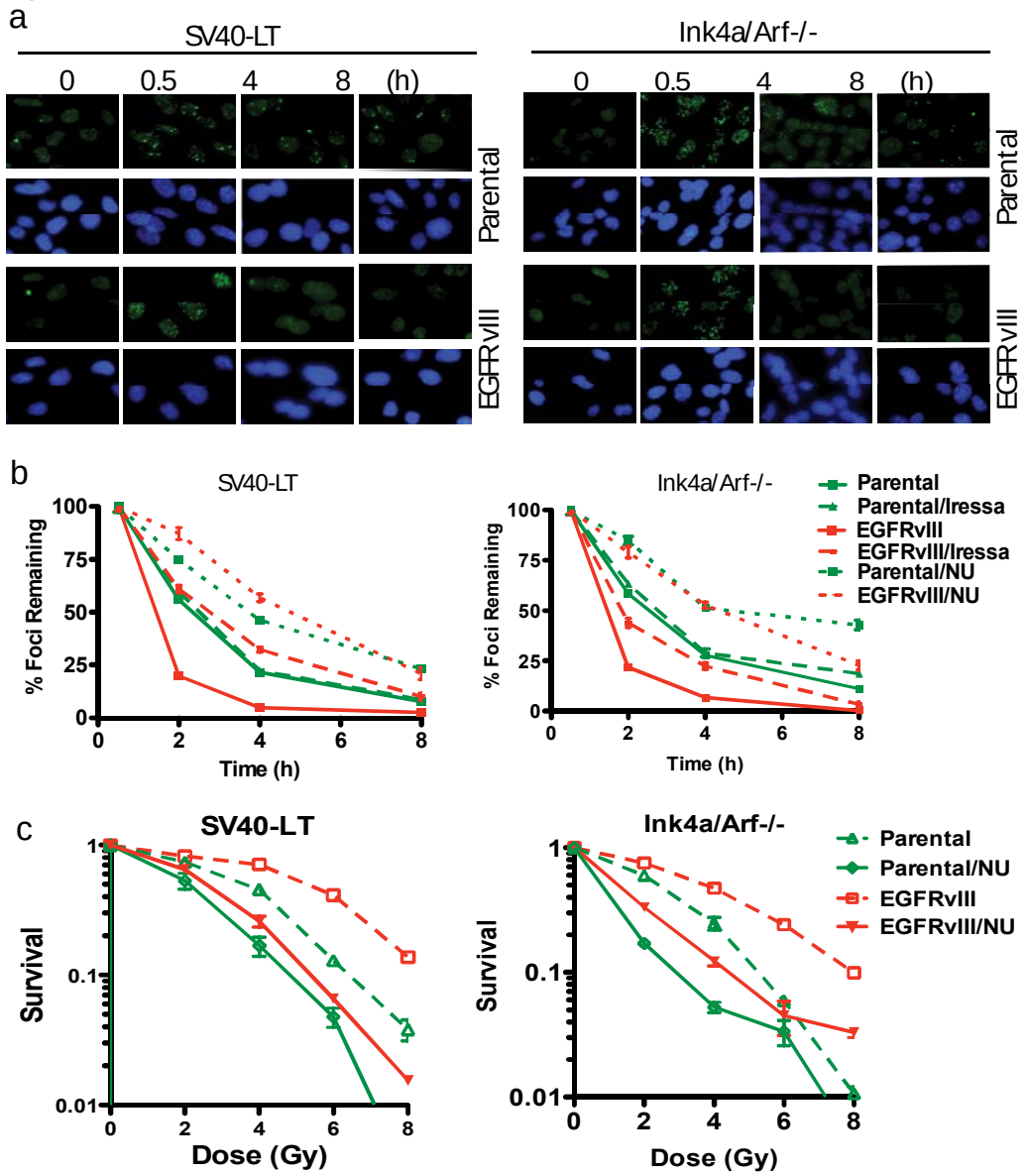

Figure 2.2 Increased radioresistance of EGFRvIII-expressing astrocytes correlates with proficient DSB repair (A) SV40-LT-expressing mouse astrocytes or Ink4a/Arf−/− primary mouse astrocytes were irradiated with 1 Gy of γ rays and immunostained for 53BP1 foci at various time points ranging from 0.5 to 8 h post-irradiation. The pictures depict initial DNA damage (0.5 h) and DNA damage remaining at 4 and 8 h. **(B)** 53BP1 foci were scored at 0.5, 2, 4, and 8 h post-irradiation. The number of 53BP1 foci was determined for each time point (average of 100 nuclei) and, after subtracting background (number of foci in unirradiated nuclei), the percentage foci remaining was plotted against time to obtain DNA repair kinetics. Error bars represent standard error of the mean.

Conversely, activation of this pathway, due to loss of PTEN, results in proficient DSB repair and radioresistance (Kao et al., 2007). Moreover, Akt-1 is reported to translocate into the nucleus upon irradiation and interact and co-localize with DNA-PKcs at DSBs (Bozulic et al., 2008; Lees-Miller, 2008; Boehme et al., 2008). Therefore, we investigated whether EGFRvIII expression directly affected DSB repair *via* the PI3K-Akt-1 pathway. Towards this end, we ectopically expressed constitutively active, myristylated-Akt-1 in SV40-LT astrocytes (Fig 2.3a). Expression of myristylated-Akt-1 resulted in efficient DSB repair similar to that noted upon EGFRvIII expression (Fig 2.3b). Conversely, treatment of EGFRvIII-expressing SV40-LT-astrocytes with LY294002, a specific inhibitor of PI3K (Cuenda and Alessi, 2000), resulted in slower DSB repair similar to levels seen in parental cells (Fig 2.3b). These results raise the possibility that EGFRvIII expression might influence DSB repair *via* the PI3K-Akt-1 pathway.

EGFRvIII enhances DSB repair in a mouse orthotopic glioma model

Upon completion of the *in vitro* project with Dr. Mukherjee, I wanted to investigate whether this phenotype is recapitulated *in vivo.* Given that cell culture conditions *in vitro* may not necessarily replicate the complex microenvironment within a tumor *in vivo*, it is possible that the efficient DSB repair observed upon EGFRvIII

Figure 2.2 (continued) Note nearly complete repair by 4 h in cells expressing EGFRvIII. Pre-treatment of cells with the EGFR inhibitor Iressa (dashed lines) or with the DNA-PKcs inhibitor NU7026 (dotted lines) abrogated DSB repair. **(C)** Radiation survival of astrocytes pre-treated with NU7026 was quantified by colony formation assays. The fraction of surviving colonies (*y*-axis) was plotted against corresponding radiation dose (*x*-axis). Error bars represent standard error of the mean of experiments performed three or more times.

Figure 2.3

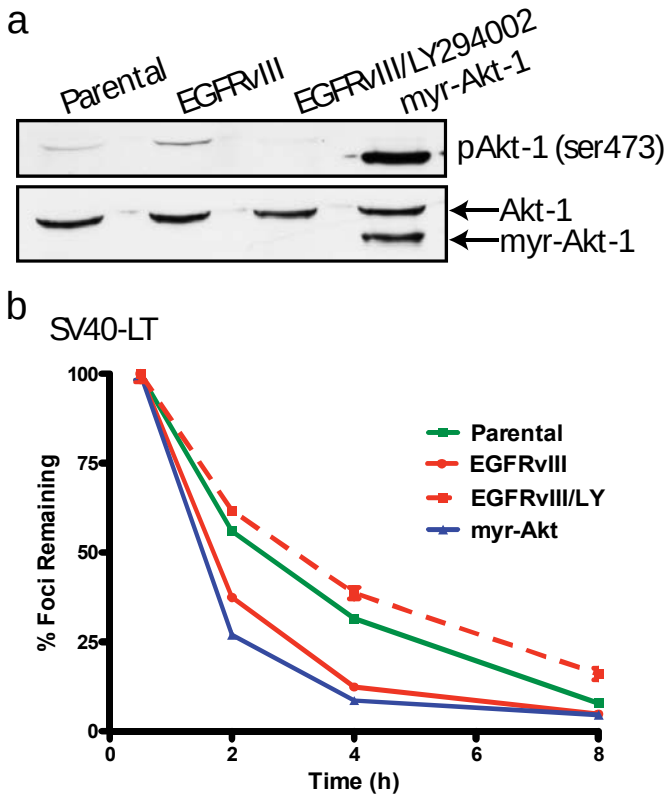

Figure 2.3 Akt-1 activation in mouse astrocytes mimics effects of EGFRvIII expression on DSB repair (A) Phosphorylation of Akt-1 (at ser 473) was assayed by Western blotting of SV40-LT-expressing mouse astrocytes (parental), SV40-LT-astrocytes with EGFRvIII over-expression, EGFRvIII-expressing astrocytes pre-treated with a PI3K inhibitor (LY294002), or SV40-LT-astrocytes expressing myristylated-Akt-1. **(B)** Astrocytes were irradiated (1 Gy) and immunostained for 53BP1 foci to obtain DSB repair kinetics. Error bars represent standard error of the mean. Note proficient repair in cells expressing myr-Akt-1 (blue line), while repair was abrogated in EGFRvIII-expressing cells treated with LY294002 (dashed red line).

expression may not hold true in the context of GBMs. Therefore, I used a mouse orthotopic glioma model to visualize DSBs and quantify DNA repair *in vivo*. U87-parental and U87-EGFRvIII cells (both expressing luciferase reporters) were stereotactically injected into the striatum of a cohort of nude mice (Bachoo et al., 2002). Intracranial tumor growth was monitored by serial luciferase imaging, with the help of Shyam Sirasangandala. Once tumors reached 50% maximal tolerated size (established in pilot experiments and corresponding to approximately 11–13 days post-implantation for U87-EGFRvIII cells and 16–18 days for U87-parental cells), mice were anaesthetized and received cranial irradiation (total dose: 2 Gy). Mice were anaesthetized and cardiac perfused with fixative at 0.5, 2, 4, or 8 hours post-irradiation. Brains were paraffin embedded for routine immunohistochemistry and all tumor sections were H&E stained to determine the size and location of tumors (Fig 2.4a). Tumor sections were then stained with α-53BP1 antibody to visualize DSBs and quantify repair kinetics (Fig 2.4a,b). DSB repair kinetics indicated significantly faster DSB repair rates in tumors derived from U87-EGFRvIII cells (Fig 2.4b). These results, demonstrating *in vivo* tumor cell repair kinetics for the first time, suggest that EGFRvIII over-expression in glioma-relevant orthotopic tumors significantly augments the repair of radiation-induced DNA damage.

Mouse orthotopic tumors expressing EGFRvIII are refractory to radiation therapy

To test whether proficient DNA repair mechanism(s) observed in EGFRvIII-expressing tumors translates into *in vivo* radioresistance, we exposed nude mice bearing intracranial U87-parental or U87-EGFRvIII tumors to whole brain radiotherapy (WBRT).

Figure 2.4

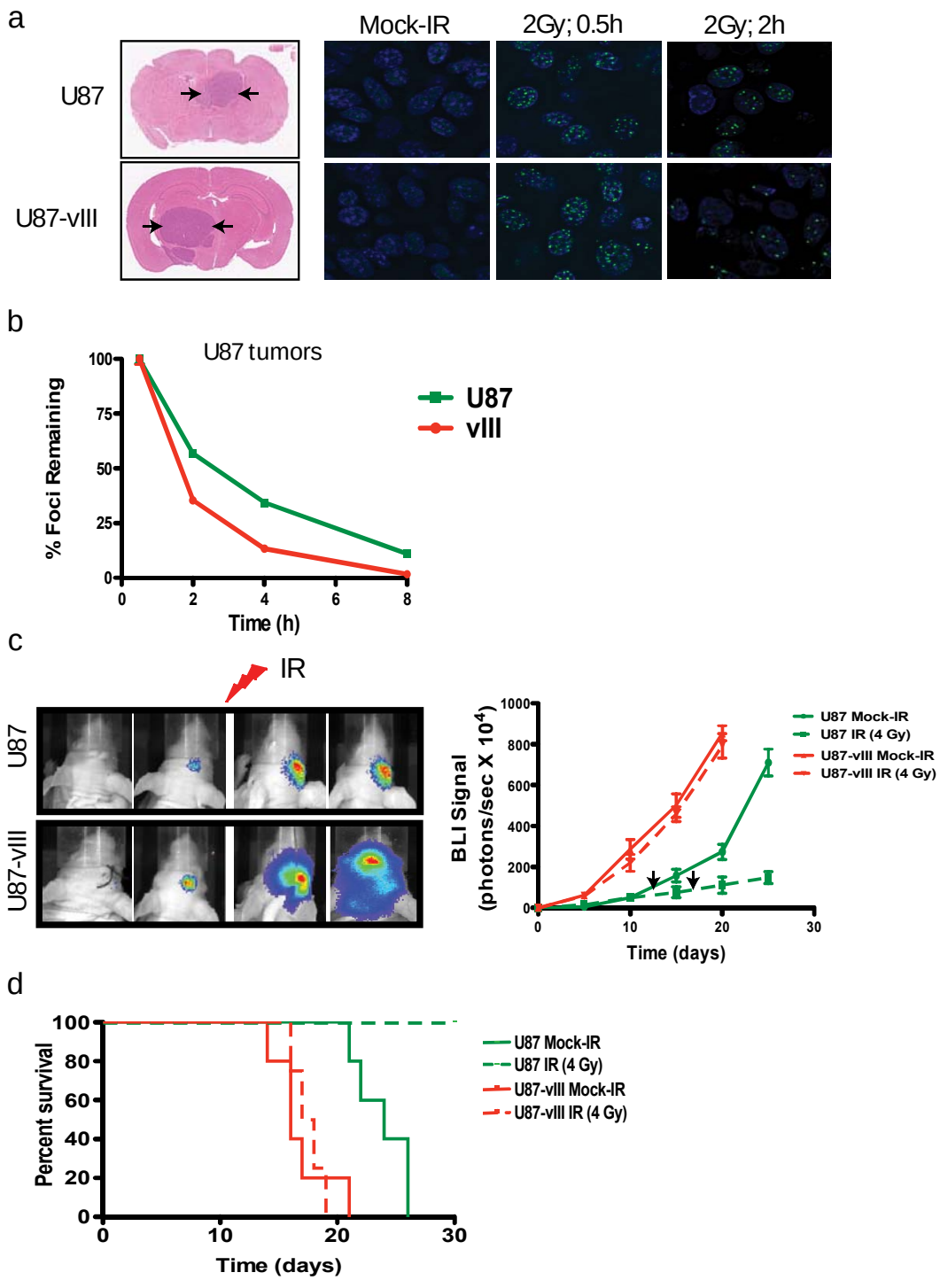
a
Mock-IR
2Gy; 0.5h
2Gy; 2h
U87
U87-vIII
b
U87 tumors
% Foci Remaining
Time (h)
U87
vIII
c
IR
U87
U87-vIII
BLI Signal (photons/sec X 10^4)
Time (days)
U87 Mock-IR
U87 IR (4 Gy)
U87-vIII Mock-IR
U87-vIII IR (4 Gy)
d
Percent survival
Time (days)
U87 Mock-IR
U87 IR (4 Gy)
U87-vIII Mock-IR
U87-vIII IR (4 Gy)

As reported previously (Nishikawa et al., 1994), the rate of U87-EGFRvIII intracranial tumor growth is significantly higher than that of U87-parental tumors. Due to the faster growth rate of U87-EGFRvIII glioma cells, the timing of WBRT was adjusted such that IR(4 Gy, one time dose) was delivered when the tumors were approximately of similar size (at day 6 post-implantation for U87-EGFRvIII tumors and at day 10 for U87-parental tumors) **(**Fig 2.4c). Mice were sacrificed when they became moribund or at day 30 post-implantation. Following WBRT, the growth rate of U87-parental tumors was significantly reduced compared to growth of mock-irradiated tumors **(**Fig 2.4c). In contrast, there was no difference in the rate of U87-EGFRvIII tumor growth with or without radiation. Correspondingly, following WBRT, there was little improvement in

Figure 2.4 EGFRvIII enhances DSB repair in a mouse orthotopic glioma model *in vivo* (A) Orthotopic U87-parental and U87-EGFRvIII tumors were generated in nude mice. Once tumors reached 50% maximal tolerated size, mice received cranial irradiation (2 Gy) and were sacrificed at 0.5, 2, 4, and 8 h post-IR to obtain DNA repair kinetics. Intracranial tumors were identified in coronal brain sections by H&E staining. Brain regions occupied by tumor mass were stained with α-53BP1 antibody to visualize radiation-induced DSBs. **(B)** 53BP1 foci were scored to obtain DSB repair kinetics. Error bars represent standard error of the mean. **(C)** Growth of orthotopic U87-parental and U87-EGFRvIII tumors was monitored by serial luciferase imaging (representative images are shown). Nude mice with intracranial U87-parental or U87-EGFRvIII tumors were either mock-irradiated or irradiated (4Gy) (n=5 per cohort) and luciferase intensities were quantified over a period of 20 days. The plot represents average signal intensity (photons/sec $\times 10^4$) for each cohort (*y* axis) plotted *versus* time post-implantation (*x* axis). Arrows represent time of radiation. Error bars represent standard error of the mean. Note marked decrease in the rate of U87-parental tumor growth (dashed green line) following IR ($p<0.01$) while U87-EGFRvIII tumors (dashed red line) show no significant difference in rate of tumor growth ($p>0.05$). **(D)** Kaplan-Meier analyses of mice with intracranial U87-parental or U87-EGFRvIII tumors (n=6 per cohort). Note no significant increase in post-radiation (4 Gy) survival of mice harboring U87-EGFRvIII tumors (dashed red line) ($p>0.05$) in contrast to marked increase in survival of mice bearing U87-parental tumors (dashed green line) ($p<0.01$).

overall survival (Kaplan- Meier analyses) of mice bearing U87-EGFRvIII tumors compared to mock- irradiated mice **(**Fig 2.4d). In contrast, all mice with U87-parental intracranial tumors that were irradiated were alive at time of sacrifice. These data indicate that proficient DSB repair in EGFRvIII-expressing tumors contributes to tumor radioresistance. We speculate that the extremely rapid and complete DSB repair observed in EGFRvIII-expressing cells may prevent the initiation of programmed cell death upon IR resulting in tumors that are refractory to radiation.

B. PTEN loss suppresses homologous recombination

PTEN loss in immortalized astrocytes sensitizes astrocytes to DNA to alkylating agents

The next step was to characterize how loss of PTEN in primary Ink4a/Arf-/- astrocytes impacted responses to radiation and drug treatment (McEllin et al., 2010). Primary astrocytes were generated from Ink4a/Arf-/- PTEN+/+ or Ink4a/Arf-/- PTENf/f transgenic littermates. Once in culture, conditional PTEN alleles were deleted by adenoviral expression of Cre recombinase, generating a set of matched astrocytes with the following genotypes: Ink4a/Arf-/-PTEN+/+ and Ink4a/Arf-/-PTEN-/-. Because primary mouse astrocytes senesce within a couple of passages after extraction, the Ink4a/Arf-/- background ensures that the astrocytes are immortal (Bachoo et al., 2002), and provide a tumor-suppressor background that is very relevant to GBMs (TCGA, 2008; Parsons et al., 2008). PTEN deletion upon adenovirus infection was confirmed by Western blotting (Figure 2.5a), as well as by PCR analysis (data not shown). As expected, PTEN loss strongly activated PI3K signaling as evidenced by increased levels

of phosphorylated Akt-1 (phospho-serine 473) (Salmena et al., 2008). In accordance with previous reports (Kao et al., 2007; Wick et al., 1999), we found that loss of PTEN resulted in increased resistance to IR as assayed by colony survival (Figure 2.5b). In contrast, PTEN loss resulted in sensitization to n-methyl-n'-nitro-n-nitrosoguanidine (MNNG) (Figure 2.5c). Flow cytometric analyses revealed a significant increase in the sub-G0 population in MNNG-treated PTEN-deficient cultures indicating that the sensitivity of these astrocytes to MNNG was due to an increase in cell death (Figure 2.5d).

PTEN does not regulate the suicide repair enzyme MGMT

Toxicity from S_N1-type alkylating agents results mainly from a specific type of DNA lesion, methylation of the O^6 position of guanine (O^6meG) (Kaina et al., 2007). This lesion can be reversed by the suicide repair enzyme MGMT, which transfers the methyl group to an internal cysteine residue and inactivates the enzyme (Gerson et al., 2004). It has been previously reported that *MGMT* promoter silencing by methylation corresponds to a better therapeutic response to temozolomide (Stupp et al., 2009; Hegi et al., 2005). Therefore, we investigated whether PTEN loss can cause a decrease in MGMT levels at either the protein or RNA level. However, Western blot analyses of basal MGMT protein levels did not show a significant difference between PTEN+/+ and PTEN-/- astrocytes (Figure 2.6a). It has also been reported that MGMT transcription is induced in response to various DNA damaging agents, including MNNG (Kaina et al., 2007; Fritz et al., 1991). However, reverse transcription PCR (RT-PCR) analyses revealed that both astrocyte lines showed similar basal rates of MGMT RNA levels and

Figure 2.5

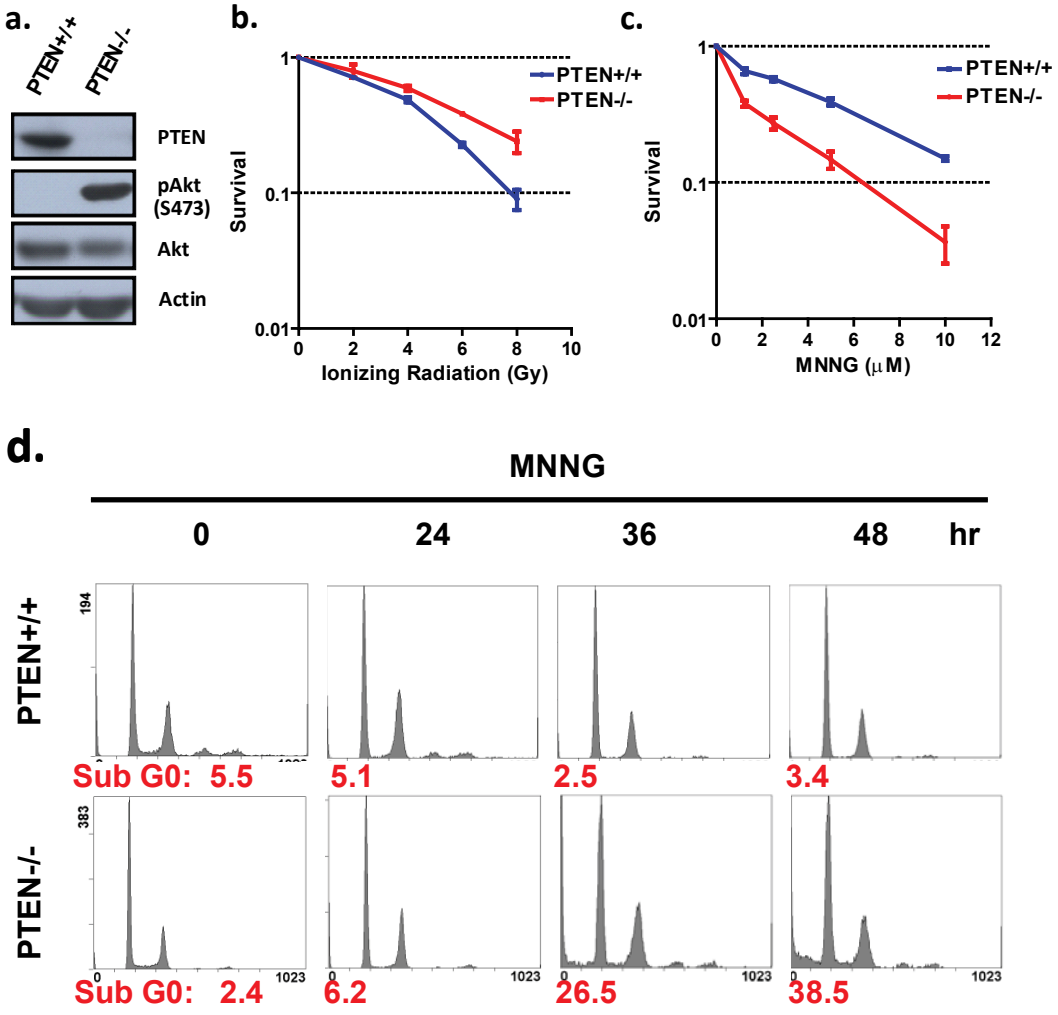

Figure 2.5. **PTEN loss sensitizes astrocytes to MNNG. (A**), loss of PTEN and activation of Akt in PTEN+/+ and PTEN−/− astrocytes were analyzed by Western blotting with α-PTEN and α-phospho-Akt(ser473) antibodies. **(B)**, the radiation survival of astrocytes was quantified by colony formation assays. The fraction of surviving colonies (y-axis) was plotted against corresponding radiation dose (x-axis). **(C)**, the sensitivity of astrocytes to MNNG was quantified by colony formation assays. Note increased sensitivity of PTEN-null cells to MNNG. Error bars, SEM of experiments done three or more times. **(D)**, induction of cell death by MNNG was assessed by quantifying the sub-G0 population in MNNG-treated cultures by flow cytometry (percentages in red).

were each capable of inducing MGMT transcription upon MNNG treatment (Figure 2.6b). Interestingly, PTEN-/- astrocytes show a greater induction of MGMT transcription after MNNG treatment. This phenotype is likely due to the persistence of DNA double-strand breaks in this cell line after MNNG treatment, as shown in Figure 2.8, rather than any changes in MGMT regulation. These data strongly suggest that the sensitivity of PTEN-null cells to MNNG was not due to changes in *MNNG* transcript or protein levels.

MNNG treatment induces replication-associated DNA DSBs

The cytotoxicity of O^6meG lesions is attributed to the recognition of O^6-meG/C or O^6-meG/T mispairs by the mismatch repair (MMR) system (Jiriciny J, 2006), with two opposing models proposed: (a) DNA damage signal transduction by the MMR complex engaged at the mismatch sites directly triggering apoptosis (direct signaling model) or (b) reiterative and futile repair attempts by MMR resulting in single-strand and double-

Figure 2.6

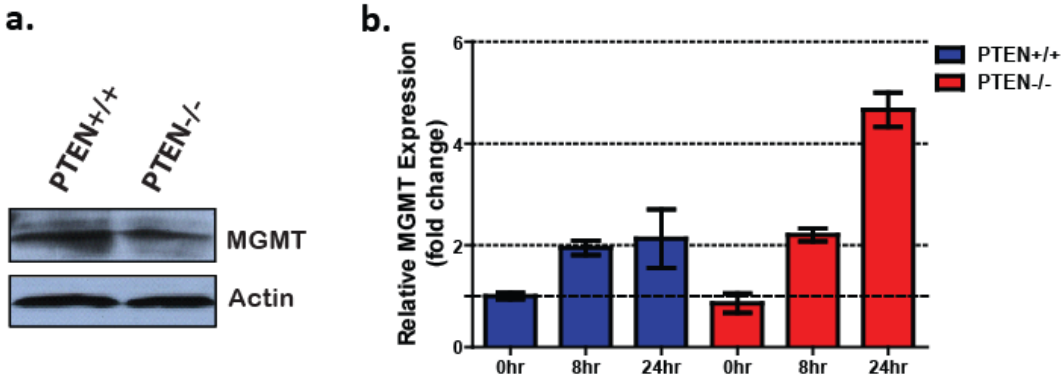

Figure 2.6. MGMT regulation is not affected by PTEN loss. (A), MGMT protein levels in PTEN+/+ and PTEN−/− astrocytes were analyzed by Western blotting with α-MGMT antibody. **(B)**, MGMT transcript levels in mock-treated and MNNG-treated astrocytes were quantified by RT-PCR. Values were normalized to glyceraldehyde-3-phosphate dehydrogenase (GAPDH) levels and expressed as fold change relative to mock-treated PTEN+/+ cells. Bars, SEM.

strand DNA breaks (futile cycle model) (Wang and Edelmann, 2006). Since DNA double-strand breaks (DSBs) are the most lethal of DNA lesions, we investigated whether such breaks were induced in MNNG-treated astrocytes. MNNG-induced breaks are presumed to occur in the S/G2 phases as DNA replication is required for mispairing. Astrocytes were treated with 5μM MNNG and harvested 9 hours later for analysis by flow cytometry. Staining for DNA content with propidium iodide (x-axis) and γH2AX, a surrogate marker for DSBs (y-axis) showed significant increases in DNA breaks in both cell lines. Furthermore, these breaks occur primarily in the S and G2 phases of the cell cycle as predicted (Figure 2.7a, b).

DSBs are repaired by NHEJ or HR in mammalian cells. While NHEJ is operative in all phases of the cell cycle, HR is limited to S/G2 and is particularly important for resolving replication-associated breaks (Branzei and Foiani, 2008). Therefore, it is likely that these breaks may be resolved by HR rather than by NHEJ. Indeed, no further sensitization was observed upon treating these cells with NU7026 (McEllin et al., 2010), a potent inhibitor of the major NHEJ repair enzyme DNA-PKcs (Veuger et al., 2003), that MNNG induces DSBs and that cells defective in HR (XRCC2 and Brca2 mutants), but not cells defective in NHEJ (Ku80 and DNA-PKcs mutants), were sensitive to MNNG, similar to PTEN-null cells (Roos et al., 2009).

PTEN-/- astrocytes show unrepaired DNA DSBs after MNNG treatment

Since both cell lines showed an induction of DSBs after MNNG treatment, the next step was to determine whether these breaks were more persistent in PTEN- deficient

Figure 2.7

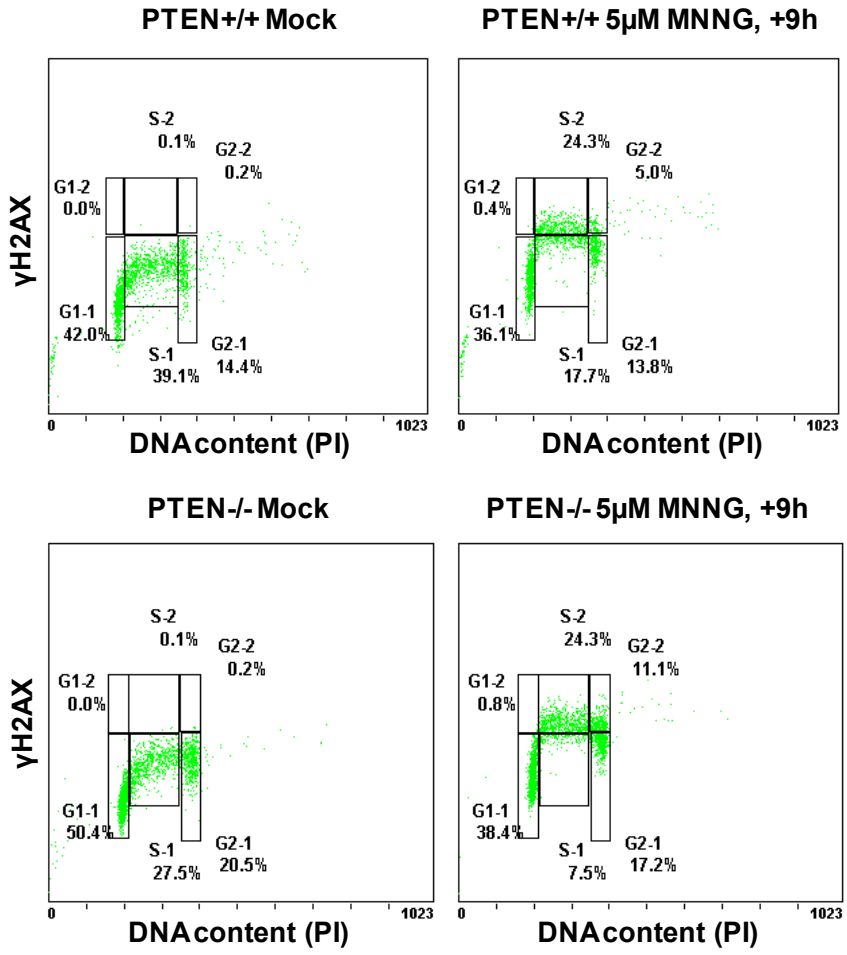

Figure 2.7. DNA double strand breaks after MNNG treatment occur in the S/G2 phases. H2AX phosphorylation in PTEN+/+ **(A)** and PTEN-/- **(B)** cells after MNNG treatment was analyzed by dual-parameter flow cytometry. Staining for DNA content (*x* axis) and for histone γH2AX phosphorylation (*y* axis) is shown (lower compartments represent unphosphorylated G1, S and G2 cells while upper compartments represent cells with phosphorylated H2AX; relative percentages are indicated). Please note that γH2AX signal increases dramatically in the S/G2 phases upon MNNG treatment.

cells. I analyzed the formation and dissolution of γH2AX and 53BP1 foci upon pulse-treatment with MNNG (Mukherjee et al., 2008; Stojic et al., 2004), these foci being *bona fide* surrogate markers for DSBs (Fernandez-Capetillo et al., 2004; Mochan et al., 2004). While the initial rate of DSB formation was equivalent in both cell lines (0-12h), PTEN-/- astrocytes show an increased number of DSBs at 16 and 24 hours post MNNG treatment, indicating that there is a failure to repair these breaks (Figure 2.8a).

PTEN-/- astrocytes show decreased levels of homologous recombination

Cells deficient in various HR components show a decrease in the number of sister chromatid exchanges (SCEs) after treatment with DNA damaging agents (Sonoda et al., 1999), especially agents that induce replication-associated DSBs such as camptothecin (CPT) (Amaudeau et al., 2001). Also, HR-deficient cells are sensitive to CPT (Amaudeau et al., 2001) and we found that PTEN-deficient astrocytes were more sensitive to this drug compared to their PTEN-proficient counterparts (Figure 2.8b). We quantified the number of SCEs in PTEN+/+ and PTEN-/- astrocytes after treatment with CPT or MNNG to determine relative HR proficiencies of these lines. A statistically significant reduction in SCE events was observed in PTEN-/- astrocytes relative to PTEN+/+ astrocytes indicating a defect in HR (Figure 2.8c). Consequently, PTEN-null cells surviving MNNG treatment exhibited greater numbers of chromosome breaks and radial chromosomes (Figure 2.8d)**,** similar to that seen in HR-deficient cells, particularly those deficient in Brca1 or Brca2 (Venkitaraman, 2009). These aberrations are indicative of a diminished capacity to repair MNNG-induced DSBs by error-free HR and subsequent repair of these lesions by error-prone pathways such as NHEJ.

Interestingly, a recent report demonstrated that PTEN is important for maintaining basal levels of transcription of the *Rad51* gene in mouse embryonic fibroblasts (Shen et al., 2007), providing a potential mechanism to explain the reduced HR capability of PTEN-null astrocytes. However, no significant changes in Rad51 protein or mRNA levels in mouse astrocytes upon PTEN loss were noted (Figure 2.9a,b). While Rad51 forms a presynaptic nucleofilament that is critical for HR, ancillary proteins such as BRCA1, BRCA2, Rad52, and the Rad51 paralogs (Rad51B, Rad51C, Rad51D, XRCC2, and XRCC3) facilitate multiple steps during the repair process (San Filippo et al., 2008). Because there are numerous recent reports of PTEN acting as a transcriptional regulator (Yin et al., 2008), we screened several of these "recombination mediators" for expression changes upon PTEN loss by qRT-PCR and observed decreases in the transcript levels of Rad51B, C, and D (Figure 2.9b). As these proteins are known to exist in complexes facilitating Rad51 nucleofilament formation (San Filippo et al., 2008), it is plausible that reduced levels of these proteins could result in attenuated HR upon PTEN loss.

PTEN loss sensitizes astrocytes to PARP inhibitors

A very important prediction from the observed reduction in HR is that PTEN-null astrocytes should be sensitive to PARP inhibitors, as these agents are thought to function by indirectly causing replication-associated DSBs. This phenomenon of "synthetic lethality" was originally identified in the context of BRCA1 and BRCA2 mutations in breast cancer (Bryant et al., 2005; Farmer et al., 2005), and PARP inhibitors are now in clinical trials for treating HR-deficient breast and ovarian cancers (Fong et al., 2009). We found that PTEN-null cells were significantly more sensitive to the PARP

Figure 2.8

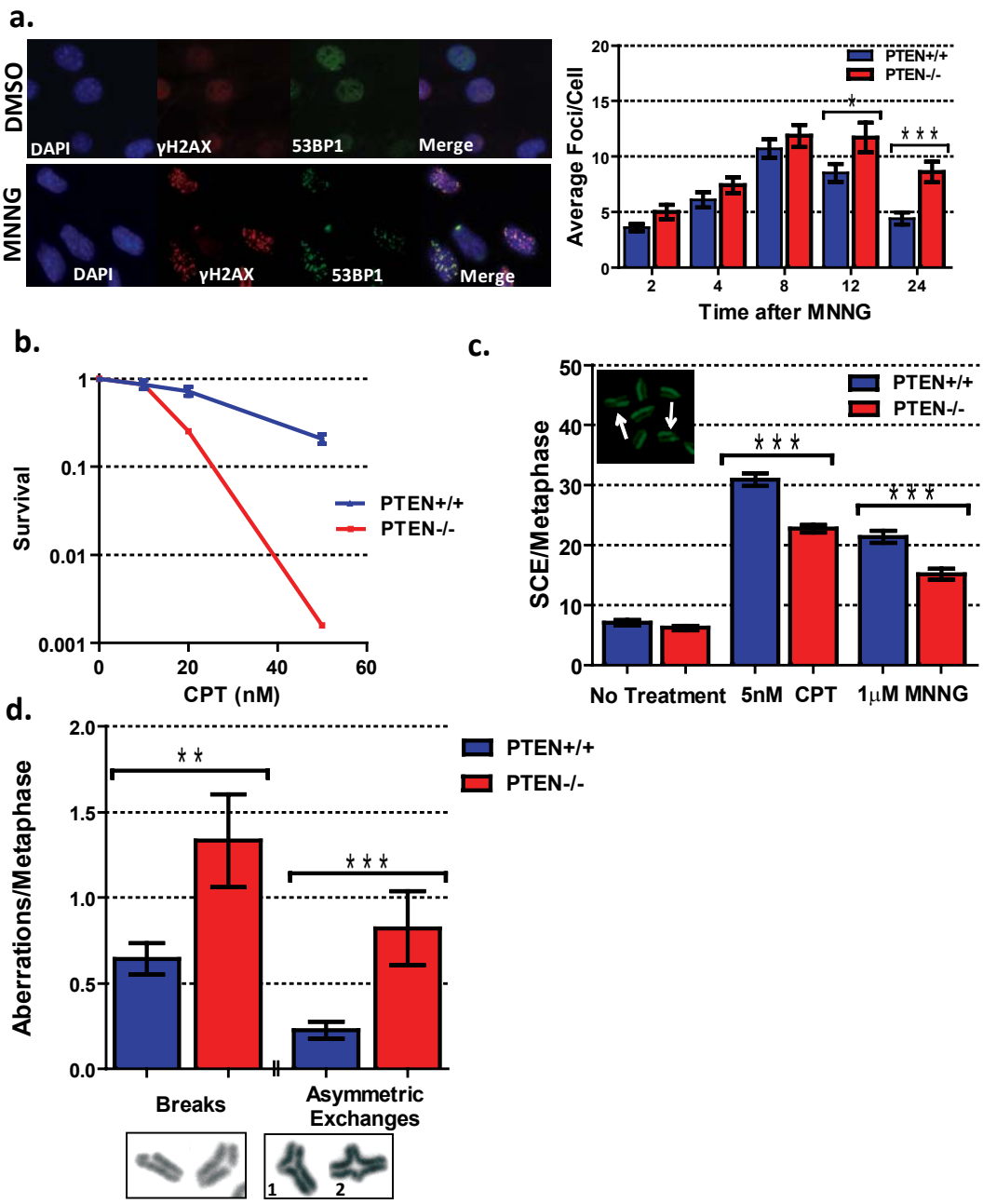

Figure 2.8. PTEN loss compromises HR repair. (A), induction and repair of DSBs in astrocytes pulsed for 1 h with 5 μmol/L MNNG. Cells were co-immunostained for γH2AX (red) and 53BP1 (green) foci at various times after MNNG treatment. Representative pictures are shown. Foci were scored at the indicated times (average of 100 nuclei) and, after subtracting background (number of foci in untreated nuclei), (cont.)

inhibitor, ABT-888 (Donawho et al., 2007), compared to PTEN WT astrocytes (Figure 2.9c). The sensitivity to ABT-888 is consistent with a HR-deficiency in PTEN-null cells, and suggests that it might be logical to treat PTEN-deficient GBMs with PARP inhibitors in the future.

Human astrocyte and glioma lines recapitulate phenotypes of PTEN loss seen in mouse astrocytes

The isogenic murine astrocytes used in this study are ideal for analyzing the effect of a single genetic change (PTEN loss) on MNNG sensitivity. However, in the context of human GBMs, the effect of a single genetic lesion could be modulated by innumerable background genetic changes (TCGA, 2008; Parsons et al., 2008, Verhaak et al., 2010). To explore the relevance of our findings in human GBMs, we compared two commonly used glioma lines (U87MG and U251MG) with a normal human astrocyte line (NHA) that had been immortalized by expression of human telomerase catalytic component (hTERT) and human papillomavirus 16 E6/E7 proteins (Sonoda et al., 2001b). Both glioma lines are PTEN-null (Ishii et al., 1999) and were more sensitive to

Figure 2.8 (continued) average foci per nucleus was plotted against time. *, $P < 0.05$; ***, $P < 0.001$ (two-way ANOVA with a Bonferroni post-test). **(B)**, the sensitivity of astrocytes to CPT was quantified by colony formation assays. Note increased sensitivity of PTEN-null cells to CPT. **(C)**, to quantify SCEs, metaphase spreads were prepared from astrocytes treated with MNNG or CPT as indicated. Reciprocal exchange events (see arrows, inset) were counted and plotted as average number of SCEs per metaphase. At least 40 metaphases were counted per treatment. ***, $P < 0.0001$ (two-tailed t test). **(D)**, metaphase spreads from astrocytes treated with 10 μmol/L MNNG were analyzed for chromatid breaks and asymmetrical exchanges. At least 40 metaphases were counted per treatment and average aberrations per metaphase were plotted. Representative pictures of aberrations are shown. **, $P = 0.0027$; ***, $P = 0.0004$ (two-tailed t test). Bars, SEM (for all plots).

Figure 2.9

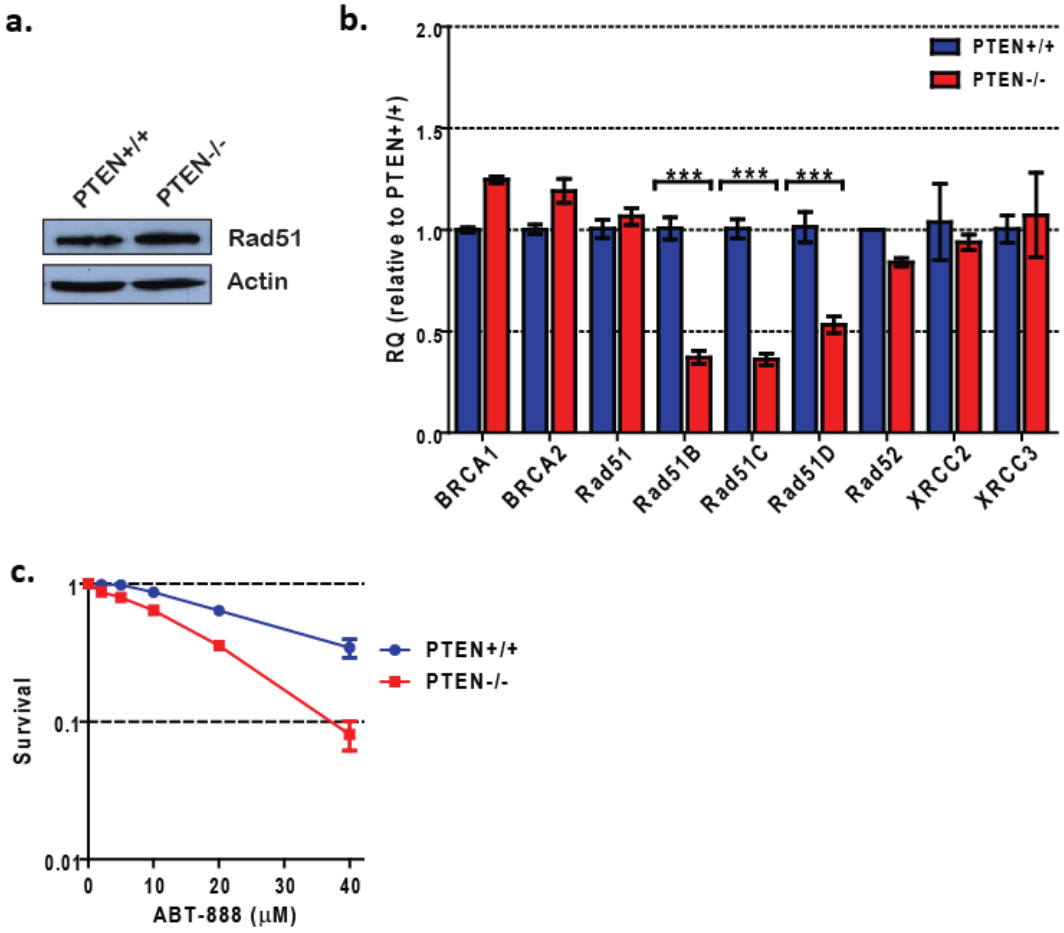

Figure 2.9. PTEN-null astrocytes express lower levels of Rad51 paralogs and are sensitive to PARP inhibitors. (A), Rad51 levels in PTEN+/+ and PTEN−/− astrocytes were analyzed by Western blotting with α-Rad51 antibody. **(B)**, transcript levels of critical HR genes were analyzed by qRT-PCR. Values were normalized to GAPDH levels and expressed as fold change relative to PTEN+/+ astrocytes. **, $P < 0.01$; ***, $P < 0.001$ (two-way ANOVA with a Bonferroni post-test). **(C)**, the sensitivity of astrocytes to the PARP inhibitor ABT-888 was quantified by colony formation assays. Note increased sensitivity of PTEN-null cells to ABT-888. Bars, SEM (for all plots).

MNNG compared to the NHA line, which has an intact *PTEN* gene (Figure 2.10a,b). Importantly, siRNA-mediated depletion of PTEN rendered the NHA line more sensitive to MNNG as quantified by the colony formation assay (Figure 2.11a,b). This was possibly due to attenuated HR, as we observed a reduced induction of SCEs upon PTEN depletion (Figure 2.11c). Interestingly, SCE induction in PTEN-null U87 cells were also reduced compared to the PTEN-proficient NHA line (Figure 2.11c). Finally, PTEN depletion could also sensitize transformed, gliomagenic NHAs (expressing E6, E7, hTERT, H-Ras, and myristylated Akt-1) (Sonoda et al., 2001), indicating that PTEN loss might result in sensitivity to DNA alkylating agents in the context of human gliomas (Figure 2.11b). In sum, these results confirm that, as observed in murine astrocytes, PTEN loss plays an important role in modulating MNNG sensitivity of normal human astrocytes and gliomagenic derivatives.

Figure 2.10

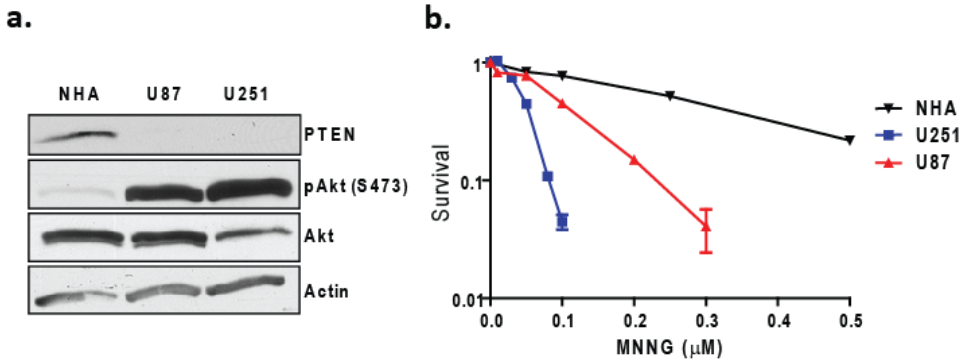

Figure 2.10. Relative sensitivities of normal human astrocytes (NHAs) and human glioma lines to MNNG. (A) PTEN levels and activation of Akt in normal human astrocytes (NHA) and in U87MG and U251MG glioma lines were analyzed by Western blotting with α-PTEN and α-phospho-Akt(ser473) antibodies. **(B)** Sensitivity of human astrocyte and glioma lines to MNNG was quantified by colony formation assays. Error bars represent standard error of the mean.

Figure 2.11

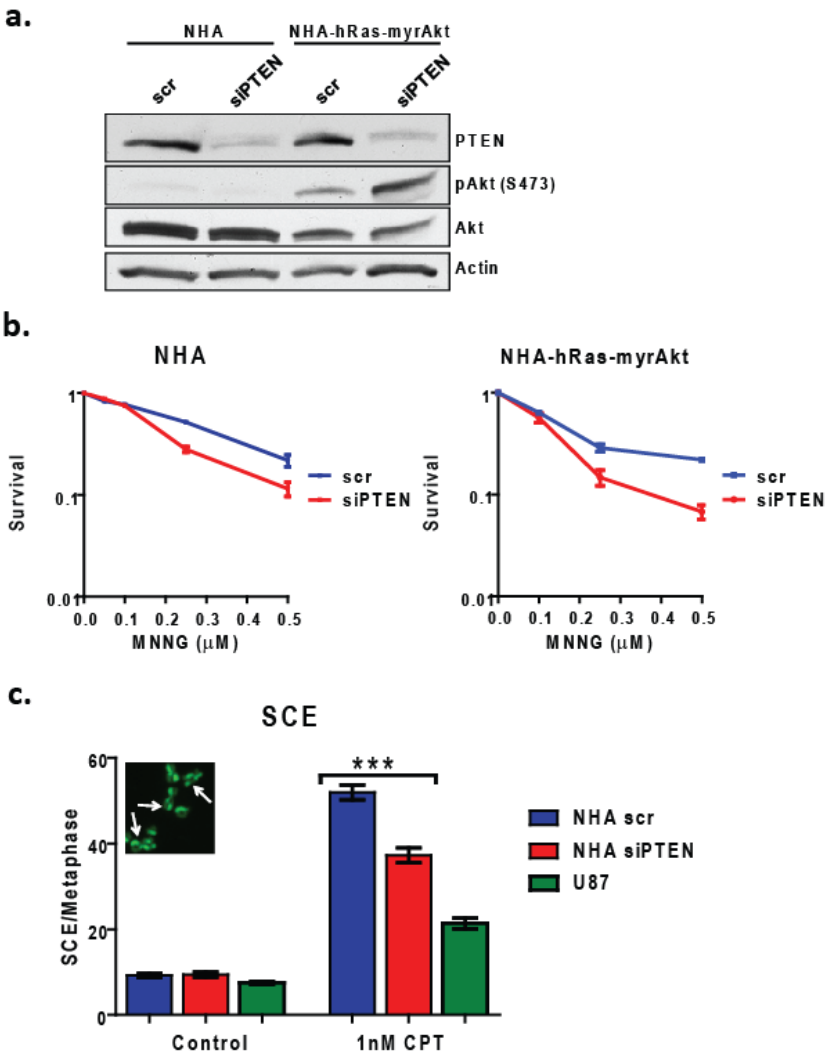

Figure 2.11. Increased sensitivities of normal human astrocytes (NHAs) and gliomagenic NHAs to MNNG upon PTEN knockdown. (A) PTEN levels and activation of Akt in normal human astrocytes (NHA) and in gliomagenic NHAs (2) transfected with a scrambled siRNA (scr) or PTEN siRNA were analyzed by Western blotting with α-PTEN and α-phospho-Akt(ser473) antibodies. **(B)** Sensitivity of human astrocyte lines to MNNG with or without PTEN knockdown was quantified by colony formation assays. Error bars represent standard error of the mean. **(C)** To quantify sister chromatid exchanges (SCEs), metaphase spreads were prepared from cells treated with CPT. Reciprocal exchange events (see arrows, inset) were counted and plotted. At least 40 metaphases were counted per treatment. Statistical significance was determined by a two-tailed t test; ***$p<0.0001$. Please note decreased SCE frequencies upon PTEN-depletion in NHAs and lower levels of SCEs in U87 cells relative to NHAs.

2.3 Discussion

Work described in this chapter supports a relatively novel concept in the DNA repair field that oncogenic signaling and DNA repair are intimately related. Here two mutations that activate oncogenic signaling have been shown to impact the rate of DNA repair, ultimately showing high correlations with therapeutic responses to radiation and alkylating agent treatment. In the first part, EGFRvIII overexpression in both genetically defined astrocyte cultures and U87 glioma cell lines conferred an increase in radiation resistance both *in vitro* and *in vivo*. This resistance was highly correlated with increases in DNA repair proficiency, as data indicated faster repair of DNA DSBs in cell culture models and in orthotopic tumor models. This resistance requires DNA-PKcs, as DNA-PKcs-/- MEFs do not show any increase in radio-resistance by overexpression of EGFRvIII (Mukherjee et al., 2009). In addition, expression of EGFRvIII promotes Akt-mediated hyperphosphorylation of DNA-PKcs, a key repair enzyme for NHEJ, after IR (Mukherjee et al., 2009). In the second piece, I have shown that loss of PTEN increases radioresistance, presumably though the same mechanisms as EGFRvIII overexpression, as they both activate the Akt pathway. In stark contrast, PTEN loss also renders astrocytes more sensitive to DNA alkylating agents, and data indicates that this phenotype is due to reduced HR frequencies in these cell lines.

These results can potentially provide the basis for exciting new therapeutic options for GBMs. There is growing evidence that the EGFR and Akt pathways and DNA repair mechanisms are linked, although the exact mechanisms remain unclear. It was first shown that EGFRvIII signals preferentially through the PI3K pathway in astrocytes, fibroblasts, and a glioma cell line. Furthermore, this expression of EGFRvIII

was sufficient to promote radioresistance in clonogenic survival assays (Li et al., 2004). Subsequent work in several cell lines has shown that inhibitors of the EGFR pathway slow down rates of DNA repair, as evidenced by increased residual damage in several different cell lines/tumor types (Friedmann et al., 2004; Tanaka et al., 2008; Golding et al., 2009; Kriegs et al., 2010). However, the exact mechanism for this effect remains elusive, with both the PI3K/Akt (Friedmann et al., 2004, Golding et al., 2009) and MAPK (Golding et al., 2009; Kriegs et al., 2010) pathways have been implicated in this response. Several reports have focused on examining the Akt pathway and radioresistance in more detail. In the U251 glioma line, inhibiting the PI3K pathway both pharmacologically and by re-expression of PTEN in glioma lines inhibits DSB repair and decreases radioresistance (Kao et al., 2007). It has also been shown that Akt is phosphorylated at S473 shortly after ionizing radiation and colocalizes with γH2AX foci, surrogate markers for DSBs. This phosphorylation appears to be dependent on DNA-PKcs, as treatment with the DNA-PKcs inhibitor NU7026 significantly reduces levels of phospho-Akt (Boehme et al., 2008; Bozulic et al., 2008). However, inhibitors of Akt1 also suppress phosphorylation of DNA-PKcs at T2609 and S2056 in lung cancer lines (Toulany et al., 2008), and our data indicates that increased signaling from EGFRvIII via the Akt pathway promotes phosphorylation of DNA-PKcs in response to IR (Mukherjee et al., 2009). Thus, it seems there may be a feedback loop between activated Akt and DNA-PKcs with these proteins acting in the same complex (Bozulic et al., 2008; Toulany et al., 2008). Such a feedback loop could both promote DNA repair through hyperactivated DNA-PKcs and promote anti-apoptotic pathways through the Akt pathway, thus enhancing cell survival/radio-resistance.

Thus, while the exact mechanism is not completely understood, a novel strategy for treatment is to concurrently give EGFR inhibitors with ionizing radiation (and temozolomide). This methodology has been tried in a Phase II trial of newly diagnosed GBM (Prados et al., 2009). Though small, the study did show promising overall survival numbers, with progression free survival increasing from 4.9 to 8.2 months and median survival increasing from 14.1 to 19.3 months. The survival benefit was found in both MGMT methylated and unmethylated tumors. It is interesting to note that the largest benefit came in tumors with methylated MGMT and intact PTEN, while no statistically significant benefit was found in EGFR expressing tumors. This result is not entirely unexpected given data presented here, which shows that the major pathway involved in promoting resistance to IR is the Akt pathway. Loss of PTEN constitutively activates this pathway, even in the absence of EGFR amplification. Therefore, inhibiting EGFR in the setting of mutant PTEN may not downregulate Akt signaling, resulting in no therapeutic benefit.

The connection between PTEN loss and reduced HR frequencies may have novel therapeutic implications: GBM patients with PTEN loss (about 36%) may benefit from the addition of PARP inhibitors to therapeutic regimens. This prediction is supported by data from multiple other groups, who have shown that PTEN-null cells and a large panel of tumors lines show decreased homologous recombination and increased sensitivity to PARP inhibitors (Mendes-Pereira et al., 2009; Dedes et al., 2010). In addition, a recent report indicates that acquired resistance of cancer cells to combinatorial treatment with temozolomide and PARP inhibitors is linked to upregulation of HR (Liu et al., 2009).

These results complement our data showing that downregulation of HR due to PTEN loss results in sensitivity to DNA alkylating agents or PARP inhibitors.

Nonetheless, there is not currently a consensus on the correlation between PTEN status and PARP sensitivity or any mechanism for this sensitivity. After the initial report linking PTEN to Rad51 in MEFs (Shen et al., 2007), there has been conflicting data concerning this relationship. While both Mendes-Pereira and Dedes show strong correlations between PTEN status and Rad51 levels, other reports have failed to show this correlation (Gupta et al., 2009; Fraser et al., 2012). However, as discussed in Fraser et al., there does appear to be significant correlation between PTEN status and sensitivity to DNA damage agents when PTEN is knocked down experimentally in isogenic lines, in contrast to results correlating PTEN status across panels of cancer lines. This may be due to complex other interactions of many genotypic changes over time in cancer cell lines. Thus, PTEN status alone may not be predictive of responses to PARP inhibitors, and a more pathway centered mechanism may be at play.

Indeed, work presented here has shown that endpoints of HR as a whole (SCEs, chromosome aberrations) are reduced with PTEN deletion, but no changes are seen in Rad51 levels. Thus, it is possible that while the HR pathway is not completely impaired, failed activation of cell cycle checkpoints due to PTEN loss (Puc, Keniry et al., 2005; Puc and Parsons, 2005) may decrease the available time to complete repair from occurring, resulting in unrepaired lesions and increased cell death. An alternate hypothesis relates to data in Figures 2.1-2.4, which demonstrates that activation of the Akt pathway by EGFRvIII enhances rates of NHEJ-mediated repair in astrocytes. While HR is thought to be the main pathway of DNA DSB repair in S and G2 phases of the cell cycle, NHEJ is

still known to be active, but suppressed (Branzei and Foiani, 2006). Hyperactivation of this pathway in an Akt dependant manner may result in an increased number of replication-associated breaks being erroneously repair via NHEJ, necessarily causing a reduction in total HR events (less SCE) and an increase in chromosomal abnormalities, similar to data shown in Figure 2.8. This mechanism may explain why genetically defined mouse systems and comparisons of isogenic cancer lines with siRNA knockdowns show significant sensitization – in these situations, Akt pathway activity is tightly controlled across all groups of cells, whereas levels of the Akt pathway and/or other relevant pathways can be highly variable and not always correlated with PTEN status.

Regardless of these potential mechanisms, both temozolomide and PARP inhibitors are in clinical trials to treat GBMs, and PARP inhibitors are being extensively tested in other cancers (Plummer 2006). Successful Phase II trials of BSI-201 (Iniparib) were first presented in 2009, showing an increase in overall response rate from 32% to 52% and OS from 7.7 months to 12.3 months in triple negative breast cancer (O'Shaughnessy et al., 2011). Similar increases in survival have been seen in early trials using olaparib (Tutt et al., 2010) and veliparib (Isakoff et al., 2009; Burstein, 2011). Because some of the recent efficacy has come in patients without BRCA1/2 mutations, the hope is that PARP inhibitors may have a broader applicability in other cancers with impaired DNA repair.

2.4 Methods

Cell culture

Primary astrocytes were isolated from wild type or Ink4a/Arf−/− 5 day old pups as described previously (Bachoo et al., 2002). Primary wild type astrocytes were immortalized by retroviral expression of the SV40-large T antigen (SV40-LT). Plasmid construction, virus production and infection protocols have been described in detail previously (de la Iglesia et al., 2008). Transfection of astrocytes with retroviruses expressing mutant, constitutively active EGFR (EGFRvIII), wild type EGFR (EGFRwt), or kinase-dead EGFR (EGFRkd) was carried out as described (Bachoo et al., 2002).
For generating the PTEN astrocytes, cortical astrocytes were isolated from five day old pups from littermates of an Ink4a/Arf-/- PTENf/+ × Ink4a/Arf-/- PTENf/+ cross (You et al., 2002; Serrano et al., 1996). The floxed PTEN allele was deleted using an adenovirus expressing Cre. All cell lines were maintained in αMEM or DMEM media containing 10% FBS in a humidified 37°C incubator with 5% CO2.

Irradiations

A 137Cs source (JL Shepherd and Associates, CA) was used for γ-ray irradiation of cells. Mid-brains of mice were irradiated with an X-ray device (Pantak, 300kV, 12mA, 1.65 mm Al) fitted with a specifically-designed collimator providing a 1 cm-diameter field size iso-dose exposure.

Drug treatments

MNNG (Sigma) and CPT (Sigma) were dissolved in DMSO and stored at -20°C in aliquots of 100mM. ABT-888 (Alexis Biochemicals) was dissolved in cell culture grade water and stored at -20°C. MNNG treatments were given as a 1 h pulse, while CPT and ABT-888 were added continuously at the indicated concentrations. The DNA-PKcs inhibitor [10 μM NU7026 (Calbiochem)], the EGFR inhibitor [5 μM Gefitinib (Iressa) (Astrazeneca Co.)], or the PI3K inhibitor [50 μM LY294002 (Sigma)] was added to cells one hour (h) before irradiation. Control cells were treated with DMSO.

Colony formation assays

Cells were plated in triplicate onto 60 mm dishes (300 cells per dish) and irradiated with graded doses of radiation or treated with increasing concentrations of MNNG, CPT, or ABT-888. Surviving colonies were stained with crystal violet about 7 days later. Colonies with more than 50 cells were scored and mean values for triplicate counts determined as described (Kurimasa et al., 1999; Mukherjee et al., 2008).

DSB repair assay

DSB repair rates were assessed by quantifying the rates of dissolution of 53BP1 foci as described (Mukherjee et al., 2008). Approximately 4×10^4 cells were seeded overnight in glass chamber slides under reduced serum (0.5% FBS) conditions. The following day, cells were treated with irradiation (1 Gy) or drug treatment (5μM MNNG), fixed at the indicated times and immunostained with α-53BP1 primary antibody (Cell Signaling) and FITC-conjugated goat anti-rabbit secondary antibody (Molecular Probes) as described.

The number of 53BP1 foci was determined for each time (at least 50 nuclei) and, after subtracting background (number of foci in control population), the percentage foci remaining was plotted against time to obtain DSB repair kinetics.

Immunofluorescence (IF) staining and Western analyses

IF staining of cells and Western blot analyses of whole-cell extracts were performed as described (Mukherjee et al., 2008). Antibodies used were anti-Rad51 (Santa Cruz), anti-γH2AX (Upstate), anti-53BP1 (Cell Signaling), anti-actin (Sigma), anti-Akt, anti-phospho-Akt(Ser473) (Cell Signaling), anti-MGMT (Santa Cruz), rhodamine red-conjugated goat anti-rabbit, and FITC-conjugated goat anti-mouse (Molecular Probes).

Stereotactic injection of cell lines

Orthotopic tumors were generated as described (Nagane et al., 1996; Bachoo et al., 2002). U87-parental or U87-EGFRvIII cells were infected with a puromycin-selectable retrovirus expressing luciferase. Equivalent levels of luciferase expression in the two cell lines was verified by Western blotting with an α-luciferase antibody (Sigma). For intracerebral stereotactic inoculation, 5×10^5 cells were suspended in PBS (5μl) and injected into the right corpus striatum of the brains of 4–5 week-old Nu/Nu nude mice (Charles River). Tumors were allowed to develop and monitored by luciferase bioluminescence imaging. All animal studies were performed under protocols approved by the Institutional Animal Care and Use Committee (IACUC) of UT Southwestern Medical Center.

Noninvasive intracranial bioluminescence imaging

Serial bioluminescence images (BLI) of tumor-bearing mice were obtained using the IVIS Lumina System (Xenogen Corp., Alameda CA) coupled to Living Image data acquisition software (Xenogen Corp.). During imaging, mice were anaesthetized with isoflurane (Baxter International Inc., Deerfield, IL) and a solution of D-luciferin (450 mg/kg in PBS; total volume: 250 µl; Biosynthesis, Naperville, IL) was administered subcutaneously in the neck region. Images were acquired between 10 and 20 minutes post-luciferin administration and peak luminescence signals were recorded. The BLI signals emanating from the tumors were quantified by measuring photon flux within a region of interest (ROI) using the Living Image software package.

Brain sectioning and immunohistochemistry

For pathological analyses and immunohistochemistry, brains were fixed in 10% formaldehyde and processed for hematoxylin and eosin (H&E) staining by standard techniques. Entire brains were sectioned in 1–2 mm coronal blocks and submitted in one cassette for paraffin embedding and sectioning. Sections (5µm) were treated with xylene and washed with ethanol. Antigen retrieval was performed by sodium citrate (10 mM, 20 min) treatment. Sections were then permeabilized in Triton X-100 and blocked with 5% goat serum. After incubation with α-53BP1 antibody (Cell Signaling) (at 4°C, overnight) cells were treated (at room temperature, 2 h) with FITC-conjugated goat anti-rabbit antibody (Molecular Probes). Sections were washed and mounted in Vectashield containing DAPI (Vector Labs).

Metaphase chromosome preparations and Sister Chromatid Exchange (SCE) assay

To examine chromosome aberrations, astrocytes were treated with MNNG and, 24 hours later, 1μg/ml colcemid (Sigma) was added for 3 hours. Metaphase chromosome spreads were then prepared using standard procedures. Aberrations were counted and categorized as breaks or asymmetric exchanges (radial chromosomes). To visualize SCEs, cells were incubated in the presence of BrdU (BD Biosciences, 10μM) for two cell divisions, after which metaphases were prepared according to the above protocol. For drug treatments, MNNG was added as a 1 h pulse immediately prior to BrdU, while CPT was added concurrently. Aberrations and SCEs were quantified by analyzing 100 metaphase spreads and differences were statistically analyzed as described below.

Small interfering RNA (siRNA) transfections.

For siRNA-mediated knockdown of PTEN, cells were transfected with PTEN siGENOME SMARTpool (Dharmacon) by lipofection (Invitrogen) and analyzed 72 h later.

Flow Cytometry.

Cell cycle stage was assayed by single-parameter flow cytometry (propidium iodide staining for DNA content) using a BD CYTOMICS FC500 Flow Cytometer (Becton, Dickinson and Company) as described in (Tomimatsu et al., 2009). For quantification of H2AX phosphorylation by flow cytometry, cells were stained for both DNA content and phosphorylated H2AX using anti-γH2AX antibody (Upstate).

NU7026 treatment

NU7026 (Sigma) was dissolved in DMSO to generate 10 mM stocks and was used at a concentration of 10μM. NU7026 was added 2 hours prior to drug and/or radiation treatment in colony formation assays.

Statistical analyses

P values for experiments were calculated using GraphPad Prism. SCE and chromosome aberration data were analyzed by a two-tailed t-test, while qRT-PCR data and repair kinetics were analyzed using two-way ANOVA.

PCR conditions and primers.

PCR amplification of mouse tails and cell lines was performed using the following primer sets. 1) For *PTEN*, the primers were: P1 5' AAG CAC TCT GCG AAC TGA GC 3'; P2 5' TTG CCA GAC ATG CTC CGA AG 3'; P3 5' GCT TGA TAT CGA ATT CCT GCA GC 3'. Expected products were as follows – P1/P2: PTENwt (400bp); P1/P2: PTENfloxed (550bp); P1/P3: PTENnull (370bp). 2) For *Ink4a/Arf*, the primers were: I01 5' GTG ATC CCT CTA CTT TTT CTT CTG ACT T 3'; I02 5' CGG AAC GCA AAT ATC GCA C 3'; I03 5' GAG ACT AGT GAG ACG TGC TAC TTC CA 3' with expected products - I01/I02: Ink4a/Arf+/+ (313bp) and I01/I02: Ink4a/Arf-/- (278bp).

RT-PCR.

For RT-PCR, astrocytes were harvested during log-phase growth and RNA was extracted using RNeasy Mini Kit (Qiagen). Flow cytometry for DNA content showed similar cell

cycle distributions for both cell lines (data not shown). A cDNA library was then made using the iScript cDNA Synthesis Kit (Biorad) using random primers. qRT- PCR was carried out using the LightCycler-FastStart DNA Master SYBR-Green I kit (Applied Biosystems) on the cDNA library using primer sets (Invitrogen) designed with Primer3 (http://frodo.wi.mit.edu/primer3/). Reactions were carried out using the comparative Ct (□Ct) method as described (Bookout et al., 2006) to provide a relative measure of expression between the two astrocyte lines. Raw values were normalized twice – first to the housekeeping gene glyceraldehyde 3-phosphate dehydrogenase (GAPDH) and then to the expression levels in PTEN+/+ cells to obtain relative change in gene expression in PTEN-/- cells. The primer sets are shown in Table 2.1.

\

Table 2.1 List of Primers for RT-PCR

Gene (NCBI Record #)	Primer Sequence
BRCA1 (NM_009764.3)	F 5' TGA CAG TGC CAA AGA ACT CG 3' R 5' GAT ACG CTG GTG CTC TCC TC 3'
BRCA2 (NM_001081001)	F 5' ACC AGT CGC CTT TCA GAG AA 3' R 5' CAC AGG GTC CAC TTT GGT CT 3'
MGMT (NM_008598.2)	F 5' AAA CAC TGA CCC CAC AGA GG 3' R 5' AAC ACA GGG TGA TGG AGA GC 3'
Rad51 (NM_011234)	F 5' AGC TCC TTT ACC AAG CGT CA 3' R 5' CCG CCC TGA GTA GTC TGT TC 3'
Rad51B (NM_009014.3)	F 5' AGA CCT CAC TTC GGA GCA GA 3' R 5' CTG CGA GGC TAT GCA CAA TA 3'
Rad51C (NM_053269.2)	F 5' TCT GTG TGT CCT CCT TGC TG 3' R 5' GCA CAG ACC TTC AAC CCC TA 3'
Rad51D (AF034955.1)	F 5' AGG ATA CAG GTG GTG CGT TC 3' R 5' CCA CCA TCA CAA CCT TCA CG 3'
Rad52 (NM_011236.1)	F 5' AGG ACA GCG TCC CAC ATA TC 3' R 5' GAA CAT GCT GGT TGG TGT TG 3'
XRCC2 (NM_020570.2)	F 5' GAA GCT CCC TCC TCT CTG GT 3' R 5' TTT CCC TGG GTC AGA AGA TG 3'
XRCC3 (NM_028875.2)	F 5'TGG ACC TTC ACC AAG GAG TC 3' R 5' ACT GGA GTG GGG ACA GTG AC 3'

Chapter 3

Baseline Characterization of Radiation Responses in the CystatinC-CreER^{T2} Rosa26-YFP inducible mouse model

3.1 Introduction

The cancer stem cell hypothesis

The long held view that all neoplastic cells in a tumor all equally endowed with tumorigenic capacity has been challenged by the emerging concept that cancers may be organized in a hierarchical fashion, with rare, relatively quiescent cells being responsible for tumor growth. It is postulated that such cancer stem cells (also often referred to as 'tumor initiating cells') , like their normal stem cell counterparts are capable of asymmetric cell division, with one progeny undergoing unlimited self- renewal, while the other undergoes rapid, but limited proliferation, before terminal differentiation (Ward and Dirks, 2007). This concept was put forth by the pioneering work investigating the cellular origins of acute myelogenous leukemia (Lapidot et al. 1994, Bonnet and Dick, 1997). This work has provided novel insights into explaining the cellular and molecular heterogeneity that are one of the hallmarks of both hematological malignancies and solid tumors. Since these landmark studies, subsequent studies have identified cancer stem cell populations in almost every type of malignancy, including breast (Al-Hajj et al., 2003), brain (Singh et al., 2003; Singh et al., 2004), colorectal (O'Brien et al., 2007; Ricci-Vitiani et al., 2007). It is important to emphasize that despite the growing support for the cancer stem cell hypothesis, this remains a work in progress (Quintana et al., 2008;

Quintana et al., 2010). The alternative view– the 'stochastic model' of cancer postulates that random mutagenesis, driven by genomic instability, an inherent feature of cancer, gives rise to multiple clonal populations of tumor cells within a single cancer (Reya et al., 2001). Because of this inherent genetic diversity, subpopulations of tumor cells may be inherently endowed with a greater ability to tolerate various cytotoxic and genotoxic therapies. At present these two mutually exclusive views of tumor origins and organization are the subject of intense debate with no clear consensus. It is important to note that with respect to malignant brain tumors, the focus of my thesis, the current view is that brain tumors are organized in a hierarchical fashion in accordance with the cancer stem cell hypothesis. At its core, the 'cancer stem cell hypothesis' proposes that a small (<1-5%) fraction of the tumor cells are exclusively responsible for maintaining tumor burden and that effective cancer therapies must be able to target and destroy the cancer stem cells. At present there is little insight into the molecular mechanisms which underlie the aggressive, recalcitrant nature of these cells. All current cancer therapies, including radiation, are based on the assumption that the tumor cell population responds in a homogenous fashion to eradicate proliferating cells. The cancer stem cell model predicts that these rarely dividing cells, distinct from the transient-amplifying population, would lead to recurrence, which is consistent with the clinical experience. Selective therapies which specifically target the cancer stem cells would be required to achieve a disease free survival. In this chapter of my thesis, using a novel genetic mouse model system which permits indelible cell-fate mapping, I provide an in-depth kinetic analysis of how the normal brain stem cell compartment responds to ionizing radiation and how select glioma relevant mutations (p53 and PTEN) impact this cellular response.

Cancer stem cells may be prospectively identified from a freshly resected tumor that is dissociated into single cells using single or multiple cell surface receptors, these may include a combination of positive and negative markers, dye exclusion and markers of metabolism (Ward and Dirks, 2007; O'Brien et al., 2009). Estimation of 'true' cancer stem frequency within a tumor mass is based on a limiting dilution transplantation assay. Limiting dilutions of subpopulations of tumor cells are transplanted into immunocompromised mice and assayed for tumor formation. The lowest possible number of injected cells that can reproducibly produce a tumor provides an estimate of 'true' cancer stem cell frequency. Of course, this assay is based on the assumption that a 'single' cancer stem cell is capable of establishing a tumor mass.

Recent evidence suggests that a minor subpopulation (<5%) of GBM cells, that fulfill the criteria for cancer stem cells may be prospectively identified by a 120 kilodalton cell-surface glycoprotein, called Prominin 1, or CD133. Remarkably, Prominin 1, or CD133, has also been shown to identify normal embryonic NSC from both mouse and human embryonic brain tissue. The CD133 positive, but not CD133 negative GBM cells, *in vitro* have been shown to undergo rapid self-renewal by symmetric cell division, form clonal aggregates, known as neurospheres, which in culture continue to proliferate indefinitely and when exposed to certain cytokines (BMP4, LIF, serum) appear to undergo differentiation into neurons, astrocytes and oligodendrocytes, hence displaying normal NSC like properties (Singh et al. 2003; Singh et al. 2004; Galli et al., 2004; Bao et al. 2006; Piccirillo et al. 2006). Subsequent studies have investigated the inherent radio-resistant and drug resistant phenotypes of these CD133-positive cancer stem cells. It has been reported that the CD133+ population may

be more radioresistant than the CD133-ve population due to increased activation of checkpoint responses and enhanced rates of DNA repair (Bao et al., 2006). Multiple other reports have linked other proteins to an increase in radiation resistance, including COX-2 (Ma et al. 2011), Notch (Wang et al., 2010), BMI1 (Facchino et al., 2010), and L1CAM (Cheng et al., 2011). It is noteworthy that BMI1 and L1CAM were shown to promote radiation resistance through impacts on the DNA damage repair machinery, either by recruitment of repair proteins (BMI1) or enhanced expression of a key DNA repair protein (L1CAM). It is unclear how expression of each of these proteins may correlate to common genotypic changes in GBM, though some links have been identified. One report does show a correlation between mutant p53 and increased L1CAM in gliomas (Tsuzuki et al., 1998). In addition, other reports have shown nuclear PTEN suppresses BMI1 (Fan et al., 2009) and an inverse relationship between the p16/p14^{ARF} tumor suppressors/mutated p53 and BMI1 levels in breast cancer (Pietersen et al., 2008). It should be noted, however, that the some of the glioma stem cell papers relied on CD133 as a marker for the stem cell population, and recent reports are now challenging its utility as a stem cell marker (Wang et al., 2008; Zheng et al., 2007; Beier et al., 2011). Wang et al. have recently shown that CD133- glioblastoma populations are able to form GBMs in xenograft models that do regenerate CD133+ cells. Nonetheless, there is substantial evidence that the glioma stem cell population may be driving the resistance seen in these cancers, possibly through signaling mechanisms that enhance DNA repair capacity. A key unknown is how these resistant proteins become aberrantly expressed during gliomagenesis, and which of the signature mutations/pathways may be driving this resistant phenotype.

As noted above, there are many similarities between the normal stem cell compartments and glioblastoma stem cells. In a simplified kinetic view, both GBM and the endogenous neural stem cell compartment may be assumed to be made of three basic types of cells, (i) quiescent stem cells that are capable of unlimited self-renewal, (ii) a transiently amplifying (proliferating) that are lineage restricted, and (iii) post-mitotic, terminally differentiated cells. Each cell type can be identified by immunohistochemical markers which define each developmental stage. Therefore, one approach to understanding the genetic basis of radioresistance is to use the endogenous stem cell compartment as a reductionist model for cancer *in vivo*. Along these lines, I undertook two major steps – (i) a detailed kinetic analysis of stem cell dynamics and radiation sensitivity along the stem cell to neuron differentiation axis (Chapter 3) and (ii) introducing combinations of relevant GBM mutations into the NSC compartment to identify which cell types show changes in radioresistance with different combinations of GBM relevant gene deletions (Chapter 4). This process allows one to identify what specific role each genetic mutation has in promoting resistance, both alone and in combination, along the entire process of transformation.

Adult neurogenesis in the SGZ

In the last 10-15 years, enormous progress has been made in understanding many of the mechanisms of adult neurogenesis and the functional consequences of this process. There are two major adult neural stem cell niches – the subventricular zone (SVZ) and the subgranular zone (SGZ) in the hippocampus. For the purposes of this chapter, I will focus entirely on the SGZ stem cell niche. The SGZ is a thin region between the granule

Figure 3.1

a.

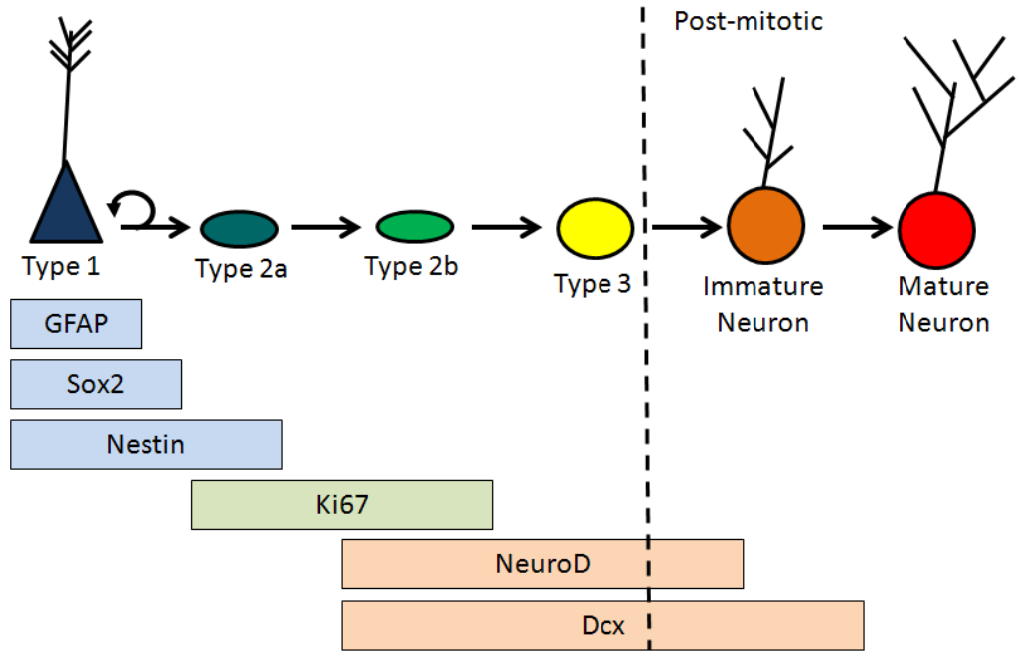

Adapted from Kempermann et al., 2004; von Bohlen und Halbach 2011

Figure 3.1. Basic organization of the adult stem cell compartment in the SGZ. Type I cells are the relatively quiescent population, with morphology similar to radial glia. The proliferating populations are Type 2a and 2b, and immature neuronal markers first being expressed in Type 2b cells. Type 3 cells are capable of proliferating under stress, but normally do not. Dcx expression continues up until the mature neuron phase, where neurons express NeuN (not shown).

cell layer of the dentate gyrus and the hilus. Progenitors divide and migrate into the granule cell layer of the dentate gyrus, where they will differentiate into granule cell neurons. There are multiple types of stem cells/progenitors thought to exist in this niche that represent progressive stages of differentiation, and these are characterized by panels of differentiation markers and morphologic criteria, described in Figure 3.1 (reviewed extensively; see Kempermann et al., 2004; Ehninger and Kempermann 2008; von Bohlen und Halbach 2011). These can be broken up into broad categories – quiescent/rarely dividing stem cells (Type I), transient amplifying cells (Type 2a, 2b), and rarely dividing/post-mitotic lineage-committed progenitors (Type 3 cells, immature neurons and mature neurons). The quiescent stem cells demonstrate a classic radial glial morphology, with a triangular soma and long apical process that extends through the granule layer (Ehninger and Kempermann 2008; von Bohlen und Halbach 2011). These also express a variety of stem cell markers, including nestin, SRY-related HMG-box gene 2 (Sox2), and GFAP (Ehninger and Kempermann 2008; von Bohlen und Halbach 2011). The transient amplifying, proliferative population can be identified by the expression of cell-cycle specific proteins (Ki67 and Mcm2). Immature neuronal markers, such as NeuroD1 and Doublecortin (DCX), are first expressed in the proliferating Type 2b cells (Steiner et al., 2006) and continue to be expressed into the Type 3 and post-mitotic, immature neuron phase. Doublecortin continues to be expressed for 2-3 weeks after cells cease proliferating (Ehninger and Kempermann, 2008). Though there is some overlap between these populations, Sox2 primarily serves as a marker for the quiescent population (with small overlaps in the Type 2 population – Steiner et al., 2006), Ki67 marks the highly proliferative, transient amplifying population, and DCX and NeuroD represent varying

stages of neuronal fate commitment, with a large segment either post mitotic or rarely dividing.

Radiation Effects on Neurogenesis

When combined with other methodologies, ionizing radiation (IR) can serve as a very powerful tool for studying the process of stem cell differentiation. In the past 10-15 years, there have been numerous reports detailing the effects of ionizing radiation on neurogenesis, beginning with work by Tada et al., 2000. In this report, the authors identified several key findings concerning the acute and long-term effects of IR. First, apoptosis induction in the SGZ peaks at 6 hours after irradiation, and is completed by 24 hours. In addition, dose-dependent increases in apoptosis induction peak at 3Gy, showing very little additional killing at higher doses. Proliferation markers (BrdU and $p34^{cdc2}$) are significantly reduced 24 hours after IR, and recover over a time period of 7-14 days in a dose-dependent fashion. It is noteworthy that although higher doses did not increase apoptosis induction, they were sufficient to reduce long-term recovery rates in the SGZ (Tada et al., 2000). Subsequent studies focused on elucidating whether this overall reduction in stem cell proliferation had functional consequences for the formation of new neurons. Monje et al. demonstrated that reductions in proliferation from high dose (10Gy) result in a significant reduction in new neurons formed from cells that proliferate after IR. In addition, this group showed a potent inflammatory response after 10Gy that has subsequently been linked to suppression of neurogenesis (Monje et al., 2003). Mizumatsu et al., 2003 investigated the effects of low dose irradiation on SGZ neurogenesis. Importantly, this study uncovered several key insights**.** Low dose IR (2Gy) was sufficient

to fully reduce Ki67 levels and induce the majority of apoptosis seen (consistent with Tada et al., 2000), but loss of DCX expression was incomplete (~50% reduction) and steadily increased up to 10Gy (assayed up to 48 hours after IR). There was also a dose-dependence in changes in fate commitment for BrdU labeled cells (BrdU given 3 weeks after IR), with 2Gy showing minimal disruptions in new neuron formation and 10Gy showing maximal effects (~75% reduction). This result correlated highly with the extent of inflammatory response, which was minimal at 2Gy and significant at 10Gy. Collectively, this data shows that a range of irradiation doses can disrupt neurogenesis, but this is a reversible phenomenon at low doses (Mizumatsu et al., 2003; Tada et al., 2000; Abdallah et al., 2007). Many other studies have solidified the link between radiation-induced impairments in neurogenesis and cognitive deficits in adult mice (Rola et al., 2004; Fan et al. 2007).

3.2 Results

Over four decades of clinical experience and laboratory based research have shown that radiation can kill rapidly dividing cells; however, some cells are able to escape cell death and are able to repopulate a tumor mass or a normal stem cell compartment. The identity of such cells is of immense clinical significance. The molecular mechanisms by which tumor cells and stem cell compartments escape cell death are not well understood. To date, almost all studies that have focused on how radiation impacts stem cell dynamics have relied on immunohistochemistry to label cell cycle associated proteins (Ki67, PCNA, P-H3) or most commonly, the incorporation of BrdU into DNA during S-phase of the cell cycle.

It is postulated that quiescent adult NSC in the SVZ and SGZ undergo asymmetric division to produce a population of transient amplifying cells that supply new cells at a rate that precisely matches the rate of replacement of damaged or dying neurons. At present it is unclear whether cell death associated with low dose radiation is limited to transient amplifying cells or whether it also negatively impacts the quiescent population and/or lineage committed progenitors. It is also not clear whether the recovery of neurogenesis following radiation is driven by transient amplifying cells that escape cell death, or by the quiescent / dormant population that respond to replace their downstream progeny, perhaps triggered by the loss of a negative feedback signal.

To better understand radiation sensitivity of the SGZ stem cell compartment and mechanism of recovery I have designed and carried out experiments using the CystatinC-CreERT2 (CstC-CreER^{T2}) tamoxifen inducible transgenic mouse line that genetically labels a large population of mature non-dividing astrocytes throughout the gray and white matter regions of the forebrain. In addition to mature cortical astrocytes, this transgenic model also labels an astrocyte population with stem cell like properties in the SGZ and SVZ. CstC-CreERT2 mediated recombination labels progenitor cells that sequentially transition to transient amplifying progenitors and then mature neurons. Detailed characterization of this transgenic mouse model was focus of a recent Ph.D. dissertation (Dr. Lori Boies, Bachoo Lab., Cancer Biology Program, UTSW.2011, manuscript in preparation). For the experiments described below, I have focused exclusively on describing how radiation impacts SGZ stem cell dynamics (Chapter 3) and how deletion of P53 and/or PTEN modifies this response.

CystatinC-CreER2 labels a population of quiescent astrocytes with stem-like properties in the SGZ of the dentate gyrus

Previous cell-fate mapping data work from our lab showed that a novel astrocyte specific transgenic mouse line, CstC-CreERT2, when crossed to the Rosa26-YFP reporter line, exclusively labeled mature astrocytes throughout the gray and white matter regions of the brain and spinal cord. In addition to labeling mature astrocytes, Rosa-YFP (here after referred to as YFP+ve) labeling was also seen along the subventricular zone (SVZ) and subgranular zone (SGZ) of the adult mouse brain. However, the precise identity of the cell types that were labeled by the CstC-CreERT2 mediate recombination was unclear. Therefore, I undertook a temporal analysis of the CstC-CreER^{T2} Rosa26-YFP compound mouse to identify the precise cell type in which the CstC-CreER^{T2} mediated recombination takes place. This detailed analysis was an essential first step to understanding how ionizing radiation affects neurogenesis.

To determine if CstC-CreER^{T2} mediated expression recombination is limited to an astrocyte population with true stem cell-like properties, and is not expressed to any significant extent in transient amplifying cells (Type2a/b) or immature neuroblasts (Type 3 cells and immature neurons), young adult (4-6 weeks of age) CstC-CreER^{T2} Rosa26-YFP mice were injected (intraperitoneal) daily with tamoxifen (180mg/kg, see methods for details) for 5 consecutive days (Figure 3.2a). I then sacrificed 1 mouse 1 day after the final tamoxifen treatment. At this time, it was clear that substantial numbers of YFP immunoreactive cells were present throughout the SGZ. A significant fraction of the YFP+ve cells exhibited a classic Type I/radial glial morphology, with a triangular cell body with a single process through the granular layer and extending into the molecular

Figure 3.2

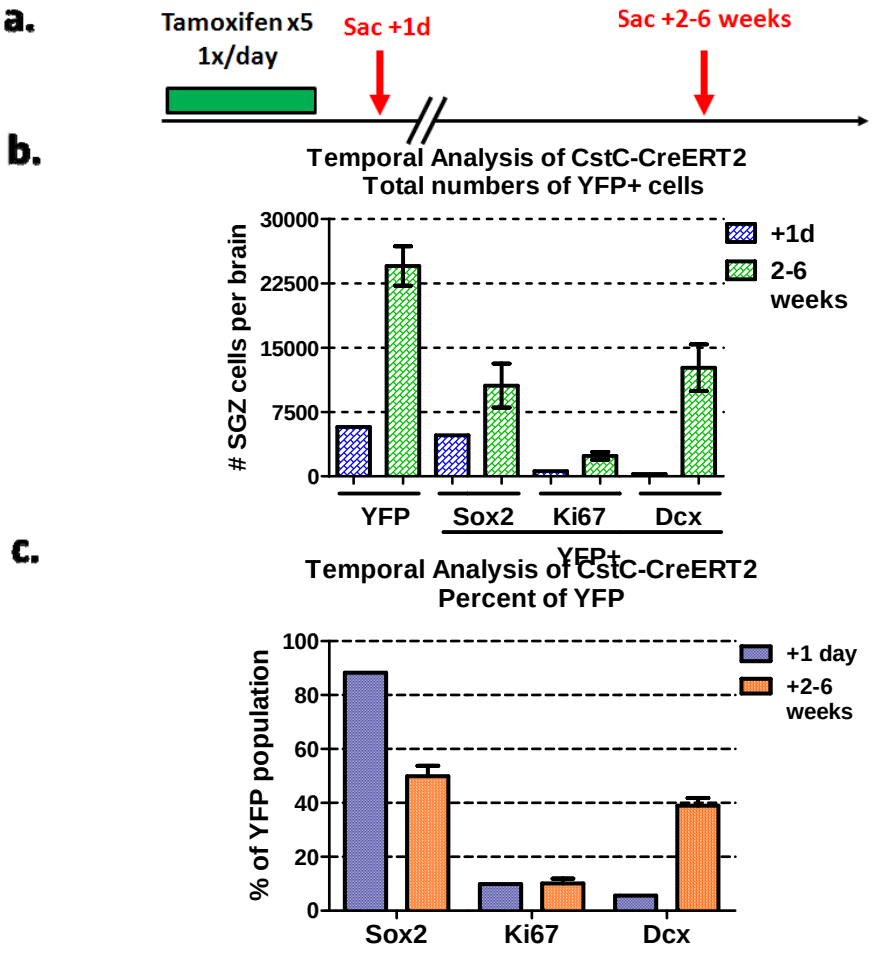

Figure 3.2 Temporal Analysis of YFP-labeled cells in the CstC-CreER^{T2} Rosa26-YFP mouse. (A) Schematic of tamoxifen treatment and sacrifice of CstC-CreER^{T2} animals used in this characterization. Tamoxifen was given 1x per day for 5 consecutive days. 1 animal was sacrificed 1 day after tamoxifen, while the rest were sacrificed between 2 and 6 weeks later (these represent the shielded hemisphere of hemi-brain irradiated mice; see Figure 3.4). **(B)** Mean values +/- SEM of each cell type in the SGZ per brain are plotted. For +1d, YFP+ve = 5,760; Sox2+ve/YFP+ve = 4,788; GFAP+/YFP+ve = 2,184 (not shown); Ki67+/YFP+ve = 600; Dcx+/YFP+ve = 288 (n=1 for all). For 2-6 weeks, YFP+ve = 24,500 +/- 2,300 (n=10); Sox2+/YFP+ve = 10,570 +/- 2,560 (n=2); Ki67+/YFP+ve = 2,400 +/- 1,210 (n=6); Dcx+/YFP+ve = 12,700 +/- 2,720 (n=9). **(C)** Data from **(B)**, expressed as a percent of the total YFP population. For +1d, Sox2+/YFP+ve = 88.3%, Ki67+/YFP+ve = 9.8%; Dcx+/YFP+ve = 5.6%. For 2-6 weeks, Sox2+/YFP+ve = 49.9 +/- 3.8% (n=2), Ki67+/YFP+ve = 10.2 +/- 1.7% (n=6); Dcx+/YFP+ve = 38.9 +/-2.9% (n=9).

layer. Quantification estimates (Figure 3.2b,c) showed that the SGZ contained 5,760 YFP+ve cells; of these 4,788 co-expressed Sox2 (83%) and 2,184 co-expressed GFAP (38%). Immunolabeling of the cell proliferation marker Ki67 was only seen in 600 of the total number YFP+ve cells, representing 10.4% of the total population, while doublecortin and YFP co-labeling was seen in a minor population of approximately 5% of YFP+ve cells (288 total DCX+ve). Taken together, the combination of Type1/radial glial morphology and co-labeling with Sox2+ve and GFAP+ve in the YFP+ve population suggests that CstC-CreER^{T2} induced recombination labels a population of quiescent (or slow dividing) adult neural stem cells. To assess what effects time has on this distribution, the shielded hemispheres of CstC-CreER^{T2} mice were analyzed (see Figures 3.4, 3.6). In this cohort, the interval between the last dose of tamoxifen and euthanasia was between 2-6 weeks. At this time, there was a global increase in total YFP positive cells across all lineages (Figure 3.2b). The most significant increase was seen in the DCX+ve/YFP+ve population, which now represents 38.9 +/-2.9% of the total YFP population (raw values increased to 12,660 +/- 2,720 total DCX+ve/YFP+ve cells, n=9). Meanwhile, the percent Ki67+ve of the YFP+ve population remained unchanged (10.2 +/- 1.7% of the total YFP population; raw numbers are 2,400 +/- 460 total Ki67+ve/YFP+ve, n=6) and the Sox2+ve percent of the YFP+ve population was reduced (down to 49.9 +/- 3.8%; total #s of 10,570 +/- 2,560 Sox2+ve/YFP+ve cells, n=2). Taken together, these observations suggest that the increased interval time permits quiescent stem cells/transient amplifying cells to proceed to DCX+ve neuroblasts, supporting the idea that CstC-CreER^{T2} is initially expressed in a quiescent population. Using this model, I can generate a population of YFP+ve cells that encompasses both the quiescent neural

stem cells and actively dividing/differentiating progenitors, making it an ideal system to assay how radiation affects progenitors in each stage along the differentiation process.

Image guided mouse hemi-brain irradiation

For Chapter 3, my goal was to quantitatively follow over time the recovery of neurogenesis with co-labeling of genetically labeled cells and lineage specific markers that define quiescent stem cells (Sox2), transient amplifying cells (Ki67) and lineage committed neuroblasts (DCX), following 3Gy radiation of the SGZ. Because of the temporal aspects of this experimental design, it is especially important to minimize biological and experimental variability. There is extensive research that the basal levels of neurogenesis among mice housed under standard laboratory conditions can be readily modified by external factors such as exercise, cognitively enriched environments and social stress (Kempermann et al., 1997; Brown et al., 2003; Lucassen et al., 2010). In an effort to minimize this biological variability, I adopted a strategy which radiation is limited to only one hemisphere, allowing the contralateral hemisphere (SGZ) to serve as an internal control. This procedure was done with the assistance of a stereotactic image guidance system developed by Dr. Solberg's group in the Division of Radiation Physics (Song et al., 2010; Pidikiti et al., 2011). At our request, this group also custom designed, built and tested a D-shaped collimator to use with their image-guided system, allowing for irradiation of one hemisphere of the mouse brain with great accuracy (Figure 3.3a,b; see methods for details of design of collimator and use of hemi-brain radiation).

Figure 3.3

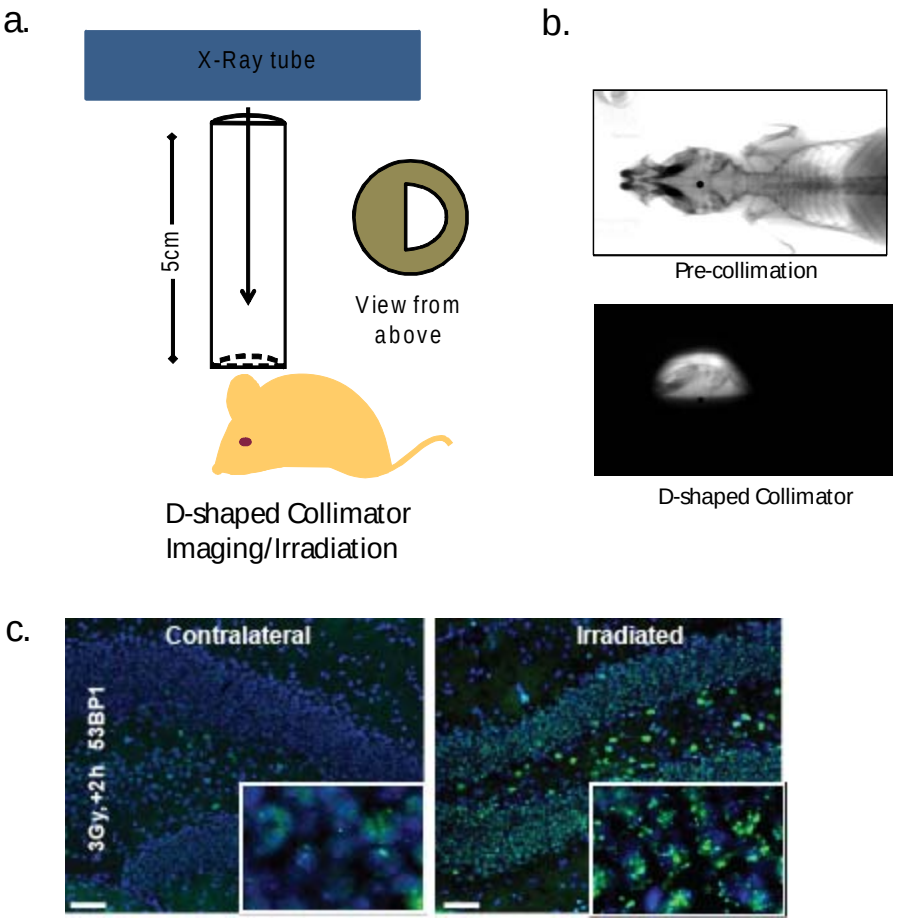

Figure 3.3. Development of a stereotactic system for mouse hemi-brain irradiation. A simplified schematic of the image-guidance irradiation set-up is shown. For details, see Song K et al., 2010 and Pidikiti et al., 2011. Mice are first anesthetized and placed in the irradiator at a distance of 5cm from the beam source **(A)**. After initial imaging **(B, top)**, the pre-collimation image is used to position the mouse so that the center of the beam (black dot) is centered in the skull. After verification of positioning with another image, a D-shaped collimator is inserted above the mouse to block all radiation outside of the D shape. To verify proper insertion, a final post-collimation image is taken **(B, bottom)**, followed by irradiation with the desired dose. **(C)** Analysis of mouse brains sacrificed shortly after irradiation. At 2h, there are robust levels of 53BP1 foci (surrogate markers for DNA DSBs) in the irradiated hemisphere, but in the contralateral (shielded) hemisphere 53BP1 is pan-nuclear, indicative of a lack of DNA damage. Scale bars 50µm.

To experimentally verify that radiation is strictly limited to one hemisphere, I analyzed the brain of a mouse that was sacrificed 2 hours after 3Gy hemi-brain radiation. Ionizing radiation causes DNA double strand breaks, which can be visualized by the formation of nuclear foci of many DNA damage proteins, including 53BP1 (Mochan et al., 2004). Immunohistochemical analysis showed that 53BP1 foci were limited entirely to the irradiated hemisphere, with no evidence of foci formation in the contralateral hemisphere (Figure 3.3c). In pilot experiments, my data also indicated that low dose radiation (3Gy) does not induce reactive gliosis. Evidence of reactive gliosis would raise the possibility that hemi-brain radiation could have unanticipated consequences on neurogenesis in the contralateral SGZ. Furthermore, Radiation 'bystander' effects are limited to cells in the vicinity of the radiation field and not likely to extend to the contralateral hemisphere (Prise and O'Sullivan, 2009). Taking these facts into consideration, it is reasonable to suggest that the biological effects were limited to the radiated hemisphere, making direct comparisons of the irradiated hemisphere to the contralateral hemisphere valid. However, this does not exclude the possibility that the contralateral hemisphere may alter baseline rates of proliferation and differentiation to compensate for any effects of radiation in the ipsilateral hemisphere. In future experiments, I will formally test the possibility that irradiating one hemisphere can induce compensatory changes in the contralateral SGZ by comparing levels of neurogenesis in age matched, sham irradiated mice with the SGZ from the shielded hemisphere of mice which were irradiated.

Dynamic analysis of how radiation affects transient amplifying progenitors and lineage committed neuroblasts

At 4-6 weeks of age, Cystatin-C CreER^{T2} Rosa26-YFP mice were treated with tamoxifen (180mg/kg, x 5 daily i.p. injections). After 2-3 weeks, one hemisphere was given a 3Gy dose of radiation, and mice were sacrificed at varying times after IR (Figure 3.4a). The initial effects were analyzed at 3 days after IR, a time point that was selected on the basis of several prior studies (Mizumatsu et al., 2003; Rola et al. 2004; Tada et al., 2000), which reported minimal proliferation recovery at 2 days post IR. Total number of YFP+ve cells and YFP+ve/Sox2+ve co-labeled cells in the shielded hemisphere were 13,924 +/- 2473 (n=4) and 6,566 (n=1), and total numbers in the irradiated hemisphere were 10,721 +/- 1919 (n=4) and 5,515 (n=1), respectively (Figure 3.4d). Surprisingly, only a small fraction of the total YFP+ve population was lost (YFP+ve cells in the irradiated hemisphere were 76.8 +/- 1.0% of the contralateral hemisphere, n=4, Figure 3.4e). The modest 16% decrease in the Sox2+ve/YFP+ve population following radiation suggests that this quiescent population is remarkably resilient to radiation (Figure 3.4e). Total numbers of actively proliferating (Ki67+ve) and Ki67+ve/YFP+ve cells in the shielded SGZ were 3,612 +/- 60 and 1,788 +/- 168, which was significantly higher compared with 408 +/- 24 (Ki67+ve) and 156 +/- 36 (Ki67+ve/YFP+ve) cells in the irradiated SGZ (n=2 for all, Figure 3.4d). Similarly, total number of DCX+ve and DCX+ve/YFP+ve cells in the shielded and irradiated SGZ were 14,456 +/- 3,362 (DCX), 6,276 +/- 2,060 (DCX/YFP) and 2,106 +/- 729 (DCX IR), 648 +/- 302 (DCX/YFP IR), respectively (n=3; Figure 3.4d). These data clearly suggest that radiation causes a marked loss of both actively proliferating (Ki67 and Ki67+ve/YFP+ve) as well as lineage

Figure 3.4

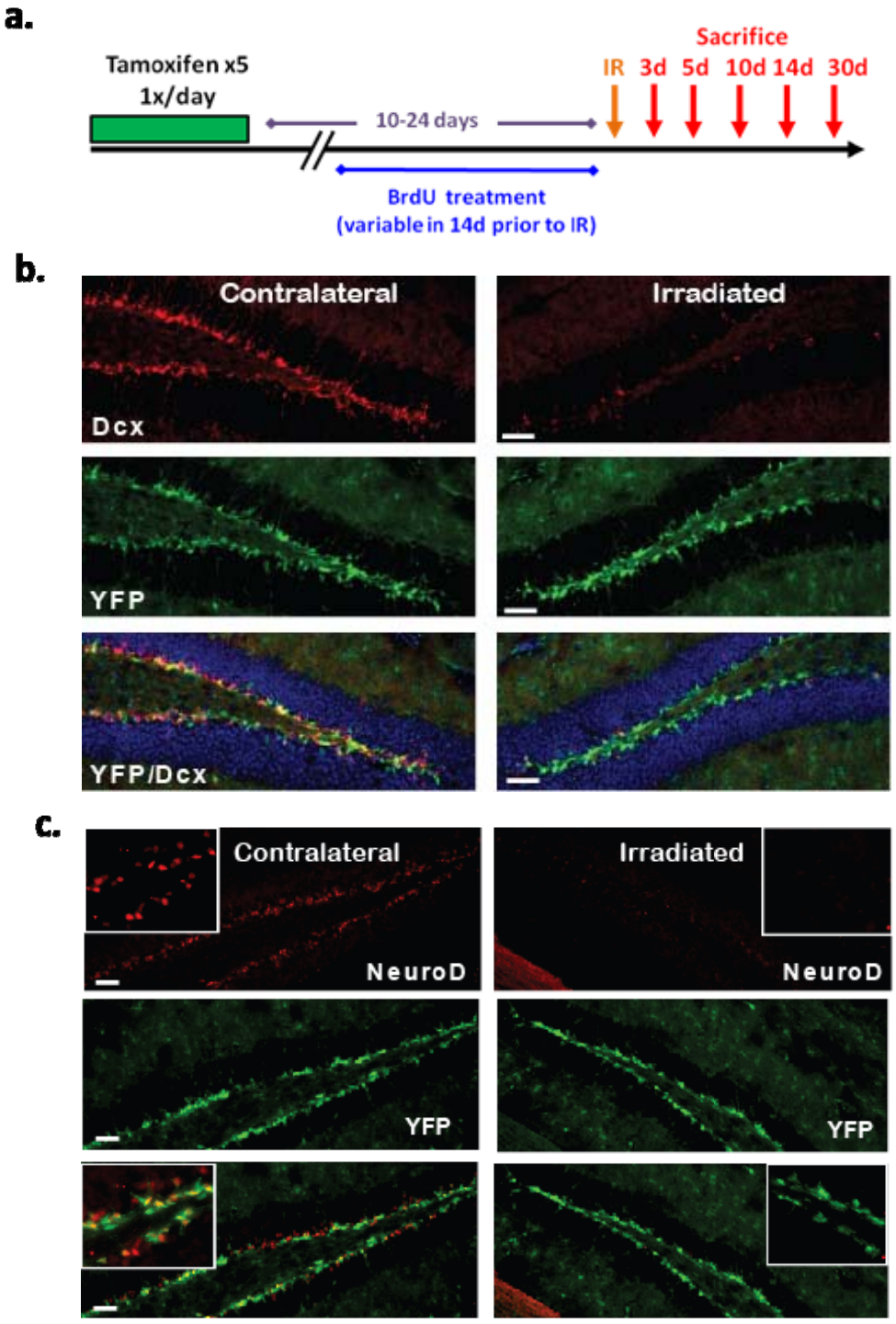
a.
Tamoxifen x5
1x/day
10-24 days
Sacrifice
IR 3d 5d 10d 14d 30d
BrdU treatment
(variable in 14d prior to IR)
b.
Contralateral
Irradiated
Dcx
YFP
YFP/Dcx
c.
Contralateral
Irradiated
NeuroD
NeuroD
YFP
YFP

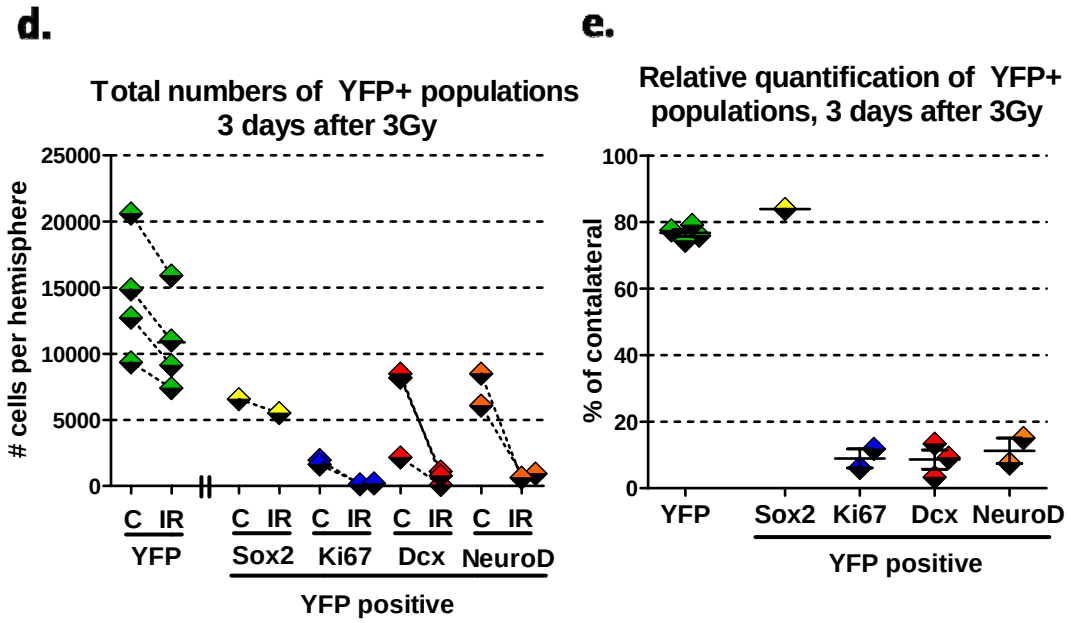

Figure 3.4 Acute effects of IR on neurogenesis in the SGZ – CstC-CreER^{T2} Rosa26-YFP mice. (A) Schematic of tamoxifen and hemi-brain IR treatment in CstC-CreER^{t2} Rosa26-YFP mice. After tamoxifen treatment at 4-6 weeks of age, mice were irradiated with 3Gy hemi-brain between 10 and 24 days after tamoxifen treatment. BrdU pulse-chase labeling was given in the two weeks prior to irradiation (optional; see Figure 3.5 and Table 3.1 for details). **(B), (C)** Representative images of Dcx/YFP **(B)** and NeuroD/YFP **(C)** immunofluorescence staining of CstC mice 3 days after hemi-brain irradiation, showing both the contralateral (shielded) and irradiated hemispheres. Scale bars 50µm. **(D)** Quantification of total YFP (n=4), Sox2/YFP (n=1), Ki67/YFP (n=2), Dcx/YFP (n=3), and NeuroD/YFP (n=2) 3 days after IR, with C = contralateral (shielded), IR = irradiated. Dotted lines connecting each point represent the paired values from a single mouse. Mean values +/- SEM per SGZ per hemisphere are as follows: YFP C 14,400+/-2,370, IR 10,900+/-1,840; Sox2/YFP C 6,570, IR 5,520; Ki67/YFP C 1,790+/-170, IR 156+/-36; Dcx/YFP C 6,280+/-2,060, IR 650+/-300; NeuroD/YFP C 7,290+/-1,200, IR 780+/-140. **(E)** Relative numbers for data plotted in (c). Values are expressed as number of cells in the irradiated hemisphere divided by the number in the contralateral hemisphere. Mean values +/- SEM are as follows: YFP 76.8+/-1.0%; Sox2/YFP 84.0%; Ki67/YFP 9.0+/-2.9%; Dcx/YFP 8.6+/-2.9%; NeuroD/YFP 11.3+/-3.8%.

committed neuroblasts (DCX+ve and DCX+ve/YFP+ve) populations by ~91% and 91.4% , respectively (Figure 3.4b, e). Radiation induced loss of Ki67+ve cells was not surprising in view of previous reports, that have reported similar findings (Mizumatsu et al., 2003; Tada et al., 2000; Abdallah et al., 2007) and knowledge that activation of a DNA damage process in cells actively replicating their DNA can readily trigger cell death. However, the almost complete loss of DCX immunoreactivity was a somewhat unexpected finding, since a significant number of DCX+ve cells are no longer actively proliferating. To ensure that this was not limited to DCX immunoreactivity, I also tested for NeuroD labeling, another marker of neuronal lineage-committed progenitors that is essential for adult neurogenesis (Gao et al., 2009). NeuroD labeled 7,286 +/-1,211 YFP+ve cells in the shielded SGZ and 774 +/- 144 YFP+ve cells on the irradiated side, representing an 89% reduction after IR (Figure 3.4c,d,e). Based on the similar and dramatic loss of DCX and NeuroD positive cells it would be reasonable to suggest that the DCX+ve/NeuroD+ve population and actively proliferating cells (Ki67) are both highly radiosensitive and undergo apoptosis. However, this seemingly logical interpretation is inconsistent with the modest loss of total YFP+ve cells in the SGZ (13,924 +/- 2,473 shielded vs. 10,721 +/- 1,919 irradiated; relative survival is 76.8 +/- 1.0%, n=4). Taken together, the Ki67+ve/YFP+ve plus DCX+ve/YFP+ve population represent approximately 50% of the total YFP+ve cells in the SGZ (Figure 3.2c). My data shows that at 3 days post IR there is almost complete (90%) loss of Ki67 and DCX expression, while total YFP loss is a modest 23.2% (Figure 3.4b,c,e). The expected loss of total YFP+ve cells in the radiated SGZ, based a simple calculation (0.9*(40-50%)) would be 36-45%, a range greater than the observed loss in YFP (23.2 +/- 1.0%). The

simplest explanation of this discrepancy is the possibility that, following genotoxic stress caused by radiation induced DNA damage, some immature neurons may markedly down-regulate DCX/NeuroD expression without activating a cell death program at the time the mice were sacrificed (3day post-radiation). Here it is important to stress that I am speculating only that the there is down-regulation of neuronal (DCX and NeuroD) lineage markers, and am in no way implying that the loss of these markers causes reprogramming to an immature, undifferentiated state.

Combination of BrdU pulse chase experiments with genetic fate-mapping

To more directly test the hypothesis that immature neurons may lose DCX/NeuroD expression following radiation, and yet remain viable, I designed a set of experiments using a BrdU pulse chase labeling strategy. Pilot studies using two BrdU pulses per day at -2 to -1 days, labeling mostly Type 2a/2b cells (based on data from Kronenberg et al., 2003) were first performed. In this experiment, qualitative assessments showed virtually no survival of the BrdU+ve cells 3 days after 3Gy, supporting the interpretation that IR kills actively dividing cells (Type2a/2b). More detailed quantitative analysis of this experiment will be completed in the future. Therefore, my next strategy was to first BrdU label actively dividing neural progenitors in the SGZ, and then allow time for these progenitors to develop into DCX+ve neuroblasts. At this point, I would irradiate and quantitatively asses how many BrdU+ve/DCX+ve cells were present in the shielded and irradiated SGZ. I designed two BrdU pulsing strategies (BrdU -1wk and BrdU -2wk), outlined in Figure 3.5a. Control experiments in 4-6 week old mice demonstrated that at the time of IR, mice given the BrdU -1wk mice had 12,200

BrdU+ve, 6,790 BrdU+ve/DCX+ve, and 3,650 BrdU+ve/Ki67+ve cells in the SGZ (n=1). Mice given the BrdU -2wk pulse showed 5,190 +/- 390 BrdU+ve (n=3), 4,370 +/- 550 BrdU+ve DCX+ve (n=3), and 36 +/-0 BrdU+ve, Ki67+ve (n=2). Thus, the BrdU -1wk pulse labeled a mixed population of Ki67+ve (26.6%) and DCX+ve (63.6%) cells at the time of irradiation, while the BrdU -2wk pulse labeled DCX+ve progenitors almost exclusively (80.1+/-2.5%, n=3) (Figure 3.5b). The latter pulse represents an ideal strategy to quantitatively assess the overall survival and protein expression of DCX+ve neuroblasts after IR.

With this information, I BrdU pulse labeled 4 CstC-CreER^{T2} Rosa26-YFP mice once per day for 7 days (-14 days to -8 days, BrdU -2wk) to IR. Two mice were sacrificed at both 3 days and 14 days after IR. In addition, 1 mouse was BrdU pulsed on days -7 to -1 (BrdU -1wk) and sacrificed 1 day after 3Gy hemi-brain IR. This experimental strategy (Figure 3.6a) allows me to assess the effect of increased maturation on radiation sensitivity. At short term intervals after IR, the relative survival of BrdU+ve cells labeled from -7 to -1 day was 24.6% for all BrdU+ve cells and 15.4% for BrdU+ve, YFP+ve cells (Figure 3.6b). For BrdU+ve cells labeled from -14 to -8 days, the survival was 45.6 +/-5.2% for all BrdU+ve and 42.5 +/-3.0% for BrdU+ve, YFP+ve cells (Figure 3.6b). This result shows that the relative survival of BrdU labeled cells increases with age, with >40% of all cells labeled in the BrdU -2wk pulse showing survival in the short term after IR. I further analyzed these populations for DCX expression. Total number of BrdU+ve and DCX+ve/BrdU+ve co-labeled cells in the shielded and radiated hemispheres from the BrdU -2wk pulse labeled mice are presented in Table 3.1. At 3 days post IR, the total number of BrdU+ve and DCX+ve/BrdU+ve cells in the

Figure 3.5

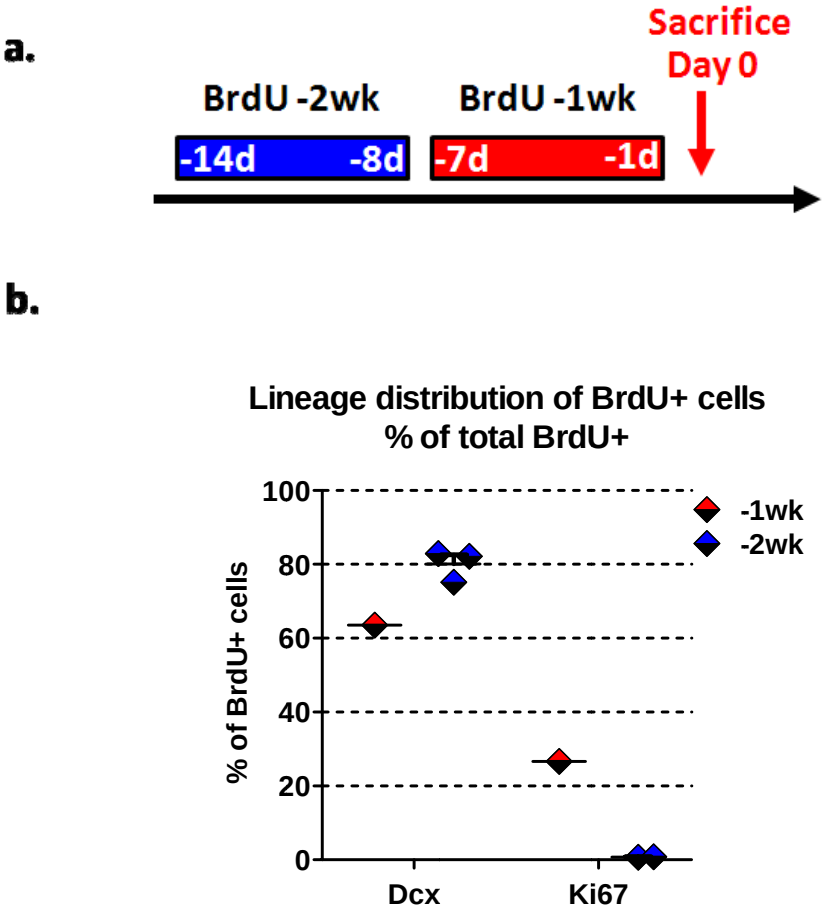

Figure 3.5. Design of BrdU pulse-chase experiments. (A) Schematic of the two BrdU labeling strategies, BrdU -2wk and BrdU -1wk. Injections were given once a day, for 7 days, either from days -14 to -8 (-2wk) or from days -7 to -1 (BrdU -1wk). Mice were sacrificed on Day 0. **(B)** Quantification of the % DCX+ve and % Ki67+ve cells in the total BrdU+ve population for each labeling strategy. Values +/- SEM are as follows. For BrdU -1wk, 63.6% of BrdU+ve cells were DCX+ve and 26.6% were Ki67+ve (n=1). For BrdU -2wk, 80.1+/-2.5% of BrdU+ cells were DCX+ve (n=3), while 0.8+/-0.06% were Ki67+ve. Raw counts +/- SEM for the entire SGZ (both hemispheres) are as follows. Values for BrdU -1wk are 12,200 BrdU+ve, 6,790 BrdU+ve DCX+ve, and 3,650 BrdU+ve Ki67+ve (n=1). Mean values +/- SEM for BrdU -2wk are 5,190+/-390 BrdU+ve (n=3), 4,370+/-550 BrdU+ve/DCX+ve (n=3), and 36+/-0 BrdU+ve/Ki67+ve (n=2).

contralateral hemisphere were 2,705 +/- 425 and 2,169 +/- 153 (identical to sham IR, expressed per hemisphere), while the irradiated hemisphere showed 1,203 +/- 63 BrdU+ve and 414 +/- 42 BrdU+ve/DCX+ve (n=2). The percent of total BrdU that was DCX positive was 81.3 +/-7.1% in the contralateral hemisphere and 34.7 +/- 5.3% in the irradiated hemisphere. At +14 days, number of BrdU+ve and DCX+ve/BrdU+ve cells in the contralateral hemisphere were 854 +/- 100 and 306 +/- 78, while the irradiated hemisphere showed 288 +/- 28 BrdU+ve and 6 +/- 6 BrdU+ve/DCX+ve (n=2). The percent of total BrdU that was DCX positive was 32.1 +/-5.1% in the contralateral hemisphere and 2.6 +/- 2.6% in the irradiated hemisphere.

Overall, the data shows reductions in the DCX positive fraction of total BrdU+ve at both 3days and 14days post-radiation, providing preliminary evidence that immature neurons can lose neuronal lineage marker expression following radiation induced DNA damage. Future experiments to increase the number of mice used and decrease the SEM are necessary to strengthen this data. Most importantly, surviving BrdU labeled cells at 14 days post IR showed no evidence of recovery of DCX expression to levels seen in the contralateral shielded SGZ. This further suggests that the potential loss of DCX expression is not a transient, reversible process within the time frame of these experiments. To rule out the possibility that radiation-induced DNA damage caused neuronal progenitors to undergo an aberrant default differentiation into an astrocyte lineage, I examined the number of S100β/BrdU co-labeled cells (GFAP/BrdU co-labeling is being assessed in on-going experiments). The number of BrdU+ve/S100β+ve cells in the shielded and irradiated hemispheres was not significantly different. Therefore, IR does not appear to cause a change in fate commitment. All raw

Figure 3.6

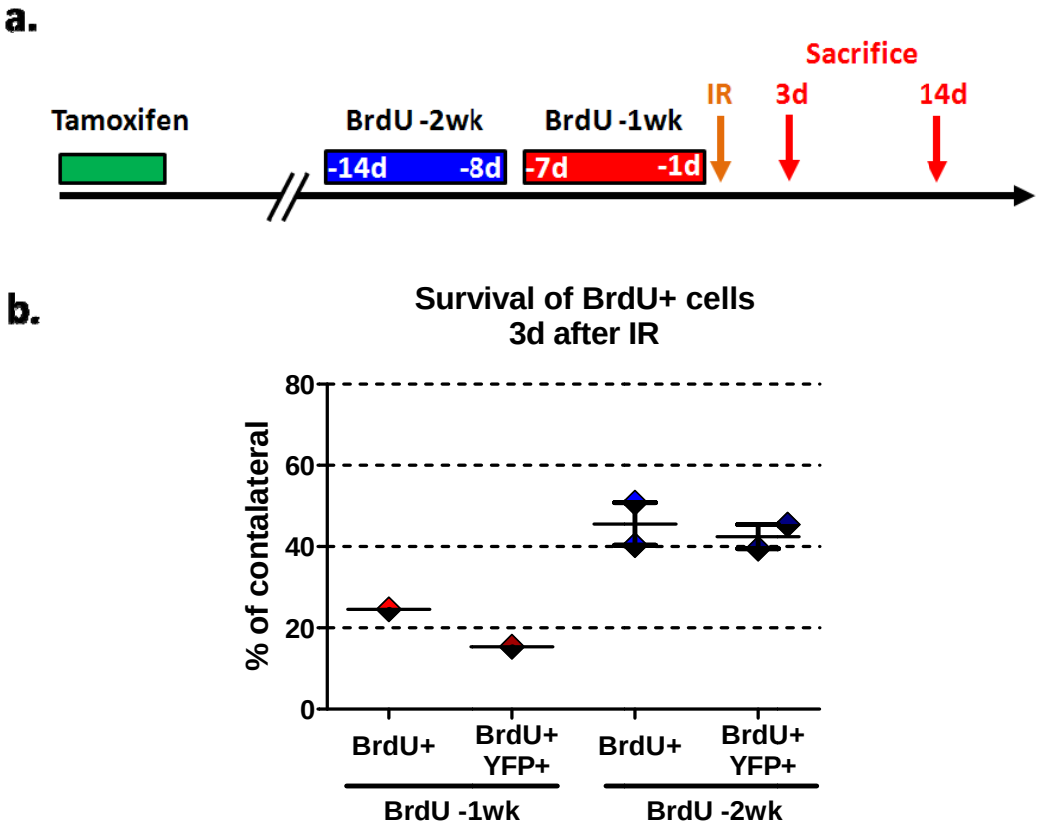

Figure 3.6 Combination of BrdU pulse labeling strategies and IR. (A) Schematic showing the tamoxifen treatment and BrdU labeling strategies for CstC-CreER^{T2} Rosa26-YFP mice. The "BrdU -2wk" pulse refers to BrdU injections on days -14 to -8 (Day 0 = 3Gy IR), while the "BrdU -1wk" pulse refers to BrdU injections on days -7 to -1. Time between tamoxifen and BrdU was at least 10 days. **(B)** Relative survival of BrdU labeled cells short term after 3Gy hemi-brain IR. Values for BrdU -1wk (sacrificed at +1d) are 24.6% for BrdU+ve total and 15.4% for BrdU+ve/YFP+ve cells (n=1). Values for BrdU -3wk (sacrificed at +3d) are 45.6 +/-5.2% for BrdU+ve total and 42.5 +/-3.0% for BrdU+ve/YFP+ve cells (n=2). This data indicates that survival increases as BrdU labeled cells become more mature. Raw numbers per hemisphere are as follows: BrdU -1wk – shielded BrdU+ve 2,784, BrdU+/YFP+ve 780; IR BrdU+ve 684, BrdU+/YFP+ve 120, n=1. BrdU -2wk shielded BrdU+ve 2,705 +/- 425, BrdU+/YFP+ve 654 +/- 258; IR BrdU+ve 1,203 +/- 63, BrdU+/YFP+ve 270 +/- 90 (n=2).

data is presented in Table 3.1. Thus, the irradiated BrdU+ve progenitors do not appear to be actively undergoing neurogenesis at 14d post IR. Future experiments will investigate integration rates for BrdU-labeled cells and co-labeling of BrdU with NeuN, calretinin, and calbindin.

Quiescent progenitors are resistant to low-dose radiation and drive neurogenesis recovery

It is well known that neurogenesis in the adult hippocampus can fully recover following low-dose radiation (Mizumatsu et al., 2003; Tada et al., 2000; Abdallah et al., 2007). However, what is not clear, is whether the recovery of first proliferation followed by reemergence of immature neurons is mediated by a minor population of proliferating

Table 3.1

	Sacrificed at 0d	Sacrificed 3 days post IR		Sacrificed 14 days post IR	
	Mock IR	Shielded	Irradiated	Shielded	Irradiated
Dcx+ BrdU+	2,085 +/- 211	2,169 +/- 153	414 +/- 42	306 +/- 78	6 +/- 6
BrdU+	2,593 +/- 195	2,705 +/- 425	1,203 +/- 63	854 +/- 100	288 +/- 28
Dcx+ Percent of BrdU	80.1+/-2.5%	81.3 +/- 7.1%	34.7 +/- 5.3%	32.1 +/-5.1%	2.6 +/- 2.6%
S100β+ BrdU+	no data	no data	no data	72 +/- 48	60 +/- 36
Number of animals	n=3	n = 2	n = 2	n = 2	n = 2

Table 3.1. Results of BrdU pulse-chase labeling strategies. Raw numbers for all data derived from BrdU pulse-chase experiments described in Figure 3.5, normalized at total counts per SGZ per hemisphere. Both total numbers of DCX+ve/BrdU+ve and the DCX+ve % of the total BrdU+ve cells are reduced relative to the shielded hemisphere at 3 days and 14 days after IR. There is no change of S100β+/BrdU+ cells at 14 days.

progenitors that escape cell death, dedifferentiation of more mature lineage committed progenitors that re-establish an undifferentiated hierarchy, or the results of activation of quiescent (Type I) stem cells that respond to reestablish normal homeostasis. To distinguish between these possibilities, I used the CstC-CreER^{T2} Rosa26-YFP transgenic model. At 4-6 weeks of age, Cst-C CreER^{T2} Rosa26-YFP mice were treated with tamoxifen (standard dose, x 5 daily i.p. injections). After 2-3 weeks, one hemisphere was given a 3Gy dose of radiation and sacrificed at varying times after IR, ranging from 3 days to 1 month. As discussed earlier, the number of YFP+ve/Sox2+ve cells in the shielded and irradiated SGZ were similar, suggesting that radiation has a minor impact on the quiescent (Type 1) stem cell population. This contrasted sharply with the Ki67+ve/YFP+ve and DCX+ve/YFP+ve cells, which were almost completely gone in the radiated hemisphere after IR. The Ki67 immunolabeling was the first to recover, reaching peak values at 10 days after IR and dropping slightly at 14 days. The total number of Ki67+ve cells and Ki67+veYFP+ve cells at 10d was 3,570 +/- 606 and 1,176 +/-144 in the shielded hemisphere and 4,038 +/- 654 and 1,380 +/- 432 in the irradiated side (Figure 3.6a, c). Levels of DCX recovered at a slower pace, showing only partial recovery by 14 days after IR. The total number of DCX+ve cells and DCX+ve/YFP+ve cells at 14d was 11,788 +/- 1,448 and 4,766 +/- 1,005 in the shielded hemisphere and5,640 +/- 391 and 2,504 +/- 672 in the irradiated hemisphere (Figure 3.6b, d). By 1 month after IR, recovery of DCX+ve and DCX +/YFP+ve cells reaches its peak recovery, showing 71.8 +/- 8.6% and 77.0 +/- 18.2% of the contralateral hemisphere (10,407 +/- 5,001 contralateral; 7,071 +/- 1,893 irradiated DCX+ve/YFP+ve, n=2, Figure 3.6b,d). This temporal pattern of neurogenesis recovery is consistent with a model in which a

Figure 3.7

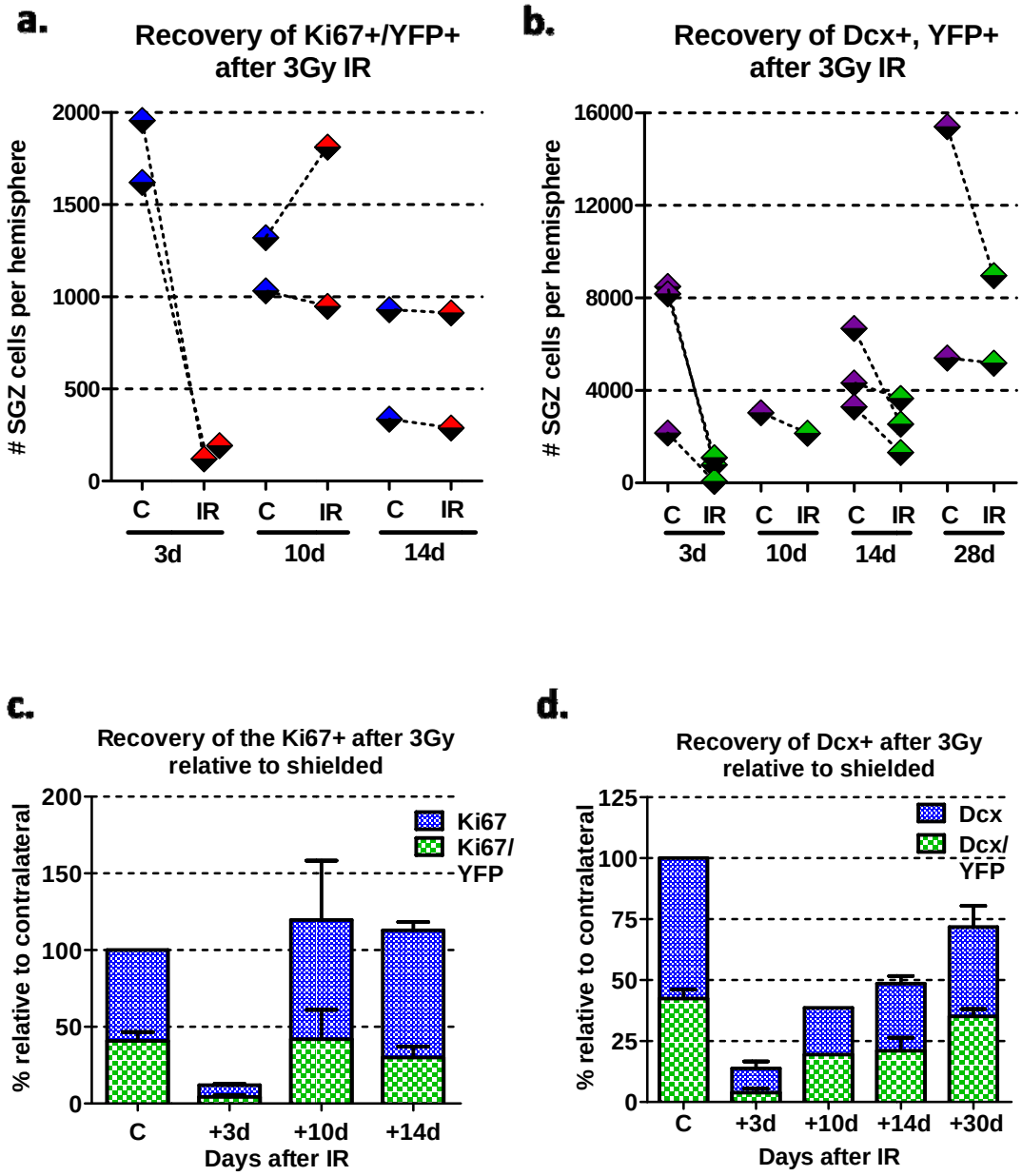
a.
Recovery of Ki67+/YFP+ after 3Gy IR
SGZ cells per hemisphere
2000
1500
1000
500
0
C IR C IR C IR
3d 10d 14d
b.
Recovery of Dcx+, YFP+ after 3Gy IR
SGZ cells per hemisphere
16000
12000
8000
4000
0
C IR C IR C IR C IR
3d 10d 14d 28d
c.
Recovery of the Ki67+ after 3Gy relative to shielded
% relative to contralateral
200
150
100
50
0
Ki67
Ki67/ YFP
C +3d +10d +14d
Days after IR
d.
Recovery of Dcx+ after 3Gy relative to shielded
% relative to contralateral
125
100
75
50
25
0
Dcx
Dcx/ YFP
C +3d +10d +14d +30d
Days after IR

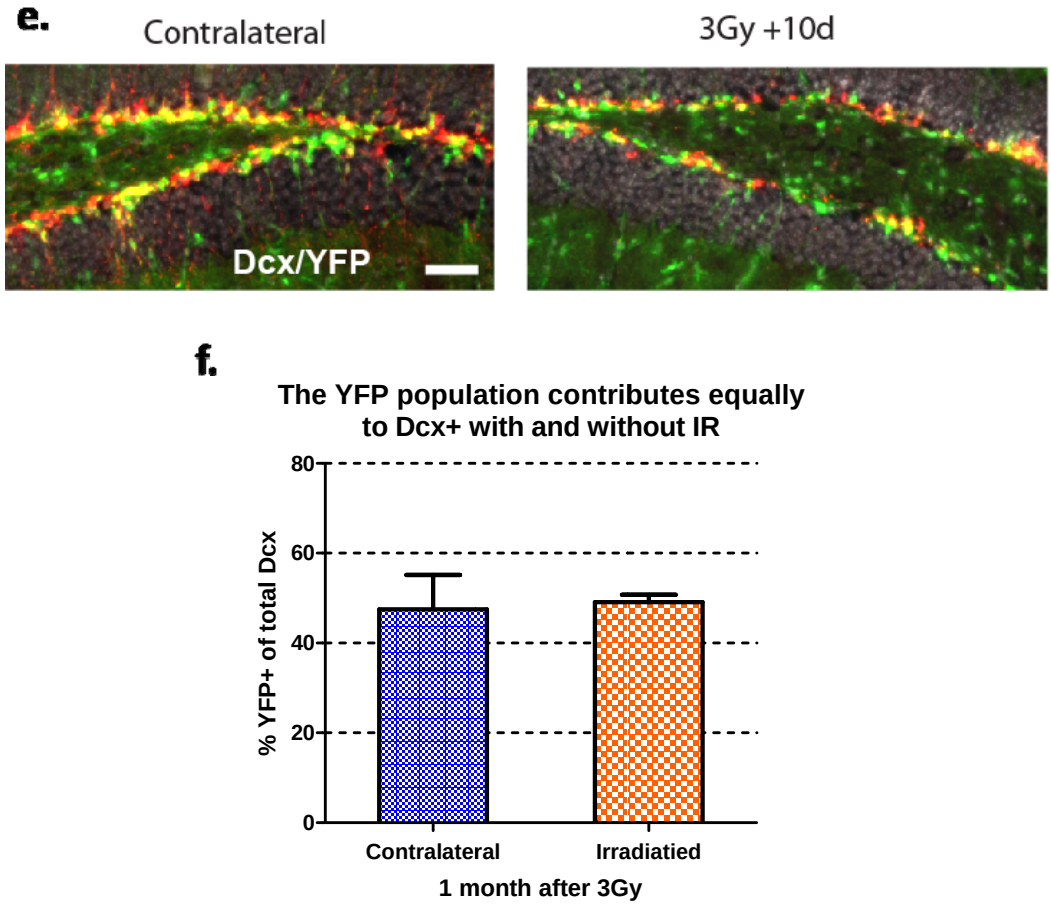

Figure 3.7. Recovery in CstC-CreER^{T2} Rosa26-YFP mice is partially derived from a pre-labeled YFP-positive compartment. (A) Quantification of Ki67 recovery over time, shown as raw numbers from the contralateral (C) and irradiated (IR) hemispheres. Dotted lines connect the counts from the each hemisphere of the same mouse. Mean values +/- SEM are as follows: 3d C 1,790 +/-170, IR 156 +/- 36; 10d C 1,176 +/- 144, IR 1,380 +/- 432; 14d C 633 +/- 297, IR 600 +/- 312 (n=2 for all). **(B)** Same plot as in **(A)**, except for Dcx recovery. Mean values +/- SEM are as follows: 3d C 6,280+/-2,060, IR 650 +/- 300 (n=3); 10d C 3,036, IR 2,148 (n=1); 14d C 4,770 +/- 1,010, IR 2,500 +/- 672 (n=2); 30d C 10,400 +/- 5,000, IR 7,070 +/-1,890 (n=2). **(C), (D)** Data from **(A)** and **(B)**, plotted as values relative to each contralateral (shielded) hemisphere. **(E)** Pictures of a 3Gy hemi-brain irradiated mouse brain sacrificed 10 days after IR. Note that there is partial recovery of Dcx (red) and YFP (green), and that populations of YFP+ Dcx+ and YFP- Dcx+ exist. Scale bars 50µm. **(F)** Quantification of the YFP+ fraction of the total Dcx in the irradiated and contralateral hemispheres at 1 month post irradiation (n=2). Mean values +/- SEM are 47.5 +/- 7.7%, n=2 for the contralateral hemisphere and 49.1 +/- 1.7%, n=2 for the irradiated hemisphere.

quiescent stem cell is mobilized to replace lost progenitors. In this scenario, one would expect to see DCX lag behind Ki67, as the quiescent stem cell first produces a transient amplifying (rapidly proliferating) population, which expands and then exits the cell cycle to produce immature neurons. Another interesting note is that the YFP positive and YFP negative progenitors show similar kinetics of recovery (Figure 3.6c, d, e). In fact, the percent of the DCX population that is YFP positive is virtually identical in the shielded and irradiated hemispheres at 30 days post IR (49.5 +/-5.5% contralateral and 46.5 +/- 4.5% irradiated, n=2; Figure 3.6f). This data describing the dynamic recovery of neurogenesis supports the idea that the CystatinC-CreER^{T2} mouse model labels a representative sub-population of approximately half of the adult neural stem cells in SGZ.

Quiescent progenitors are resistant to high-dose irradiation

Recovery mediated by a quiescent population suggests that non-dividing stem-like cells have inherent resistance to radiation, even in the absence of any key genetic lesions. To test whether this resistance is dose-dependent, CstC-CreER^{T2} mice were tamoxifen treated and hemi-brain irradiated with 10Gy. At this dose, it has been reported that permanent deficits in neurogenesis are seen, as marked by minimal recovery of proliferation and differentiation (Monje et al., 2002; Mizumatsu et al., 2003; Fike et al., 2009). This decrease in neurogenesis may be due to cell intrinsic factors (killing of the quiescent population) or due to cell extrinsic factors (disruption of the NSC niche). Intriguingly, preliminary data indicates that increasing the dose did not result in significant additional killing of the YFP+ve cells at three days post IR (Figure 3.9a).

Figure 3.8

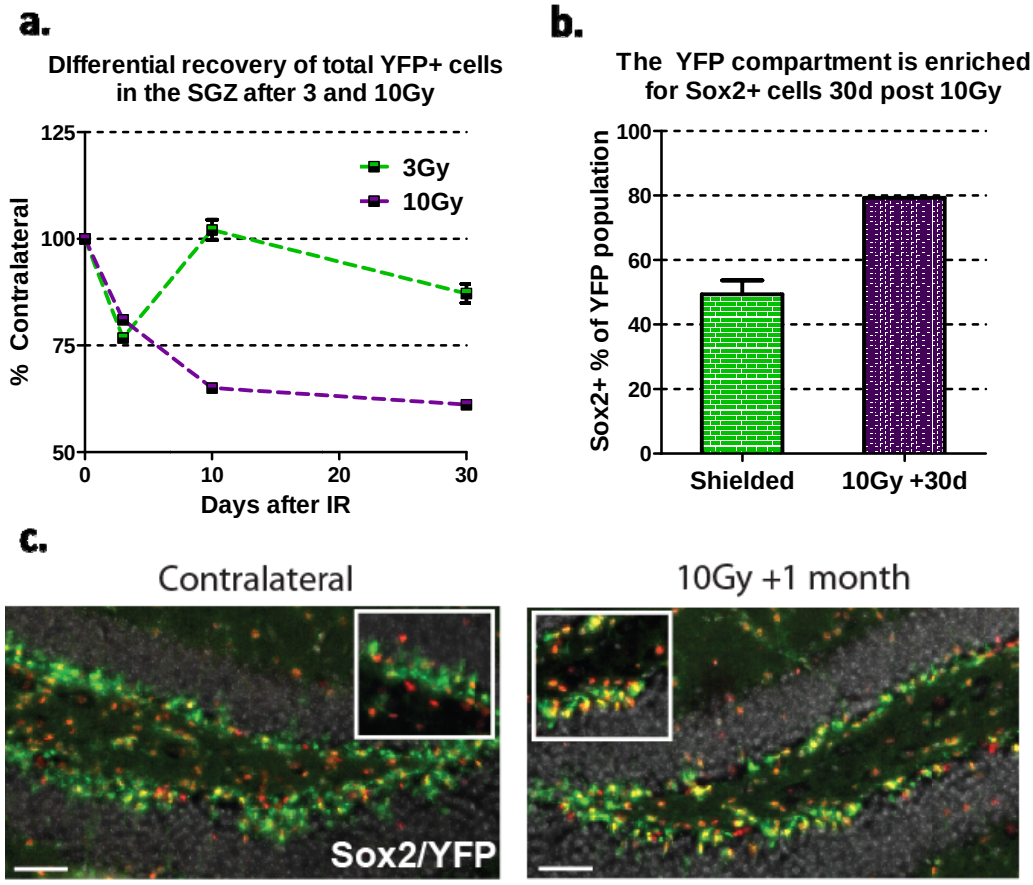

Figure 3.8. Quiescent progenitors show resistance to high dose IR. (A) Quantification of total YFP positive progenitors in the SGZ of mice treated with 3Gy or 10Gy hemi-brain IR, expressed relative to the contralateral hemisphere. For 3Gy – 3d 76.8 +/- 1.0%, n=4; 10d 102.1 +/- 2.4%, n=2; 30d 87.2 +/- 2.2%, n=2. For 10Gy, 3d 81.0%, 10d 65.0%, and 30d 61.1%, n=1 for all. At +30 days, raw numbers for YFP+ve cells are: 3Gy shielded 22,200 +/- 8,060, IR'd 19,200 +/- 6,540, n=2; 10Gy shielded 13,500, IR'd 8,220, n=1. **(B)** Quantification of the Sox2 positive fraction of the total YFP positive cells in the SGZ. The Sox2+/YFP+ve population comprises 49.9 +/- 3.8% (n=2) of the total YFP in shielded hemispheres, while the Sox2+/YFP+ve population comprises 79.3% of the total YFP population 30 days after 10Gy (n=1). **(C)** Images showing Sox2 (red) and YFP (green) co-labeling in the 10Gy hemi-brain irradiated mouse sacrificed at 30 days post IR. Note the increase in co-labeling (yellow) in the irradiated SGZ relative to contralateral. Scale bars 50μm.

Furthermore, after 10Gy the number of YFP+ve cells did not increase and continued to decay over time, relative to the contralateral hemisphere. If the quiescent population was resistant to IR, then one would expect the YFP+ve cells to be enriched for Sox2+ve immunolabeling. Therefore, I quantified the % of the YFP+ve cells that expressed Sox2 1 month after 10Gy. Preliminary data shows that 79.3% (n=1) of the remaining YFP positive cells in the irradiated hemisphere co-express Sox2, representing a large increase from control levels of ~49.4% (n=2). While this preliminary experiment is underpowered and does not directly address the differentiation capacity of these NSC, it does suggest that the inherent resistance to cell death is maintained at higher doses that suppress neurogenesis. This result has interesting implications, as it suggests that one of the major determinants of radiation resistance in the progenitor population is quiescence.

3.3 Discussion

In addition to characterizing the relationship between differentiation status and radiation sensitivity, another goal of this project was to further characterize the dynamics of adult neural stem cell proliferation/differentiation in the SGZ. In this chapter, I have used radiation to perturb normal homeostasis, and then analyzed the recovery phase in an attempt to gain insight into how homeostasis is maintained in this niche. My results indicate that low dose radiation disrupts the differentiation process for all proliferating and early post-mitotic progenitors, but does not impact the survival of the quiescent NSC population. In addition, data from this chapter suggests that radiation may lead to a suppression of fate commitment in immature neuroblasts that does not immediately coincide with radiation-induced death (summarized in Figure 3.9).

Regardless of whether this phenotype is occurring, my data suggests that radiation is significantly impairing the ability of immature neuroblasts to differentiate into functional neurons (based on Table 3.1, +14d, lack of Dcx/BrdU in the irradiated hemisphere). One key prediction is that radiation would cause decreases in the number of pre-labeled BrdU+ve cells that form NeuN+ve neurons in the granule layer of the dentate gyrus. This experiment is currently underway.

Current data from this project is not definitive regarding the radiation responses of each progenitor type. There are several potential areas that I can improve upon. Because my data relies on relative measurements between shielded and irradiated hemispheres, adequate unirradiated controls are absolutely necessary in order to rule out any unintended effects of radiation to the contralateral hemisphere. These effects could increase or decrease total neurogenesis in the contralateral side, providing altered numbers of YFP+ve, DCX+ve, Ki67+ve etc. Thus, the comparisons between hemispheres may not be completely valid, as relative data (e.g. 23% loss in YFP 3d after IR) may be based on inaccurate assumptions (i.e. contralateral = completely unirradiated).

Increased numbers of animals and further characterization of existing data sets are also necessary to strengthen my data, specifically with respect to the proposed downregulation of DCX/NeuroD proteins and survival of immature neurons (as opposed to radiation-induced cell death). To reiterate, based on >90% loss of Ki67 and Dcx expression in the YFP population after 3Gy (normally 50% of all YFP+ve cells), I would expect to see a 36-45% loss of total YFP+ve cells due to radiation-induced cell death. This is different than the observed loss of only 23% of total YFP+ve cells. Thus, at least

Figure 3.9

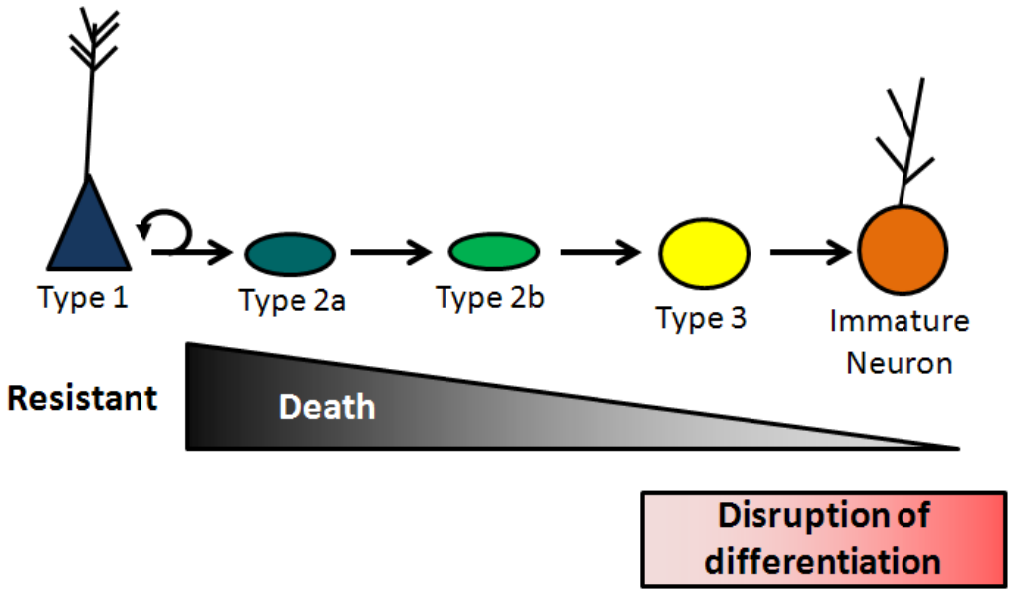

Figure 3.9. Summary of IR effects on differrent stages of differentiation in the SGZ. After 3Gy IR, the Type I cells are resistant to radiation-induced cell death (Sox2 #s, Figure 3.4, 3.8). Data from the total YFP+ve population and from BrdU pulse-chase strategies indicates that there are both surviving and dying populations of differentiating cells (Type 2a to immature neurons) (Figure 3.4, 3.6). The extent of cell killing decreases as the BrdU labeled population matures, indicating that the surviving cells are most likely enriched for Type 3 cells and immature neurons (Figure 3.6). Furthermore, irradiated populations show loss of DCX and NeuroD in the short term (Figure 3.4) and virtually no DCX co-labeling 14 days after IR (Table 3.1), suggesting that the differentiation capacity of surviving cells may be disrupted. This may promote faster rates of death in the BrdU labeled population. Overall, it appears that radiation likely prevents completion of differentiation in all non-Type 1 progenitors.

some of the YFP+, Ki67+ve and/or YFP+/DCX+ve cells must be resistant to radiation-induced apoptosis. I have favored the interpretation that the immature neuroblasts are the likely cells that survive, based on BrdU pulse-chase labeling strategies (Figure 3.6, Table 3.1) that show increased survival as the BrdU+ population becomes more mature at the time of irradiation. However, this does not exclude the possibility that proliferating Type 2 cells also survive and downregulate Ki67 due to cell cycle arrest. This interpretation is not common in the field, as most reports speculate that proliferating cells are the most sensitive (Tada et al., 2000; Mizumatsu et al., 2003; Rola et al., 2004). This is based upon data regarding the dose-dependence of total apoptosis and dose-dependence of Ki67 and DCX loss. Reports show that there is a sharp rise in apoptosis after treatment with 0 to 2Gy IR (assayed 12h after IR), which then levels off to have a slower rise as the dose increases to 10Gy (Tada et.al, 2000; Mizumatsu et al., 2003). This initial sharp rise in apoptosis correlates highly with the loss of Ki67, which is almost complete after 2Gy (assayed at 48hr after IR). Some DCX expression is lost at 2 Gy, but it is only partial, and higher doses can slightly increase further Dcx loss (Mizumatsu et al., 2003; Rola et al., 2004). Thus, while this is merely a correlative relationship, the interpretation is that proliferating cells are the most sensitive, while Dcx cells can persist (though no one has directly assessed the differentiation capacity of this population). To date, no one has utilized any fate-mapping strategies or pulse-chase labeling before IR to prove this interpretation, as has been shown in this thesis. The use of the better BrdU pulse-chase strategies (similar to Figures 3.5, 3.6) can directly address this question. By refining this strategy (using fewer injections over shorter time frames), a more defined population can be labeled and then assayed for radiation sensitivity. A final approach to complement

previous data would be to perform a more detailed analysis of morphology (using the CstC-CreER^{T2} Rosa26-YFP mouse) and other immunohistochemical markers in the surviving population. The characteristics of Type 2a, 2b, 3 cells and immature neurons have been worked out extensively (see Kempermann et al., 2004; von Bohlen und Halbach 2011).

Data presented in this chapter also provides more insight into radiation-induced suppression of neurogenesis. Previous work by multiple groups has shown that high dose radiation is sufficient to lower baseline proliferation rates in the adult hippocampus and significantly impair the formation of new neurons (Monje et al., 2002; Mizumatsu et al., 2003; Rola et al., 2004). This phenotype could be due to killing of quiescent stem cell population or simply suppression of neurogenesis through modifications to the niche and/or the quiescent stem cells themselves. In one study, it was demonstrated that progenitor cells from irradiated hippocampus are capable of neuronal differentiation in culture, suggesting irradiated stem cells retain their differentiation potential (though the spectrum of lineages was altered). They additionally showed that neurogenesis can be partially restored (3 fold increase in BrdU+ve/NeuN+ve neurons) by inhibiting the inflammatory response with indomethacin (Monje et al., 2003). While this experiment suggested that the quiescent population retains its ability to differentiate, the relative proportions of this population that survive radiation treatment were unknown. Here, data using novel Cre-ER^{T2} mice demonstrates that the majority of Sox2+ve/YFP+ve quiescent progenitors persist even up to 1 month post irradiation, indicating that suppression of neurogenesis after ionizing radiation is not due to depletion of stem cells, but may be due to altered programming or an altered NSC niche.

Based on the data presented, I propose a niche occupancy model to describe the regulation of homeostasis in adult neurogenesis, as shown in Figure 3.10. After IR, all cells undergoing differentiation are disrupted (both proliferating and post-mitotic), with a sizable portion (25%) dying within the first 72 hours (Figure 3.10, faded Type 2a/b and Type 3 cells). As a result, the quiescent stem cell pool is activated and mobilized to enter the cell cycle and replenish the niche. Based on this prediction, I would expect to see proliferating Type I cells after IR. Therefore, I plan to compare the numbers of proliferating Type I cells (by quantifying co-labeling Ki67 with Sox2, GFAP, or nestin) both before and after radiation. There are two possibilities for how this mobilization may occur. First, there may be one or multiple negative feedback loops between the quiescent stem cell and both the proliferating and post mitotic stem cell populations. This feedback would regulate the number of quiescent stem cells that actively produce transient amplifying progeny. In this scenario, one would expect that the acute loss of ~50% of the differentiating progenitors would lift a strong negative feedback on the quiescent population, resulting in a significant increase in the number of proliferating Type I cells after IR (analysis pending). This would likely also result in total proliferation levels that significantly exceed the baseline levels. However, my data does not show proliferation levels that drastically exceed normal steady state. Similar kinetics have been observed in other reports for the SGZ (Tada et al., 2000; Abdallah et al., 2007), and several reports for the SVZ (Amano et al., 2002; Tada et al., 1999). A second possibility is that mobilization of the quiescent stem cell may be governed primarily by signals between the stem cell and the niche, as has been shown in drosophila (Kai and Spradling, 2003), such that the empty niche can both activate the quiescent cell and limit the number of

Figure 3.10

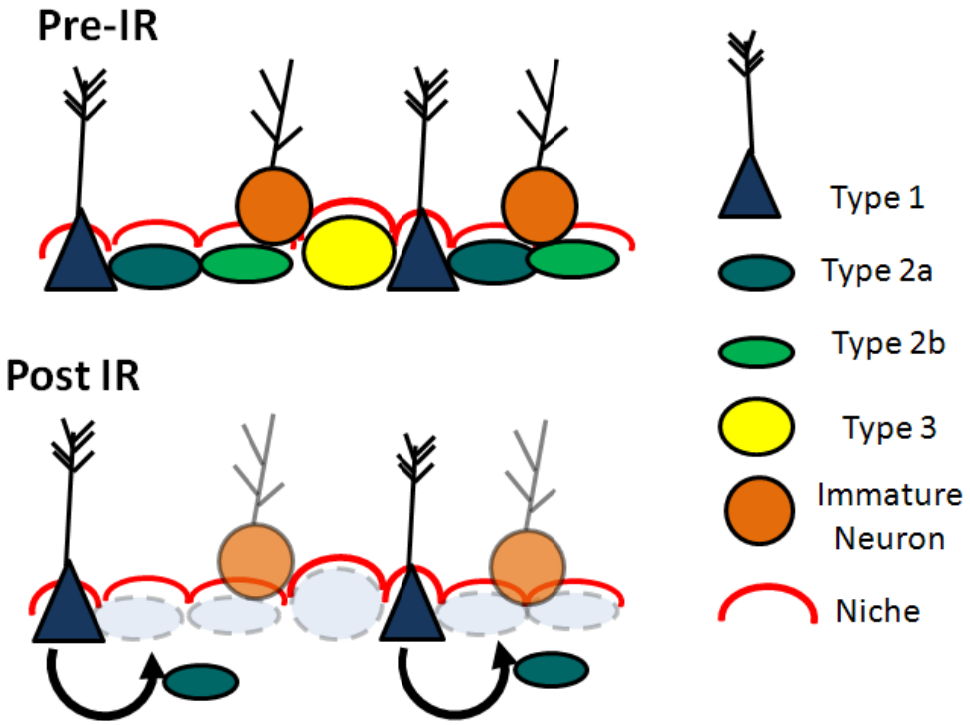

Figure 3.10. A niche occupancy model for maintenance of adult stem cell homeostasis. At steady-state, the stem cell niche is occupied by proliferating progenitors and lineage committed immature neurons. An occupied niche provides a negative feedback signal to the quiescent stem cells, preventing asymmetric division and maintaining quiescence. After ionizing radiation, the niche has been vacated by 2-3 days after IR (faded Type 2 and 3 cells), as the differentiating cells undergo cell death or are have differentiation disrupted (then resulting in accelerated death). This vacated niche can now be taken over by the quiescent population, which is mobilized and begins to produce transient amplifying progeny (new Type 2a, near arrow). The size of the niche is the limiting factor in determining the number of quiescent stem cells that are mobilized.

quiescent cells that enter the cell cycle. In this model, the number of transient amplifying clones produced is tightly controlled by the microenvironment, preventing an overpopulation of progenitors. This model would also predict that another mechanism must exist to replenish the steady-state levels of the DCX+ve, NeuroD+ve compartment. It is thought that the majority of immature neurons do not survive the differentiation process, and there are presumably stages at which these neuroblasts or immature neurons will undergo apoptosis naturally. Therefore, one possible mechanism to replenish this compartment would be to inhibit cell death/increase survival of newly generated neuroblasts. This mechanism may be plausible, as another group has demonstrated that irradiated mice actually show fewer pyknotic cells than sham irradiated mice 1 week after IR in the SGZ (Abdallah et al., 2007). This timing directly coincides with the re-emergence of new DCX+ve cells in the SGZ in my data.

To validate this model, further experiments can be performed using other perturbation methods that target only the dividing population (sparing post-mitotic cells), such as the DNA alkylating agent temozolomide, resulting in a smaller loss of progenitors in the niche. If the overall kinetics of proliferation recovery match the rate seen after IR, then this result would support a model in which rate of proliferation recovery does not depend on the extent of cell death. However, if the rate of proliferation recovery is much slower, then this result would suggest that there are feedback mechanisms between the post-mitotic progenitors and the quiescent population.

3.4 Methods

Mice

Mice used in this study were housed in the NG facility under a 12hr night/day cycle. The background for all strains is a mix between C57/B6 and FVB. The CystatinC-CreER^{T2} mouse line was developed in the Bachoo lab, as described in the thesis of Lori Boies. The Rosa26-lox stop lox YFP reporter mouse was reported in Srinivas et al., 2001. Initial work describing the inducible Cre-ER^{T2} recombinase is found in Feil et al., 1997.

Tamoxifen treatment

Tamoxifen (Sigma) was prepared fresh daily in a 30mg/ml stock according to the following protocol. Thirty milligrams of tamoxifen was weighed in a 1.5ml Eppendorf tube, after which 100µL of 200 proof ethanol (AAPER) was added and the tube was vortexed for 15-30 seconds. Then, 900µL of sunflower seed oil (Sigma) was added to the tube, it was vortexed for 15-30seconds, and then the mixture was sonicated for 2 x 5 minutes in a water bath to dissolve (while protected from light). Tamoxifen was then injected the same day, at a 180mg/kg dose by intraperitoneal injection. All mice in this study were given the standard tamoxifen regimen of 5 injections, once per day on consecutive days at 4-6 weeks of age.

BrdU Injections

For all BrdU injections, a 10mg/ml stock was dissolved in PBS before injection, and was stored at 4C while protected from light for up to 1 day. Mice were given intraperitoneal injections of 100mg/kg at the indicated times.

Hemi-brain irradiations

The stereotactic imaging system has been described in detail in Song et al., 2010 and Pidikiti et al., 2011. This system consists of a few basic steps – imaging, localization, and collimation/irradiation. Mice are first anesthetized using isoflurane, and remain under anesthesia for the remainder of the irradiation procedure (~6-10 minutes). The mouse is placed on a movable platform, and an X-ray image is taken to determine the initial position of the mouse. Once an initial position is established, the user then use the image guidance system to shift the center of the beam its desired location In this case, the center of the beam is near the center of the skull. Correct positioning is verified by taking another X-ray image of the mouse. A specially designed D-shaped collimator is then inserted, serving to block all radiation except in a semicircular region, thus allowing for 1 hemisphere of the brain to be irradiated. A final image is acquired to precisely identify the extent of irradiation, and then the mouse is irradiated with the given dose. During irradiation, mice were anesthetized using 1.5% isoflurane. The top of the mouse's head was positioned at 5cm below the X-ray source. Initial X-ray images for positioning purposed were obtained using 30kV, 5mA with an exposure time of ~5-10 seconds. For full dosing, the settings were 250kV, 5mA, and 0.7 minutes for ~3.2Gy and 250kV, 15mA, and 0.7 minutes for ~9.5Gy.

Avertin

The Avertin 40X stock is 40mg/ml, dissolved in tert-amyl alcohol; 1x working solution was made by diluting the 40X stock in PBS, while rotating overnight at 4C. Working stock was kept for 1 month while wrapped in foil to protect it from light.

Sacrifice/Tissue processing

At the time of sacrifice, mice were anesthetized with a working solution of Avertin until non-responsive to toe pinching. After opening the chest cavity, mice were then transcardially perfused with 10ml cold PBS followed by 10ml cold 4% paraformaldehyde, pH 7.4. Brains were removed and post-fixed overnight at 4 degrees C in 4% paraformaldehyde. After post-fixation, brains were moved to PBS and stored at 4 degrees Celsius. For cryosectioning, brains were moved to 30% sucrose in PBS at 4 degrees C for at least 36 hours (until the brain sank). Prior to embedding in OCT medium, the unirradiated hemisphere of any hemi-brain irradiated brains was marked with tissue marking dye. Brains were then embedded in OCT and frozen on dry ice. Coronal 30 micron sections were cut on the Leica 3050S model cryostat at -20 degrees Celsius and stored in PBS + .05% sodium azide. Sections were collected serially in 12 well plates, with each well containing $1/12^{th}$ of the entire brain (or in 96 well plates, with 1 section/well).

Immunofluorescence

For immunofluorescence staining on tissue sections, a representative sample of the SGZ (1 in every 12 sections per stain) was taken from each brain. Sections were stained free-floating and kept in primary antibody solution for at least 1d room temperature or 2 days at 4 degrees C, and secondary antibody for 1 day. Sections were washed twice after each primary and secondary antibody incubations, and stained with 0.2µg/ml DAPI in PBS for 10 minutes prior to mounting the tissue sections onto slides. Once the sections were

mounted, excess PBS was aspirated and Fluoromount G mounting media was added before sections dried out, in order to preserve the full depth of the tissue section. Antibodies and dilutions are as follows – chicken anti-GFP, Aves Labs, 1:10,000-1:20,000; goat anti-DCX, Santa Cruz Biotechnology, 1:500; rabbit anti-DCX, Cell Signaling, 1:1000; rabbit anti-Ki67, Abcam; goat anti-NeuroD, 1:400, Santa Cruz Biotechnology; rabbit anti-Sox2, Abcam, 1:1000; rabbit anti-S100β, DAKO, 1:2000; rabbit anti-GFAP, DAKO, 1:2000; and mouse anti-BrdU, BD Biosciences, 1:300. Secondary antibodies at a 1:1000 dilution were from Jackson Labs (donkey anti-chicken DyLight 488) and from Invitrogen (Alexa594, Alexa488, and Alexa 647 donkey anti-mouse, rabbit, goat, or chicken).

BrdU Immunofluorescence

For BrdU immunostaining, sections were first stained to completion for the non-BrdU antibody. After this, sections were fixed for 20 minutes in cold 4% paraformaldehyde, washed twice with PBS, and then moved to 2N HCl +0.3% Triton X-100 for 20 minutes at 37 degrees C. Sections were then transferred to a 0.1M borate buffer, pH 8.5 to neutralize the HCl for at least 10 minutes. This was followed by the standard immunofluorescence protocol, starting with two washes in PBS.

Imaging

All images of immunofluorescence staining were taken using the Leica DM5500 Upright microscope using a monochrome camera. Images were edited and merged into pseudocolor pictures using the ImageJ software.

Quantification by Stereology

Quantification of immunofluorescence staining was performed using the 40X lens of Olympus BX51 System Microscope. The optical fractionator probe in the StereoInvestigator program (MicroBrightField) was used to provide a random sampling of the counting area, which included the subgranular zone and dentate gyrus, but excluded the hilus. All brains quantified included 1 in every 12 SGZ-containing sections. Total numbers of each protein and the total number of cells in which colocalization was seen were quantified. The area sampling fraction for YFP, DCX, Sox2, and NeuroD was 1/4; for Ki67, Mcm2, and BrdU it was 1/3. The height sampling fraction was 12 microns for Dcx, Sox2 and NeuroD and 18 microns for Ki67, Mcm2, and BrdU, with an average measured section thickness between 22 and 24 microns. The same parameters were used for both the irradiated and contralateral hemispheres of hemi-brain irradiated animals, and values are expressed as the ratio of the estimated total counts using mean section thickness on the irradiated hemisphere relative to the contralateral (shielded) hemisphere. The Schaeffer coefficient of error was <25%.

Other methods of quantification

In some cases, quantification was performed without using Stereo Investigator to randomly sample the region – all positive cells in the section were counted. This procedure was only done for BrdU quantification 14 days after irradiation (Table 3.1) and for the YFP quantification 1 day after tamoxifen treatment (Figure 3.2b,c). Using the 40X lens of a Leica DM5500 upright microscope, I scanned for BrdU (or YFP) positive cells in the hippocampus and counted each individual cell. The presence or absence of the

second label (e.g. DCX, S100β) was then determined and recorded for each cell. Counts were restricted to the SGZ/dentate gyrus; cells in the hilus were not counted.

Chapter 4

Using genetic fate mapping to systematically evaluate how loss of p53 and PTEN impact the effects of IR on SGZ neurogenesis

4.1 Introduction

Current front line treatment for malignant brain tumors involves high dose fractiionated radiation and an alkylating drug, temozolomide (TMZ). The cytotoxic effects of both radiation and TMZ are mediated by DNA damage. There is extensive evidence that both p53 and PTEN tumor suppressor genes play an important role in orchestrating the cellular DNA damage response (DDR) (see Introduction and Chap.2). In this final chapter of the thesis, my goal was to build on the work describe in Chapter 3, to understand how cells at varying stages of differentiation in the SGZ stem cell compartment respond to radiation with or without deletion of p53 and/or PTEN. A systematic investigation into a defined P53/PTEN deleted population of SGZ stem cells and their progeny will not only provide basic insight into pathways affecting neurogenesis, but it can also lay the framework to better understand how GBM tumors, which may be organized in a hierarchical fashion, respond to radiation and chemotherapy. Based on the work presented in Chapter 3, it is possible that the two key populations in which tumor suppressor loss may confer radioresistance are the transient amplifying population and/or the immature neuronal population, which showed cell death and differentiation disruption after radiation. Induction of cell death may be due to prolonged DNA damage signaling in response to DSBs (as shown in Chapter 2). If Akt

activation mediated by deletion of PTEN in this context enhances DSB repair, this may also contribute to inhibiting apoptosis in these cell types. It is also conceivable that the rate of recovery may be either suppressed by the p53 pathway or driven by Akt pathway, based on previously published data described below.

There is a significant amount of literature concerning the effects of p53 and PTEN deletion in NSC, based primarily off of *in vitro* experiments or constitutive cre-mediated recombination. PTEN deletion in the brain (under the nestin-cre promoter) was first shown to produce macrocephaly due to excessive proliferation during development; furthermore, NSC isolated from these mice showed enhanced proliferation but no impact on differentiation in culture (Groszer et al., 2001). Subsequent experiments using these cells showed that loss of PTEN significantly enhanced self-renewal and proliferation rates, all while maintaining the capacity to differentiate (Groszer et al, 2006). Other groups have linked single copy loss of PTEN to increased migration, proliferation, and resistance to oxidative stress induced death (Li et al., 2002). Consistent with these papers, adult deletion of PTEN under a GFAP-cre promoter *in vivo* showed increases in total neurogenesis in the SVZ region, as evidenced by increased total numbers of progenitors and size of the olfactory bulb. Mice with PTEN deletions were also better able to mobilize progenitors in the SVZ after stroke (Gregorian et al., 2009). An analogous situation may exist with radiation, leading to a prediction that PTEN deletion may enhance the rate and degree of recovery. However, this group did not investigate what effects PTEN deletion had on hippocampal neurogenesis. This topic has been investigated briefly in a recent publication by Bonaguidi et al., 2011. In this study, clonal populations of SGZ Type 1 progenitors were labeled using a single injection of tamoxifen

in a nestin-CreER^{T2} mouse model. Analysis revealed that deletion of PTEN promoted symmetric division and entry into the cell cycle at the expense of the quiescent pool, though divisions frequently generated multiple radial glial cells and no differentiated progeny (Bonaguidi et al., 2011). These observations are consistent with previous data suggesting that PTEN negatively regulates proliferation and self-renewal. Although these studies are informative, presently there is no direct information on PTEN loss in the neural stem compartment affects radiation resistance *in vivo*.

The links between p53 function and neural stem cells have also been well characterized, though there are currently very few studies relating these phenotypes to radiation responses. In 2006, a group investigated the effects of homozygous germline p53 deletion on the adult SVZ compartment. This group noted increased proliferation rates and immature neuroblast formation both *in vitro* and *in vivo*. In addition, they noted an increase in mobilization of the quiescent pool after treatment with the mutagen ENU (Gil-Perotin et al., 2006). One might expect similar phenotypes to occur after radiation. There do appear to be differences between total deletions and mutant forms of p53; Wang et al., 2009 show that expression of a mutant p53 capable of DNA binding, but without transcription functions did not confer a proliferative advantage to NSC. As one might expect, a constitutively active form of p53 (the delta 44 mutant) showed reductions in SVZ proliferation, differentiation, and self renewal *in vivo* and *in vitro* (Medrano et al., 2009). Finally, the initial characterization of the hGFAP-cre p53f/f PTENf/+ tumor model did examine the phenotypes of p53-/-, PTEN-/-, and p53-/- PTEN-/- NSC *in vitro*, showing that both of these mutations alone promoted an increase in total neurosphere

number, but the combination showed a synergistic increase in number and activation of Myc, ultimately preventing differentiation.

Overall, these studies using germline knockouts and constitutive cre driver mice to delete p53 or PTEN have shown that these genes do play some role in regulating adult neural stem cell dynamics. It is important to note that these previous studies focused primarily on the SVZ region, rather than the SGZ, which has been the focus of my thesis. Nonetheless, prior data suggests that deletion of p53 and/or PTEN may protect NSC from apoptosis after IR and/or promote the mobilization of the quiescent compartment. In this chapter, I have focused on using the CystatinC-CreERT2 transgenic mouse (described in Chapter 3) which revealed that quiescent stem cell SGZ are highly resistant to radiation, while the transient amplifying compartment(Type2a/b) and immature neuroblasts (DCX+ve) were exquisitely sensitive to DNA damage. Based on this information, I hypothesized the increase in resistance as a result of p53 and/or PTEN loss would like involve the transient amplifying and/or immature (DCX+) neurons.

4.2 Results

Previous reports relying on germline p53 null mice have provided seemingly conflicting data on how radiation affects neurogenesis in the SGZ. Loss of p53 was reported to prevent early induction of apoptosis in the subgranular zone after extremely high doses of radiation (17Gy) but did not prevent irreversible loss of neurogenesis (Li YQ et al., 2010). Others have reported that p53 loss does not prevent early apoptosis in response to extremely low dose (.4Gy) radiation, but that loss of p53 accelerated the recovery of neurogenesis (Uberti et al., 2001). These seemingly contradictory findings

may be reconciled if the impact of radiation is dose dependent. Indeed, radiation induced apoptosis is highly dose-dependence with an initial sharp rise followed by a shallower increase after 3-5Gy (Tada et al., 2000; Mizumatsu et al, 2003). It is possible that at low-doses not all rapidly dividing cells undergo apoptosis, but rather undergo transient cell-cycle arrest followed by return to proliferation. This scenario is consistent with the more rapid recovery of neurogenesis seen with low dose radiation (Levine et al., 2006).

One key limitation of using germline tumor suppressor mice or even conditional mice with a Cre-driver that is not cell-type specific, is that it is difficult to draw firm conclusions about whether a specific phenotype is of a cell-intrinsic mutation or an indirect effect involving multiple cell types in the local environment, or perhaps the results of a remote adaptation due to aberrant gene deletion during embryogenesis. To mitigate such confounding factors, I used the Cystatin-CreERT2 inducible mouse to target glioma relevant mutations to a subpopulation of stem cells in the SGZ (baseline characterization of this transgenic mouse line was described in chap3).

Cell-intrinsic loss of p53 attenuates radiation-induced loss of DCX

Based on the detailed characterization of Cystatin-CreERT2 Rosa26-YFP mice described in Chapter 3, YFP+ labeled cells in the SGZ will include a population of (i) quiescent astrocytes with stem cell-like properties (approximately 50%), (ii) a population of transient amplifying cells, Ki67+ve (Type2a/b) (approximately 10%) and (iii) immature, DCX positive neuroblasts (Type3; approximately 40%). To ensure that the base line numbers of these cells types in the SGZ did not change significantly following deletion of p53 and/or PTEN, I systematically quantified the (i)total number of YFP+ve

cells, (ii) YFP+/Ki67+ ; and (iii) YFP+/DCX+ cell in mice that were (a) wild type (i.e., CreERT2 R-YFP) (ii) p53f/f, (iii) PTEN f/f and (iv) p53f/f, PTENf/f (data not shown). This analysis showed that the total number of YFP+, YFP+/Ki67+, and YFP+/DCX+ cells was not significantly different among the four genotypes (data not shown). Although there does not appear to be a quantitatively significant increase in YFP+ve cells over the 2-4 week time span of these experiments, qualitatively, deletion of PTEN did produce a clear increase in overall process length and branching in immature neuroblasts (DCX+ve) (data not shown). This phenotype is consistent with data from several groups, including Dr. Luis Parada, showing the PTEN loss in the immature neurons can lead to an increase in the dendritic arborization of neurons (Kwon et al, 2006). A more detailed characterization of this result is planned.

In Chapter 3, I presented a detailed quantitative analysis of the dynamic response of YFP- and YFP+ve cell types in the SGZ , showing that the radiation response of these two populations were remarkably similar, both in the initial response and subsequent recovery. This implies that the CstC-CreER^{T2} mediated recombination effectively labeled a representative population of the total neurogenic compartment in the SGZ (approximately 40-50%; Figure 3.7). Therefore, it is reasonable to propose that the YFP-ve population represent genetic wild-type cells that are intermingled among p53-/- and/or PTEN-/- cells. This genetic mix of wild type and tumor suppressor deficient cells provides a powerful means to assess the impact of radiation on the SGZ stem cell compartment.

Adult mice of the following genotypes; wild-type mice (CstC-CreER^{T2} Rosa-YFP, n=2), CstC-CreERT2 R-YFP p53f/f (n=2), CstC-CreERT2 R-YFP PTENf/f

Figure 4.1

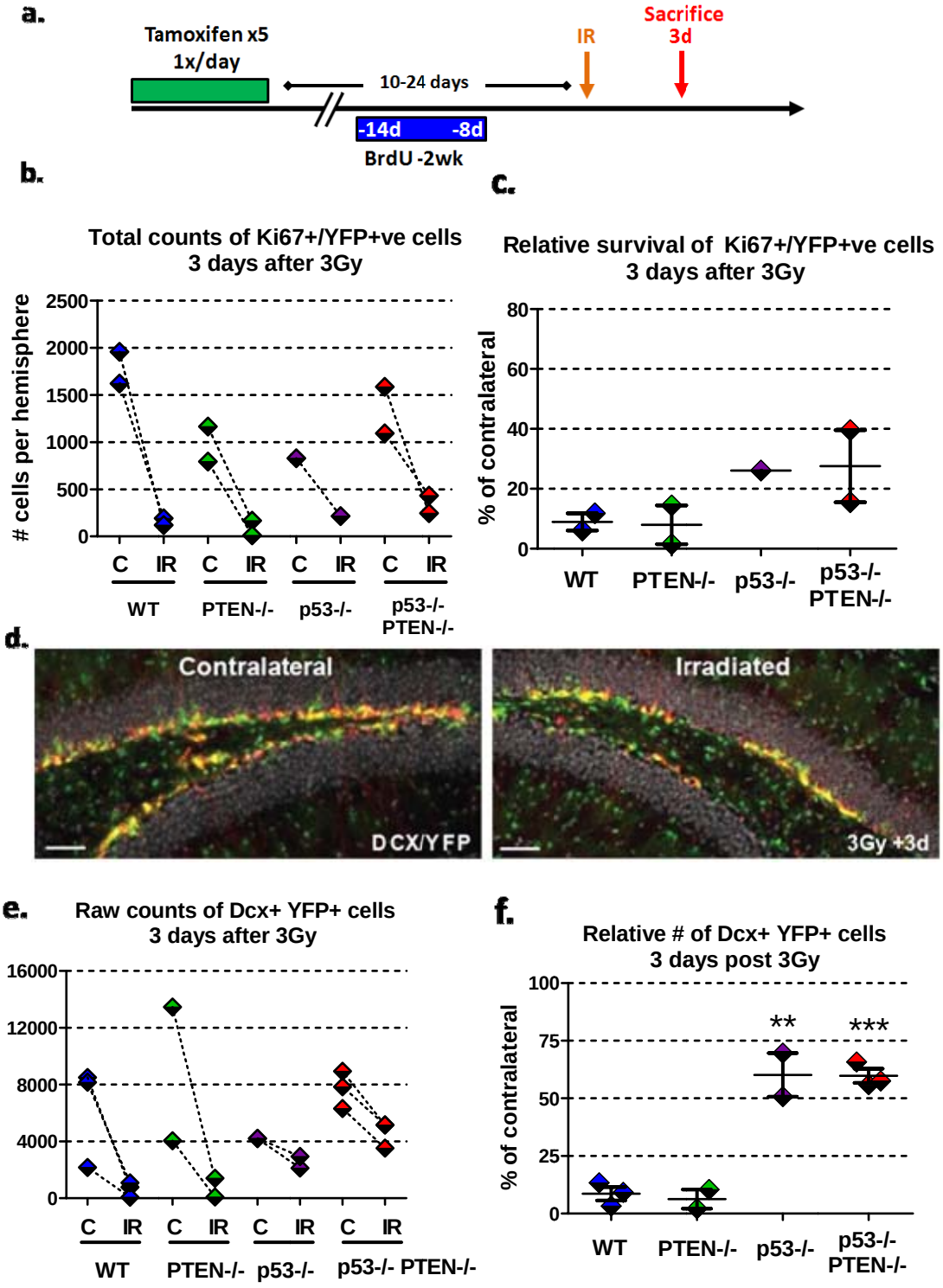
a.
Tamoxifen x5
1x/day
10-24 days
IR
Sacrifice
3d
-14d
-8d
BrdU -2wk
b.
Total counts of Ki67+/YFP+ve cells
3 days after 3Gy
cells per hemisphere
2500
2000
1500
1000
500
0
C IR C IR C IR C IR
WT
PTEN-/-
p53-/-
p53-/-
PTEN-/-
c.
Relative survival of Ki67+/YFP+ve cells
3 days after 3Gy
% of contralateral
80
60
40
20
0
WT
PTEN-/-
p53-/-
p53-/-
PTEN-/-
d.
Contralateral
DCX/YFP
Irradiated
3Gy +3d
e.
Raw counts of Dcx+ YFP+ cells
3 days after 3Gy
cells per hemisphere
16000
12000
8000
4000
0
C IR C IR C IR C IR
WT
PTEN-/-
p53-/-
p53-/- PTEN-/-
f.
Relative # of Dcx+ YFP+ cells
3 days post 3Gy
% of contralateral
100
75
50
25
0
**
***
WT
PTEN-/-
p53-/-
p53-/-
PTEN-/-

(n=2), and CstC-CreERT2 R-YFP p53f/f, PTENf/f (n=3) were treated with tamoxifen and 2-4 weeks later, hemi-brain irradiated (3Gy) and sacrificed 3 days later (see Figure 4.1a). As noted previously (Chapter 3: Figure 3.4), in wild-type mice low-dose radiation produced a marked reduction of YFP+/Ki67+ve cells (this data is shown in Figure 4.1b to provide a convenient comparison across the different genotypes). Perhaps counter to expectations, quantitative analysis of the YFP+/Ki67 populations in the radiated SGZ compared to the contralateral shielded SGZ showed a marked decrease (from 828 to 216 in p53f/f mice, n=1; from 978 +/- 186 to 90 +/-78 in PTENf/f mice (n=2) and from 1,338 +/-246 to 339 +/- 93 in p53f/f PTENf/f mice (n=2)) similar in magnitude to that seen in wild type mice. This data suggests that both p53 and/or PTEN, as single or double gene deletions, have negligible effect on the loss of Ki67 expression caused by radiation (clearly, more replicates are necessary to confirm this result). From my current data, it is

Figure 4.1. Cell-intrinsic loss of p53 is sufficient to prevent radiation-induced Dcx loss in immature neurons. (A) Schematic of tamoxifen, BrdU, irradiation, and sacrifice in the different genetic backgrounds of CstC-CreER^{T2} mice. **(B)** Raw values for YFP+/Ki67+ve cells, 3 days after IR, in all backgrounds. Dotted line connects the two hemispheres from the same brain; C= contralateral (shielded), IR = irradiated. Averages per hemisphere +/- SEM are: WT C 1,788+/-168, IR 156 +/-36 (n=2); PTEN-/- C 978 +/-186, IR 90 +/- 78 (n=2); p53-/- C 828, IR 216.0 (n=1); p53-/- PTEN-/- C 1,338+/-246, IR 339 +/-93 (n=2). **(C)** Data from (B), plotted as relative to contralateral. Averages are as follows: WT 8.9 +/-2.9 (n=2); PTEN-/- 8.0 +/- 6.5 (n=2); p53-/- 26.1 (n=1); p53-/-PTEN-/- 27.5+/-12.0 (n=2). **(D)** Pictures using a 10X lens showing persistence of Dcx+/YFP+ve cells 3 days after IR. Scale bars 50µm. **(E)** Raw values for YFP+/DCX+ve cells, 3 days after IR, in all backgrounds. Dotted line connects the two hemispheres from the same brain; C= contralateral (shielded), IR = irradiated. Averages per hemisphere +/- SEM are: WT C 6,276 +/-2,060, IR 648 +/-302 (n=3); PTEN-/- C 8,752 +/-4,706 , IR 745 +/- 659 (n=2); p53-/- C 4,206 +/-18, IR 2,532 +/- 408 (n=2); p53-/- PTEN-/- C 7,700 +/-762, IR 4,614 +/-543 (n=3). **(F)** Data from E, plotted as relative to contralateral. Averages are as follows: WT 8.6 +/-2.9 (n=3); PTEN-/- 6.3 +/-4.1 (n=2); p53-/- 60.1 +/-9.4 (n=2); p53-/- PTEN-/- 59.8 +/-3.1 (n=3). P values (t-test) for p53-/- vs. WT p=0.0075 (**); p53-/- PTEN-/- vs. WT p=0.0003 (***).

unclear whether the marked decrease in Ki67 expression represents cell death or simply cell cycle arrest; and importantly, whether there the pattern of cell death vs. cell arrest differs among the genotypes. Ongoing studies using tunnel and cleaved caspase-3 co-labeling with YFP to asses for apoptosis, as well as BrdU labeling of ransient amplifying cells (24-48hrs) before radiation will provide a more definitive answers to this important unresolved questions.

In contrast to the negligible effect of p53 or PTEN loss on progenitor cell proliferation, p53 (but not PTEN) loss may reduce the magnitude of DCX down-regulation caused by radiation (see Figure 4.1b). In wild-type mice, number of DCX/YFP+ve cells in the shielded SGZ was 6,276 +/-2,060 and 648 +/-302 (n=3) in the irradiated hemisphere, representing a >90% loss (note that this data was presented in Chapter 3, Figure 3.4 and is being presented here only for the convenience of the reader, drawing a clear comparison with PTEN-/- and p53-/- data). With a PTEN deletion only, the number of YFP+/DCX+ve cells in shielded and irradiated SGZ were 8,752 +/-4,706 and 745 +/- 659 (n=2), respectively; showing a similar marked (>90%) loss similar to that seen in wild type mice (Figure 4.1e,f). In contrast, in p53-/- mice the total number of DCX+/YFP+ve cells in the shielded and irradiated SGZ were 4,206 +/-18 and 2,532 +/-408 (n=2); and 7,700 +/-762 vs. 4,614 +/-543 (n=3) in the double p53-/-PTEN-/- mutant mice (see Figure 4.1e,f; picture in 4.1d). This data suggests that p53 deletion, but not PTEN deletion, may significantly attenuate loss of DCX expression in immature neurons (Figure 4.1f; Dcx+/YFP+ve is 60% of contralateral with p53 deleted vs. <10% in the WT). The higher number of DCX+/YFP+ve cells associated with p53 deletion could

result from either a block in IR-induced downregulation of DCX and/or increase in survival of p53-/- DCX progenitors following radiation.

Loss of p53 increases survival of lineage committed DCX positive progenitors following radiation

Data described above suggests that p53 has little impact on radiation induced loss of transient amplifying cells, but may increase survival of DCX+ lineage committed progenitors. To determine if this phenotype also enhances survival of this population, a BrdU pre-pulsing strategy described in Chapter 3.1 was combined with radiation using the CstC-CreERT2 p53f/f PTENf/f Rosa26-YFP mice. Mice were given daily injections of BrdU at -14 to -8 days (BrdU -2wk) before 3Gy hemi-brain IR (Day 0), and were then sacrificed three days after IR (Figure 4.2a). Quantification of total BrdU+ve and BrdU+/ YFP+ve cells by stereology shows a striking difference between the WT (YFP-ve) and p53/PTEN double deleted (YFP+ve) populations. As presented previously, 42.5+/-3.0% (n=2) of the total YFP+/BrdU+ve population survives a 3Gy dose in the WT setting (Figure 3.6b). Meanwhile, deletion of p53 and PTEN increases the surviving percentage to 105 +/-22.6% in the YFP+/BrdU+ cells (total numbers - shielded 1,842 +/- 54, IR 1,920+/-360, n=2) indicating that these two mutations may both prevent radiation-induced downregulation of neuronal fate commitment genes (Fig 4.1e) and increase overall survival of immature neurons. As expected, the YFP negative, BrdU+ve population shows a similar decrease in total number after irradiation as seen in the CstC-CreERT2 WT mouse (Figure 4.2 b; YFP negative BrdU+ cells – shielded 4,554 +/- 234, IR 2,052 +/-36; 45.1 +/-1.5% relative to contralateral, n=2) . Although the exact

Figure 4.2

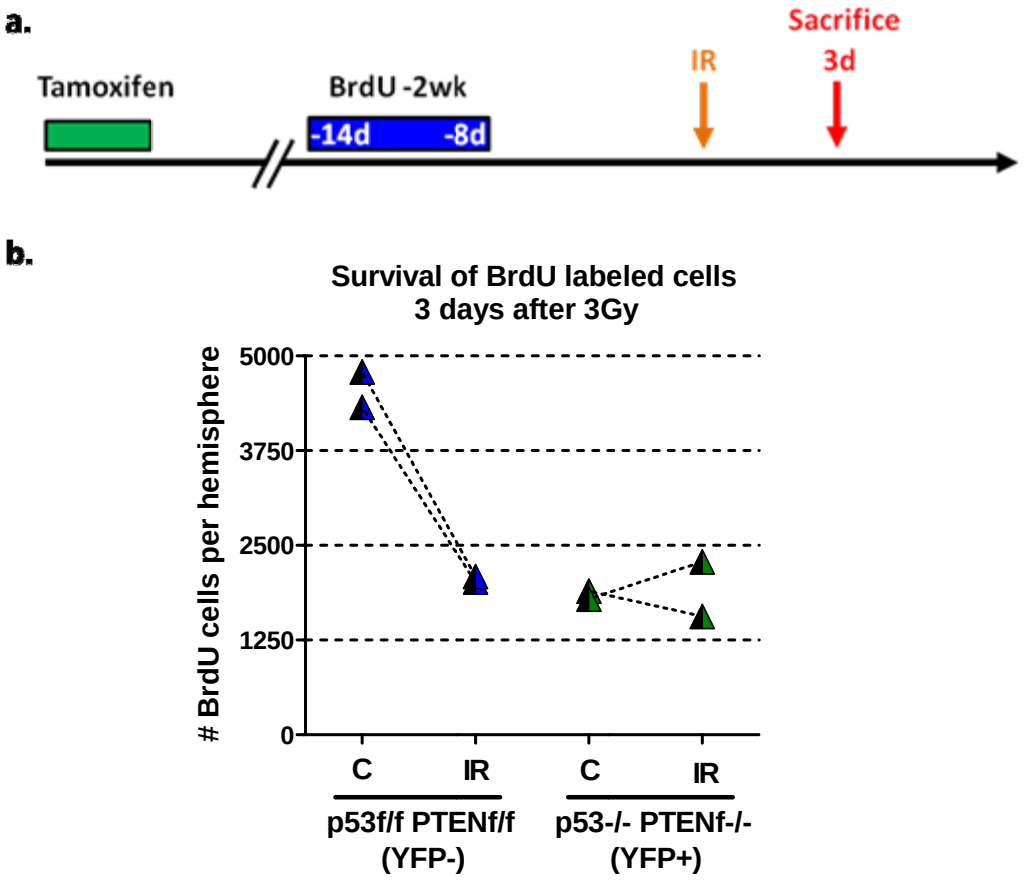

Figure 4.2. BrdU pulse-chase labeling in a CstC-CreER^{T2} p53f/f PTENf/f Rosa26-YFP mouse. (A) Schematic of all treatments, from tamoxifen treatment to sacrifice at 3 days after 3 Gy hemi-brain IR. 1-2 weeks after tamoxifen, BrdU was given from -14 to -8 days (day 0 = IR). **(B)** Graph of total BrdU numbers in two CstC-CreER^{T2} Rosa26-YFP p53f/f PTENf/f Rosa26-YFP mice. The YFP negative cells in this mouse do not have recombination, and therefore are WT C= contralateral (shielded) and IR = irradiated hemisphere. Mean values +/- SEM are as follows: YFP-ve C 4,554 +/-234, IR 2,052 +/-36; YFP+ve C 1,842 +/-54, IR 1,920 +/- 360 (n=2)

mechanism(s) for this increased survival are not clear, this observation for the first time raises the possibility that p53 deletion may selectively promote the survival of DCX+ve Type 3 progenitors and immature neurons, with little to no effect on the proliferating Type 2 cells. This phenotype may be entirely p53 mediated, or PTEN may be playing a role in activating a pro-survival pathway and/or enhancing the proficiency of DNA repair through the Akt pathway, as described in Chapter 2.

HOT lines show loss of differentiated markers after TMZ and IR treatment

Data so far has indicated that DNA damage caused by radiation downregulates genes involved in commitment to a differentiated lineage. In the setting of a non-transformed cell, this disruption coincides with accelerated death and irreversible changes in differentiation state. To what extent this phenotype can be applied to glioblastoma is unknown - certainly, there is a large body of evidence to suggest that GBM show extensive heterogeneity in expression patterns, frequently showing multiple aberrantly expressed lineage markers for astrocytes, neurons, and oligodendrocytes in the same tumor (Maher et al., 2001). These lineage markers may represent functionally different populations of the tumor that may have differential responses to treatment, with many people believing that the cancer stem cells show resistance to therapy. An alternate explanation could be that radiation and DNA damage agents are promoting global changes in expression patterns in non-CSCs that promote signatures of the cancer stem cell population, as a protective mechanism to put cancer cells into quiescence.

An ongoing project in the Bachoo lab is to isolate human glioblastoma cells from primary patient tumors and serially passage them immunocompromised mice. These

human orthotopic tumors (HOTs) maintain a high degree of similarity to the original patient tumor, including the characteristic morphology and gene expression patterns. I wanted to determine if this p53 dependent change in differentiation markers after DNA damage occurs in the context of human GBMs. In the present study (performed with Tomoyuki Mashimo, Vamsihadara Vemireddy and Nozomi Tomimatsu), six different HOT lines were grown orthotopically in NOD-SCID mice and treated with either saline or temozolomide (TMZ). The TMZ dosing schedule consisted of one 80mg/kg intraperitoneal injection per day over 3 consecutive days. The mice were then sacrificed 3 days later, and tumor tissue was then removed and analyzed for protein levels by Western blotting. Immunohistochemistry for the proliferation marker Ki67 showed that HOT lines showed drastically reduced levels of proliferation (Figure 4.3a) and some apoptosis (data not shown), but the overall density of the tumor cells does not significantly change after 1 TMZ regimen. It appears that a majoritiy of cells exit the cell cycle and perhaps enter a state of relative quiescence or dormancy. The next step was to verify that temozolomide was inducing DNA double strand breaks in the tumor cells. As shown in Figure 4.3b, all lines showed evidence of an activated DDR, as evidenced by increased levels of γH2AX (evidence for DNA DSBs) and various other DDR components, such as phosphorylated ATM (S1981) and activation of p53 (stabilization and phosphorylation at serine 15). Notably, R553 and R738 did not show stabilization or phosphorylation (S15) of p53 in response to DNA damage, leading to the prediction that these HOT lines should not show any change in lineage markers after IR or TMZ treatment. To test this, the protein extracts were analyzed for expression of a panel of lineage markers. As discussed previously, Dcx is a microtubule associated protein that is specific for lineage-committed

Figure 4.3

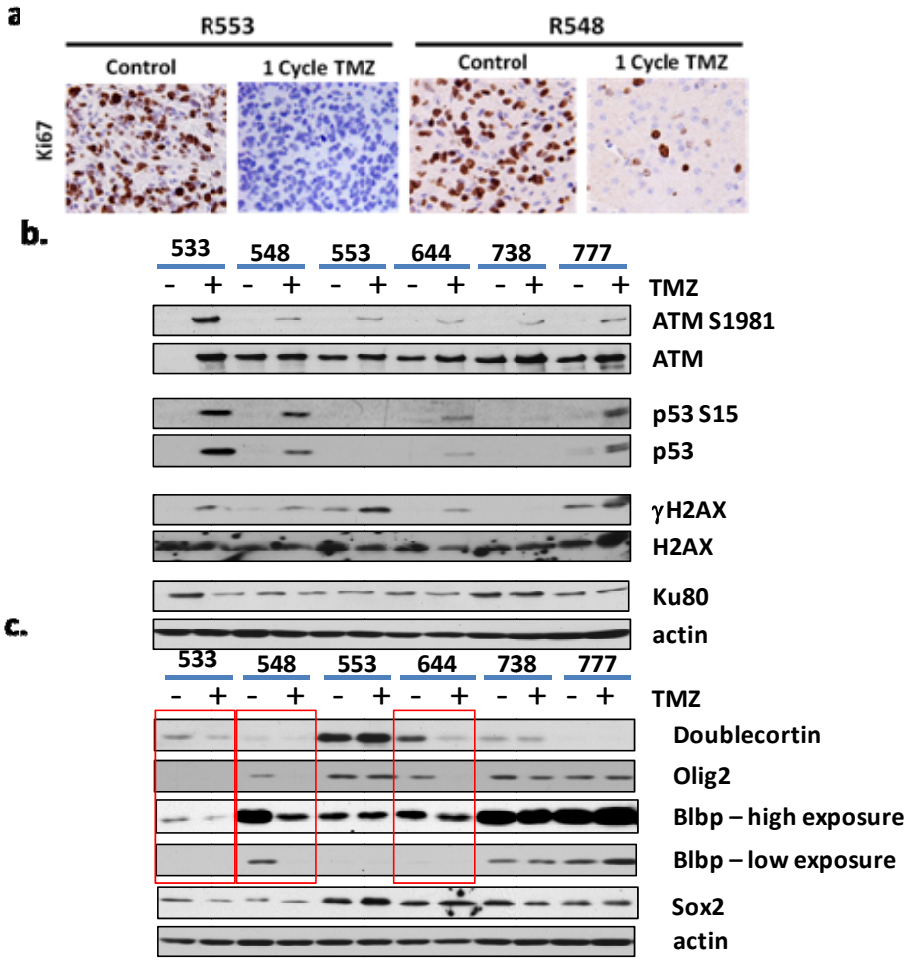

Figure 4.3. DNA damage signals downregulate differentiation markers in human orthotopic GBM. Human orthotopic tumors (HOT) were injected into the brains of NOD-SCID and serially passaged. Mice harboring one of each line were then treated with either saline or 1 regimen of TMZ (80mg/kg, 1 injection per day for 3 consecutive days) and sacrificed 3 days after treatment. Examination of total Ki67 levels **(A)** between groups is shown for 3 representative lines. **(B)** Western blot analysis of protein extracts from this cohort was performed to look for markers of DSBs and an activated DNA damage response (phospho-ATM serine 1981, phospho-p53 serine 15, and γH2AX). Note that R553 and R738 do not show stabilization or phosphorylation of p53. **(C)** Western blot analysis of the samples from **(B)** looking at various lineage-commitment markers in HOT lines after TMZ. Note that 3 out 4 lines that induce p53 show striking changes in Blbp, Doublecortin, and Olig2 expression, while the lines that showed no p53 activation have no changes in these markers.

immature neurons (von Bohlen und Halbach, 2011). Olig2 is a bHLH transcription factor expressed early in development and post-natally in NG2+ oligodendrocyte precursors (Ross et al., 2003; Ligon et al., 2006). Previous publications have shown that it is almost uniformly expressed in gliomas, both astrocytoma and oligodendroglioma (Ligon et al., 2004). Brain lipid binding protein (Blbp) is primarily a marker of radial glial cells (both in development and in the adult) (Feng et al., 1994, Steiner et al. 2006), but can be expressed in reactive astrocytes under pathological conditions such as injury and neurodegenerative disease (Kipp et al., 2011; Kim et al., 2012). Sox2 is also a well known marker of Type 1 neural stem cells and is essential for neurogenesis (Ferri et al, 2004), and it was also identified as one of the key factors needed to de-differentiate somatic cells into induced pluripotent stem cells (Takahashi and Yamanaka, 2006).

HOT lines that failed to activate p53 (R553 and R738) did not show any changes in Doublecortin, Sox2, Blbp, or OIlig2 expression after TMZ treatment (Figure 4.3c). However, three out of four lines that showed evidence of activated p53 (R533, R548, R648) all showed reductions in Doublecortin, Blbp, and Olig2, and after TMZ treatment, while Sox2 expression was relatively constant in all cases (Figure 4.3c). These data are remarkably of the data shown in Figures 4.1 and 4.2. The tumor associated expression of cell-type specific genes supports the overall idea that DNA damage signals may suppress lineage specific genes in a p53-dependent manner. It is not clear at this point whether this change in expression profile marks a transient or prolonged modification of overall transcription, and to what extent this phenotype may provide any resistance to therapy. It is also unclear why R777 does not show any phenotype after TMZ treatment, given that the p53 protein is both stabilized and phosphorylated after DNA damage. To validate this

hypothesis, the activity of downstream effectors of the p53 pathway (e.g. p21) needs to be investigated.

4.3 Discussion

Results presented in this chapter demonstrated that p53 plays a critical role in modulating radiation resistance in the neural stem cell compartment, in ways that are applicable to both basic neurobiology as well as in cancer biology. From a basic biology perspective, collectively my data suggests that activation of p53 in a lineage-committed progenitor cell due to cell stress may cause an irreversible suppression of differentiation. This phenotype also appears to be cell-intrinsic in immature neurons, as conditional deletion of p53 can reverse the loss of key neuronal fate commitment genes in a significant population. This result suggests that the underlying molecular program which regulates neurogenesis in the SGZ requires high genetic fidelity of among stem-progenitor cells and effectively eliminates those with any DNA damage. Along these lines, the central role of p53 in regulating such a process is of course not unexpected, as this transcription factor is activated in response to a variety of cell stressors, including DNA damage. The precise impact of p53 loss and PTEN loss in the stem/progenitor compartment are currently under investigation. One might expect that single or combined deletions may promote recovery at a faster rate, due to accelerated proliferation and/or increased mobilization of quiescent progenitors. In cell culture, activation of oncogenic signaling pathways like Akt can accelerate proliferation rates and give cells a proliferative advantage. Whether this happens *in vivo* in this highly defined stem cell niche seems less clear.

The ability of primary GBM cells to respond to chemotherapy and radiation by activating a p53 mediated cell arrest program provides these tumors a powerful adaptive mechanism to avoid cell death and an opportunity to develop resistance to the two front line therapies of malignant gliomas. Thus, in this case p53 would be acting as a double edged sword – while its activation may help to potentiate the pro-apoptotic signals in response to DNA damage, it also may be necessary to promote entry into a protective, dormant state.

There are multiple experiments and controls necessary to expand upon this concept. Western blot data only examines a pool of cells and can leave out critical information. First, it is not known what percentage of the total tumor cells express these markers, and whether or not these co-label with each other. Second, there is no way to determine whether these populations have died or changed expression patterns from this data. However, our qualitative analysis shows that a majority of the tumor cells are Ki67 positive, and treatment with radiation or TMZ for a single cycle reduces proliferation but does not appreciably change overall tumor cell density (Figure 4.3a). Thus, it appears that one key difference between the tumor lines and the endogenous stem cell compartment is the ability to enter cell arrest after DNA damage. The baseline experiments using BrdU pre-pulse experiments (Chapter 3, Figures 3.5-3.6) can provide a useful starting point to test both the overall extent of killing and survival of specific subpopulations. It is important to note that the dynamic analysis of the SGZ stem cell compartment that I described in chapters 3 and 4 provide an important conceptual frame work for evaluating how malignant tumors respond to conventional therapies and inevitably develop resistance to chemotherapy and radiation.

4.4 Methods – see Chapter 3; additional methods below

Mice

Mice used in this study were housed in the NG facility. The conditional p53 used were described in Jonkers et al., 2001; the conditional PTEN mice were described in You et al., 2002. NOD-SCID mice were purchased from Charles River Laboratories.

HOT lines

Human orthotopic tumors from patients with GBM were first isolated from fresh patient samples and dissociated into single cells. After dissociation, cells were intra-cranially injected into the striatum of NOD-SCID mice (see methods for Chapter 2) and allowed to grow until mice became moribund. At this time, mice were given an overdose of Avertin and decapitated. The brain was removed and sliced to 1mm thick coronal sections, after which tumor tissue was dissected and saved for DNA isolation, RNA isolation, histology, and subsequent dissociation/passaging in NOD-SCID mice. Subsequent generations were used for TMZ treatment studies. For the TMZ treated cohort, mice were injected with an 80mg/kg dose of TMZ (LKT Labs) for three consecutive days.

Temozolomide

A stock solution of 40mg/ml was first prepared in DMSO and stored at -20 degrees Celsius. This solution was then diluted in 300µl of 0.9% saline immediately before the

intraperitoneal injection. The standard TMZ regimen is 80mg/kg, once a day, for three consecutive days

Protein lysates/Western blotting

Protein Extraction and Western Blotting—Western blotting experiments were performed using whole cell extracts from frozen brain tumor specimens following standard techniques. For whole cell extracts, cells were resuspended and lysed in RIPA buffer (SIGMA). Lysates were mixed with 2XSDS buffer, then boiled for 5 min. For nuclear extracts, cells were first resuspended in hypotonic lysis buffer, then after spinning, pellets were resuspended in nuclear extraction buffer. After spinning, supernatant was collected as nuclear extract. Lysates were mixed with 2XSDS buffer, then boiled for 5 min. For Western blotting, cell extracts were electrophoresed on 8, 10, 15% SDS-polyacrylamide gels to detect medium-sized proteins or low-bis 8% SDS acrylamide gels for high molecular weight proteins. Proteins were then transferred to a polyvinylidene difluoride membrane (Biorad). Membranes were incubated in TBS- and 5% skim milk added to TBS-T. Membranes were then stained with Ponceau S dye to check for equal loading and homogeneous transfer. Hypotonic lysis buffer was 10mM Tris HCl, pH7.9, 1.5mM MgCl2, 5mM KCl, + protease and phosphatase inhibitors. Nuclear extraction buffer was 50mM Tris HCl pH7.9, .5M NaCl, 2mM EDTA, 10% sucrose, 10% glycerol, and protease/phosphatase inhibitors.

Table 4.1

Antibody	Source	Western
phospho-p53(S15)	Cell Signaling	1:1000
actin	Sigma	1:1000
ATM	Sigma	1:1000
P53	Santa Cruz	1:1000
γH2AX	Upstate	1:1000
H2AX	Bethyl	1:2000
phospho-ATM(S1981)	Genescript	1:1000
Ku80	Gift from Dr. B. Chen	1:1000
HRP-conjugated secondary antibodies	Biorad	1:3000

Table 4.1. Dilutions of primary and secondary antibodies for Western blotting.

Chapter 5

Conclusions/Future Directions

In the first results chapter, work presented here has shown novel links between a key oncogenic signaling event (activation of the Akt pathway) and pathways involved in DNA double strand break repair. While the error prone NHEJ pathway appears to be activated with overexpression of EGFRvIII, the homologous recombination pathway shows reduced activity after PTEN loss. This has functional consequences, as both of these mutations increase radioresistance, while loss of PTEN renders astrocytes more sensitive to DNA damaging agents that induce replication associated breaks. There are now numerous reports that Akt is phosphorylated shortly after IR and can translocate to the nucleus (Bozulic et al., 2008; Fraser et al., 2011). In addition to our data with EGFRvIII (Mukherjee et al., 2009), another report has shown that knockdown of Akt inhibits DNA-PKcs activity (Toulany et al., 2008). Therefore, it is possible that Akt activation may aberrantly promote NHEJ-mediated repair of breaks that would normally be repaired by HR, resulting in inappropriate error-prone repair of replication associated breaks. This can lead to increased chromosomal aberrations and cell death. A critical event in determining which DSB repair pathway to use is resection at the site of the double strand break (Symington and Gautier, 2011). It is possible that activation of Akt may be playing a role in this process. Recent reports have shown that phosphorylated Akt interacts with Mre11 in response to DNA DSBs (Fraser et al., 2011; Deng et al., 2011). Mre11 is one of the key players involved in the resection process, so it would be

interesting to investigate if Akt may be regulating the function of Mre11 to prevent resection. Indeed, a recent report has implicated Akt in suppressing DNA end processing in G2, a phase in which homologous recombination would be active (Xu et al., 2010). Evidence also points to a potential feedback loop between activated Akt and DNA-PKcs; inhibition of either component prevents phosphorylation of the other one after radiation (Bozulic et al., 2008; Toulany et al., 2008; Mukherjee et al., 2009). These proteins also are found in the same complex (Bozulic et al., 2008; Toulany et al., 2008). Activation of both proteins after IR could have dual effects to promote radiation resistance, as Akt signaling is pro-survival and activated DNA-PKcs can promote DSB repair. Further elucidating the interactions between these two proteins is an area of high importance.

In Chapters 3 and 4, I have explored the effects of radiation on the adult neural stem cell compartments using a novel Cre-ER^{T2} mouse model. From a basic stem cell biology perspective, this fate mapping system offered new insight into the responses of individual progenitor populations after irradiation. I showed that the proliferating progenitors and immature neuroblasts showed increase in cell death and disruptions in differentiation. My data supports the idea that immature neuroblasts may show suppressed expression of key neuronal lineage markers, such as Doublecortin and NeuroD, after IR while still persisting in the neurogenic niche. Any disruption in the differentiation capacity immature neuroblasts is irreversible, as re-expression of Dcx does not occur 14 days after IR. Meanwhile, quiescent stem cells were resistant to apoptosis at both low and high doses, and this population was likely responsible for recovery of proliferation and differentiation after low dose IR. This phenotype has interesting implications for GBM – wild type, quiescent stem cells have inherent resistant to

radiation treatment, even in the absence of any pro-survival mutations. Is this simply due to quiescence, or due to some inherent property of the stem cell? And if so, is this mechanism(s) conserved in cancer stem cells? Understanding how Type 1 cells might differentially cope with DNA damage is an important next step in understanding mechanisms of radiation resistance in SGZ stem cells. Ongoing experiments are testing if stem cells show altered DNA repair kinetics *in vivo*, both in the short term after low dose and long term after high does (is there persistent DNA damage, and what specific cell type is this present in?

This baseline characterization was then used to assess what role(s) p53 and PTEN may play in promoting radioresistance *in vivo*, using the adult NSC as a reductionist model for cancer. I showed that the major determinant of resistance was p53, and that this functioned only in the immature neuroblasts to prevent IR-induced loss of Dcx and/or cell death. There are many open areas of investigation in this area. First, while the acute effects of radiation in these mutant models were assessed, the extent to which deletion of p53 (with or without PTEN) provides long term protection to the immature neuroblasts is unknown. Is this a transient effect, or does p53 loss promote long-term survival and/or integration of these irradiated precursors? Second, the effects of key GBM mutations on mobilizing the quiescent population after IR have not been fully addressed with detailed kinetic analysis. Understanding mechanisms that modulate this process has fundamental importance to cancer biology, as tumor recurrence after treatment may derive from a quiescent, radio-resistant stem cell population. Preliminary data suggests that p53 deletion may accelerate the proliferation recovery in this compartment, with or without modulation of PTEN, while PTEN deletion alone does not

show any phenotype. These experiments are currently underpowered and warrant further study. Fully elucidating any additive or synergistic effects of combined deletion is of critical importance. Finally, I would ultimately like to extend this characterization into a *de novo* inducible tumor model. Work from the Bachoo lab has shown combined deletion of PTEN (with or without p53) and an activating BRAF mutation ($BRAF^{V600E}$) is sufficient to induce GBM in Nestin-$CreER^{T2}$ mice. This defined system is the perfect model to address the effects of the p53 on radiation resistance in a tumor setting.

The potential role of p53 signaling to suppressing differentiation in neuroblasts is a novel finding. Preliminary evidence suggests that this mechanism may be conserved in cancer cells, as orthotopic GBM lines treated with Temozolomide show a downregulation of lineage markers in a p53-dependent manner, similar to what may be happening in the NSC niche. This may suggest that GBM cells are "de-differentiating" to a phenotype that mimics a cancer stem cell. Future experiments will focus on addressing whether similar phenotypes occur in response other DNA damage inducing treatments, such as ionizing radiation. In addition, it is imperative to determine whether this mechanism has any protective effects for long term treatment in orthotopic xenograft models. Activation of a more stem-like gene signature may promote quiescence, resulting in an increased resistance to therapeutic modalities. This model predicts that GBM lines which fail to activate p53 should re-enter the cell cycle faster after treatment, rendering these newly proliferating cells more susceptible to treatment. Thus, p53 could be acting as a double-edged sword – while efficient activation of p53 may help promote apoptosis in tumor cells, the ones that evade this process may be more resistant to subsequent treatment options.

BIBLIOGRAPHY

Abdallah N, Slomianka L, Lipp HP. Reversible Effect of X-Irradiation on Proliferation, Neurogenesis, and Cell Death in the Dentate Gyrus of Adult Mice. *Hippocampus*. 2007;17:1230–1240.

Al-Hajj M, Wicha M S, Benito-Hernandez A, Morrison SJ, Clarke M F. Prospective identification of tumorigenic breast cancer cells. *Proc Natl Acad Sci USA*. 2003 Apr 1;100(7):3983-8.

Alcantara Llaguno S, Chen J, Kwon CH, Jackson EL, Li Y, Burns DK, Alvarez-Buylla A, Parada LF. Malignant astrocytomas originate from neural stem/progenitor cells in a somatic tumor suppressor mouse model. *Cancer Cell*. 2009 Jan 6;15(1):45-56..

Allay JA, Dumenco LL, Koc ON, Liu L, Gerson SL. Retroviral transduction and expression of the human alkyltransferase cDNA provides nitrosourea resistance to hematopoietic cells. *Blood*. 1995 Jun 1;85(11):3342-51.

Amano T, Inamura T, Wu CM, Kura S, Nakamizo A, Inoha S, Miyazono M, Ikezaki K.. Effects of single low dose irradiation on subventricular zone cells in juvenile rat brain. *Neurol Res*. 2002 Dec;24(8):809-16.

Armesilla-Diaz A, Bragado P, Del Valle I, Cuevas E, Lazaro I, Martin C, Cigudosa JC, Silva A. p53 regulates the self-renewal and differentiation of neural precursors. *Neuroscience*. 2009 Feb 18;158(4):1378-89.

Arnaudeau C, Lundin C, Helleday T. DNA double-strand breaks associated with replication forks are predominantly repaired by homologous recombination involving an exchange mechanism in mammalian cells. *J Mol Biol.* 2001;307:1235–45.

Bachoo RM, Maher EA, Ligon KL, Sharpless NE, Chan SS, You MJ, Tang Y, DeFrances J, Stover E, Weissleder R, Rowitch DH, Louis DN, DePinho RA. Epidermal growth factor receptor and Ink4a/Arf: convergent mechanisms governing terminal differentiation and transformation along the neural stem cell to astrocyte axis. *Cancer Cell*. 2002;1:269–77.

Baker SJ. PTEN enters the nuclear age. *Cell.* 2007 Jan 12;128(1):25-8.

Bao S, Wu Q, McLendon RE, Hao Y, Shi Q, Hjelmeland AB, Dewhirst MW, Bigner DD, Rich JN. Glioma stem cells promote radioresistance by preferential activation of the DNA damage response. *Nature*. 2006 Dec 7;444(7120):756-60.

Beier F, Beier CP, Aschenbrenner I, Hildebrandt GC, Brümmendorf TH, Beier D. Identification of CD133(-)/telomerase(low) progenitor cells in glioblastoma-derived cancer stem cell lines. *Cell Mol Neurobiol*. 2011 Apr;31(3):337-43.

Boehme KA, Kulikov R, Blattner C. p53 stabilization in response to DNA damage requires Akt/PKB and DNA-PK. *Proc Natl Acad Sci U S A*. 2008 Jun 3;105(22):7785-90.

Bonaguidi MA, Wheeler MA, Shapiro JS, Stadel RP, Sun GJ, Ming GL, Song H. In vivo clonal analysis reveals self-renewing and multipotent adult neural stem cell characteristics. *Cell*. 2011 Jun 24;145(7):1142-55.

Bonnet D, Dick JE. Human acute myeloid leukemia is organized as a hierarchy that originates from a primitive hematopoietic cell. *Nat Med*. 1997 Jul;3(7):730-7.

Bookout AL, Cummins CL, Mangelsdorf DJ, Pesola JM, Kramer MF. High-throughput real-time quantitative reverse transcription PCR. *Curr Protoc Mol Biol*. 2006 Feb;Chapter 15:Unit 15.8.

Bozulic L, Surucu B, Hynx D, Hemmings BA. PKBalpha/Akt1 acts downstream of DNA-PK in the DNA double-strand break response and promotes survival. *Mol Cell*. 2008;30:203–13.

Brandes AA, Franceschi E, Tosoni A, Hegi ME, Stupp R. Epidermal growth factor receptor inhibitors in neuro-oncology: hopes and disappointments. *Clin Cancer Res*. 2008 Feb 15;14(4):957-60.

Branzei D, Foiani M. Regulation of DNA repair throughout the cell cycle. *Nat Rev Mol Cell Biol.* 2008 Apr;9(4):297-308.

Brooks CL, Gu W. The impact of acetylation and deacetylation on the p53 pathway. *Protein Cell*. 2011 Jun;2(6):456-62.

Brown J, Cooper-Kuhn CM, Kempermann G, Van Praag H, Winkler J, Gage FH, Kuhn HG. Enriched environment and physical activity stimulate hippocampal but not olfactory bulb neurogenesis. *Eur J Neurosci*. 2003 May;17(10):2042-6.

Bryant HE, Schultz N, Thomas HD, Parker KM, Flower D, Lopez E, Kyle S, Meuth M, Curtin NJ, Helleday T. Specific killing of BRCA2-deficient tumours with inhibitors of poly(ADP-ribose) polymerase. *Nature*. 2005 Apr 14;434(7035):913-7.

Bublil EM, Yarden Y. The EGF receptor family: spearheading a merger of signaling and therapeutics. *Curr Opin Cell Biol*. 2007 Apr;19(2):124-34.

Burkhart D. L., Sage J. Cellular mechanisms of tumour suppression by the retinoblastoma gene. *Nat. Rev. Cancer*. 2008 Sep;8(9):671-82.

Burma S, Chen BP, Chen DJ. Role of non-homologous end joining (NHEJ) in maintaining genomic integrity. *DNA Repair (Amst)*. 2006 Sep 8;5(9-10):1042-8.

Burma S, Chen DJ. Role of DNA-PK in the cellular response to DNA double-strand breaks. *DNA Repair (Amst)*. 2004 Aug-Sep;3(8-9):909-18.

Burstein, H. Novel Agents and Future Directions for Refractory Breast Cancer. *Seminars in Oncology*. 2011 Jun;38 Suppl 2:S17-24.

The Cancer Genome Atlas Network (TCGA). Comprehensive genomic characterization defines human glioblastoma genes and core pathways. *Nature*. 2008 Oct 23;455(7216):1061-8.

Chakravarti A, Dicker A, Mehta M. The contribution of epidermal growth factor receptor (EGFR) signaling pathway to radioresistance in human gliomas: a review of preclinical and correlative clinical data. *Int J Radiat Oncol Biol Phys*. 2004 Mar 1;58(3):927-31..

Chalhoub N, Baker SJ. PTEN and the PI3-kinase pathway in cancer. *Annu Rev Pathol*. 2009;4:127-50.

Cheng L, Wu Q, Huang Z, Guryanova OA, Huang Q, Shou W, Rich JN, Bao S. L1CAM regulates DNA damage checkpoint response of glioblastoma stem cells through NBS1. *EMBO J*. 2011 Mar 2;30(5):800-13.

Chow LM, Endersby R, Zhu X, Rankin S, Qu C, Zhang J, Broniscer A, Ellison DW, Baker SJ. Cooperativity within and among Pten, p53, and Rb pathways induces high-grade astrocytoma in adult brain. *Cancer Cell*. 2011 Mar 8;19(3):305-16.

Cuenda A, Alessi DR. Use of kinase inhibitors to dissect signaling pathways. *Methods Mol Biol.* 2000;99:161–75.

Dai C, Celestino JC, Okada Y, Louis DN, Fuller GN, Holland EC. PDGF autocrine stimulation dedifferentiates cultured astrocytes andinduces oligodendrogliomas and oligoastrocytomas from neural progenitors and astrocytes in vivo. *Genes Dev*. 2001 Aug 1;15(15):1913-25.

Dang L, White DW, Gross S, Bennett BD, Bittinger MA, Driggers EM, Fantin VR, Jang HG, Jin S, Keenan MC, Marks KM, Prins RM, Ward PS, Yen KE, Liau LM, Rabinowitz JD, Cantley LC, Thompson CB, Vander Heiden MG, Su SM. Cancer-associated IDH1 mutations produce 2-hydroxyglutarate. *Nature*. 2009 Dec 10;462(7274):739-44.

de la Iglesia N, Konopka G, Puram SV, Chan JA, Bachoo RM, You MJ, Levy DE, Depinho RA, Bonni A. Identification of a PTEN-regulated STAT3 brain tumor suppressor pathway. *Genes Dev*. 2008 Feb 15;22(4):449-62.

Dedes KJ, Wetterskog D, Mendes-Pereira AM, Natrajan R, Lambros MB, Geyer FC, Vatcheva R, Savage K, Mackay A, Lord CJ, Ashworth A, Reis-Filho JS. PTEN

deficiency in endometrioid endometrial adenocarcinomas predicts sensitivity to PARP inhibitors. *Sci Transl Med*. 2010 Oct 13;2(53):53ra75.

Deng R, Tang J, Ma JG, Chen SP, Xia LP, Zhou WJ, Li DD, Feng GK, Zeng YX, Zhu XF. PKB/Akt promotes DSB repair in cancer cells through upregulating Mre11 expression following ionizing radiation. *Oncogene*. 2011 Feb 24;30(8):944-55.

Dick JE. Stem cell concepts renew cancer research. *Blood*. 2008 Dec 15;112(13):4793-807.

Dittmann K, Mayer C, Fehrenbacher B, Schaller M, Raju U, Milas L, Chen DJ, Kehlbach R, Rodemann HP. Radiation-induced epidermal growth factor receptor nuclear import is linked to activation of DNA-dependent protein kinase. *J Biol Chem*. 2005 Sep 2;280(35):31182-9.

Donawho CK, Luo Y, Luo Y, Penning TD, Bauch JL, Bouska JJ, Bontcheva-Diaz VD, Cox BF, DeWeese TL, Dillehay LE, Ferguson DC, Ghoreishi-Haack NS, Grimm DR, Guan R, Han EK, Holley-Shanks RR, Hristov B, Idler KB, Jarvis K, Johnson EF, Kleinberg LR, Klinghofer V, Lasko LM, Liu X, Marsh KC, McGonigal TP, Meulbroek JA, Olson AM, Palma JP, Rodriguez LE, Shi Y, Stavropoulos JA, Tsurutani AC, Zhu GD, Rosenberg SH, Giranda VL, Frost DJ. ABT-888, an orally active poly(ADP-ribose) polymerase inhibitor that potentiates DNA-damaging agents in preclinical tumor models. *Clin Cancer Res*. 2007 May 1;13(9):2728-37.

Ehninger D, Kempermann G. Neurogenesis in the adult hippocampus. *Cell Tissue Res*. 2008 Jan;331(1):243-50.

Facchino S, Abdouh M, Chatoo W, Bernier G. BMI1 confers radioresistance to normal and cancerous neural stem cells through recruitment of the DNA damage response machinery. *J Neurosci*. 2010 Jul 28;30(30):10096-111.

Fan C, He L, Kapoor A, Rybak AP, De Melo J, Cutz JC, Tang D. PTEN inhibits BMI1 function independently of its phosphatase activity. *Mol Cancer*. 2009 Nov 10;8:98.

Fan Y, Liu Z, Weinstein PR, Fike JR, Liu J. Environmental enrichment enhances neurogenesis and improves functional outcome after cranial irradiation. *Eur J Neurosci*. 2007 Jan;25(1):38-46.

Farmer H, McCabe N, Lord CJ, Tutt AN, Johnson DA, Richardson TB, Santarosa M, Dillon KJ, Hickson I, Knights C, Martin NM, Jackson SP, Smith GC, Ashworth A. Targeting the DNA repair defect in BRCA mutant cells as a therapeutic strategy. *Nature*. 2005 Apr 14;434(7035):917-21.

Feil R., Wagner I., Metzger D., Chambon P. Regulation of Cre recombinase activity by mutated estrogen receptor ligand-binding domains. *Biochem. Biophys. Res. Commun*. 1997 Aug 28;237(3):752-7.

Feng L, Hatten ME, Heintz N. Brain lipid-binding protein (BLBP): a novel signaling system in the developing mammalian CNS. *Neuron*. 1994 Apr;12(4):895-908.

Fernandez-Capetillo O, Lee A, Nussenzweig M, Nussenzweig A. H2AX: the histone guardian of the genome. *DNA Repair (Amst)*. 2004 Aug-Sep;3(8-9):959-67.

Ferri AL, Cavallaro M, Braida D, Di Cristofano A, Canta A, Vezzani A, Ottolenghi S, Pandolfi PP, Sala M, DeBiasi S, Nicolis SK. Sox2 deficiency causes neurodegeneration and impaired neurogenesis in the adult mouse brain. *Development*. 2004 Aug;131(15):3805-19.

Fong PC, Boss DS, Yap TA, Tutt A, Wu P, Mergui-Roelvink M, Mortimer P, Swaisland H, Lau A, O'Connor MJ, Ashworth A, Carmichael J, Kaye SB, Schellens JH, de Bono JS. Inhibition of poly(ADP-ribose) polymerase in tumors from BRCA mutation carriers. *N Engl J Med*. 2009 Jul 9;361(2):123-34.

Franceschi E, Cavallo G, Lonardi S, Magrini E, Tosoni A, Grosso D, Scopece L, Blatt V, Urbini B, Pession A, Tallini G, Crinò L, Brandes AA. Gefitinib in patients with progressive high-grade gliomas: a multicentre phase II study by Gruppo Italiano Cooperativo di Neuro-Oncologia (GICNO). *Br J Cancer*. 2007 Apr 10;96(7):1047-51.

Fraser M, Harding SM, Zhao H, Coackley C, Durocher D, Bristow RG. MRE11 promotes AKT phosphorylation in direct response to DNA double-strand breaks. *Cell Cycle*. 2011 Jul 1;10(13):2218-32.

Fraser M, Zhao H, Luoto KR, Lundin C, Coackley C, Chan N, Joshua AM, Bismar TA, Evans A, Helleday T, Bristow RG. PTEN deletion in prostate cancer cells does not associate with loss of RAD51 function: implications for radiotherapy and chemotherapy. *Clin Cancer Res*. 2012 Feb 15;18(4):1015-27.

Friedman HS, Kerby T, Calvert H. Temozolomide and treatment of malignant glioma. *Clin Cancer Res*. 2000 Jul;6(7):2585-97.

Friedmann B, Caplin M, Hartley JA, Hochhauser D. Modulation of DNA repair in vitro after treatment with chemotherapeutic agents by the epidermal growth factor receptor inhibitor gefitinib (ZD1839). *Clin Cancer Res*. 2004 Oct 1;10(19):6476-86.

Friedmann BJ, Caplin M, Savic B, Shah T, Lord CJ, Ashworth A, Hartley JA, Hochhauser D. Interaction of the epidermal growth factor receptor and the DNA-dependent protein kinase pathway following gefitinib treatment. *Mol Cancer Ther*. 2006 Feb;5(2):209-18.

Fritz G, Tano K, Mitra S, Kaina B. Inducibility of the DNA repair gene encoding O6-methylguanine-DNA methyltransferase in mammalian cells by DNA-damaging treatments. 1991 Sep;11(9):4660-8.

Fu D, Calvo JA, Samson LD. Balancing repair and tolerance of DNA damage caused by alkylating agents. *Nat Rev Cancer*. 2012 Jan 12;12(2):104-20.

Furnari FB, Fenton T, Bachoo RM, Mukasa A, Stommel JM, Stegh A, Hahn WC, Ligon KL, Louis DN, Brennan C, Chin L, DePinho RA, Cavenee WK. Malignant astrocytic glioma: genetics, biology, and paths to treatment. *Genes Dev*. 2007 Nov 1;21(21):2683-710.

Gao Z, Ure K, Ables JL, Lagace DC, Nave KA, Goebbels S, Eisch AJ, Hsieh J. Neurod1 is essential for the survival and maturation of adult-born neurons. *Nat Neurosci*. 2009 Sep;12(9):1090-2.

Galli R, Binda E, Orfanelli U, Cipelletti B, Gritti A, De Vitis S, Fiocco R, Foroni C, Dimeco F, Vescovi A. Isolation and characterization of tumorigenic, stem-like neural precursors from human glioblastoma. *Cancer Res*. 2004 Oct 1;64(19):7011-21.

Gerson SL. MGMT: its role in cancer aetiology and cancer therapeutics. *Nat Rev Cancer*. 2004 Apr;4(4):296-307.

Gil-Perotin S, Marin-Husstege M, Li J, Soriano-Navarro M, Zindy F, Roussel MF, Garcia-Verdugo JM, Casaccia-Bonnefil P. Loss of p53 induces changes in the behavior of subventricular zone cells: implication for the genesis of glial tumors. *J Neurosci*. 2006 Jan 25;26(4):1107-16.

Glassner BJ, Weeda G, Allan JM, Broekhof JL, Carls NH, Donker I, Engelward BP, Hampson RJ, Hersmus R, Hickman MJ, Roth RB, Warren HB, Wu MM, Hoeijmakers JH, Samson LD. DNA repair methyltransferase (Mgmt) knockout mice are sensitive to the lethal effects of chemotherapeutic alkylating agents. *Mutagenesis*. 1999 May;14(3):339-47.

Golding SE, Morgan RN, Adams BR, Hawkins AJ, Povirk LF, Valerie K. Pro-survival AKT and ERK signaling from EGFR and mutant EGFRvIII enhances DNA double-strand break repair in human glioma cells. *Cancer Biol Ther*. 2009 Apr;8(8):730-8.

Gregorian C, Nakashima J, Le Belle J, Ohab J, Kim R, Liu A, Smith KB, Groszer M, Garcia AD, Sofroniew MV, Carmichael ST, Kornblum HI, Liu X, Wu H. Pten deletion in adult neural stem/progenitor cells enhances constitutive neurogenesis. *J Neurosci*. 2009 Feb 11;29(6):1874-86.

Groszer M, Erickson R, Scripture-Adams DD, Dougherty JD, Le Belle J, Zack JA, Geschwind DH, Liu X, Kornblum HI, Wu H. PTEN negatively regulates neural stem cell self-renewal by modulating G0-G1 cell cycle entry. *Proc Natl Acad Sci U S A*. 2006 Jan 3;103(1):111-6.

Groszer M, Erickson R, Scripture-Adams DD, Lesche R, Trumpp A, Zack JA, Kornblum HI, Liu X, Wu H. Negative regulation of neural stem/progenitor cell proliferation by the Pten tumor suppressor gene in vivo. *Science*. 2001 Dec 7;294(5549):2186-9.

Gupta A, Yang Q, Pandita RK, Hunt CR, Xiang T, Misri S, Zeng S, Pagan J, Jeffery J, Puc J, Kumar R, Feng Z, Powell SN, Bhat A, Yaguchi T, Wadhwa R, Kaul SC, Parsons R, Khanna KK, Pandita TK. Cell cycle checkpoint defects contribute to genomic instability in PTEN deficient cells independent of DNA DSB repair. *Cell Cycle*. 2009 Jul 15;8(14):2198-210.

Haas-Kogan DA, Prados MD, Tihan T, Eberhard DA, Jelluma N, Arvold ND, Baumber R, Lamborn KR, Kapadia A, Malec M, Berger MS, Stokoe D. Epidermal growth factor receptor, protein kinase B/Akt, and glioma response to erlotinib. *J Natl Cancer Inst*. 2005 Jun 15;97(12):880-7.

Hall, E.J., and Giaccia, A.J. (2006). Radiobiology for the radiologist, 6th edition. (Philadelphia, Lippincott Williams & Wilkins).

Haupt Y, Maya R, Kazaz A, Oren M. Mdm2 promotes the rapid degradation of p53. *Nature*. 1997 May 15;387(6630):296-9.

Hegi ME, Diserens AC, Gorlia T, Hamou MF, de Tribolet N, Weller M, Kros JM, Hainfellner JA, Mason W, Mariani L, Bromberg JE, Hau P, Mirimanoff RO, Cairncross JG, Janzer RC, Stupp R. MGMT gene silencing and benefit from temozolomide in glioblastoma. *N Engl J Med*. 2005 Mar 10;352(10):997-1003.

Henson JW, Schnitker BL, Correa KM, von Deimling A, Fassbender F, Xu HJ, Benedict WF, Yandell DW, Louis DN. The retinoblastoma gene is involved in malignant progression of astrocytomas. *Ann Neurol*. 1994 Nov;36(5):714-21.

Holland EC, Celestino J, Dai C, Schaefer L, Sawaya RE, Fuller GN. Combined activation of Ras and Akt in neural progenitors induces glioblastoma formation in mice. *Nat Genet*. 2000 May;25(1):55-7.

Hollstein M, Sidransky D, Vogelstein B, Harris CC. p53 mutations in human cancers. *Science*. 1991 Jul 5;253(5015):49-53.

Honda R, Yasuda H. Association of p19(ARF) with Mdm2 inhibits ubiquitin ligase activity of Mdm2 for tumor suppressor p53. *EMBO J*. 1999 Jan 4;18(1):22-7.

Huang HS, Nagane M, Klingbeil CK, Lin H, Nishikawa R, Ji XD, Huang CM, Gill GN, Wiley HS, Cavenee WK. The enhanced tumorigenic activity of a mutant epidermal growth factor receptor common in human cancers is mediated by threshold levels of constitutive tyrosine phosphorylation and unattenuated signaling. *J Biol Chem*. 1997 Jan 31;272(5):2927-35.

Huang PH, Xu AM. White, FM. Oncogenic EGFR Signaling Networks in Glioma. *Science Signaling*. 2009 Sep 8;2(87):1-13.

Huang SM, Harari PM. Modulation of radiation response after epidermal growth factor receptor blockade in squamous cell carcinomas: inhibition of damage repair, cell cycle kinetics, and tumor angiogenesis. *Clin Cancer Res*. 2000 Jun;6(6):2166-74.

Isakoff J, Overmoyer B, Tung NM et al. A phase II trial of the PARP inhibitor veliparib (ABT888) and temozolomide for metastatic breast cancer. [abstract 1019] *J Clin Oncol*, 28 (15S, Part I) (2009), p. 118s.

Ishii N, Maier D, Merlo A, Tada M, Sawamura Y, Diserens AC, Van Meir EG. Frequent co-alterations of TP53, p16/CDKN2A, p14ARF, PTEN tumor suppressor genes in human glioma cell lines. *Brain Pathol*. 1999 Jul;9(3):469-79.

Jiricny J. The multifaceted mismatch-repair system. *Nat Rev Mol Cell Biol*. 2006 May;7(5):335-46.

Jonkers J, Meuwissen R, van der Gulden H, Peterse H, van der Valk M, Berns A. Synergistic tumor suppressor activity of BRCA2 and p53 in a conditional mouse model for breast cancer. *Nat Genet*. 2001 Dec;29(4):418-25.

Kai T, Spradling A. An empty Drosophila stem cell niche reactivates the proliferation of ectopic cells. *Proc Natl Acad Sci U S A*. 2003 Apr 15;100(8):4633-8.

Kaina B, Christmann M, Naumann S, Roos WP. MGMT: key node in the battle against genotoxicity, carcinogenicity and apoptosis induced by alkylating agents. *DNA Repair (Amst)*. 2007 Aug 1;6(8):1079-99.

Kaina B, Fritz G, Mitra S, Coquerelle T. Transfection and expression of human O6-methylguanine-DNA methyltransferase (MGMT) cDNA in Chinese hamster cells: the role of MGMT in protection against the genotoxic effects of alkylating agents. *Carcinogenesis*. 1991 Oct;12(10):1857-67.

Kamijo T, Weber JD, Zambetti G, Zindy F, Roussel MF, Sherr CJ. Functional and physical interactions of the ARF tumor suppressor with p53 and Mdm2. *Proc Natl Acad Sci U S A*. 1998 Jul 7;95(14):8292-7.

Kao GD, Jiang Z, Fernandes AM, Gupta AK, Maity A. Inhibition of phosphatidylinositol–3-OH kinase/Akt signaling impairs DNA repair in glioblastoma cells following ionizing radiation. *J Biol Chem*. 2007 Jul 20;282(29):21206-12.

Kempermann G, Kuhn HG, Gage FH. More hippocampal neurons in adult mice living in an enriched environment. *Nature*. 1997 Apr 3;386(6624):493-5.

Kempermann G, Jessberger S, Steiner B, and Kronenberg G. Milestones of neuronal development in the adult hippocampus. *Trends Neurosci*. 2004 Aug;27(8):447-52.

Kim WR, Kim JY, Moon Y, Kim HJ, Kim H, Sun W. Regional difference of reactive astrogliosis following traumatic brain injury revealed by hGFAP-GFP transgenic mice. *Neurosci Lett*. 2012 Apr 4;513(2):155-9.

Kipp M, Gingele S, Pott F, Clarner T, van der Valk P, Denecke B, Gan L, Siffrin V, Zipp F, Dreher W, Baumgartner W, Pfeifenbring S, Godbout R, Amor S, Beyer C. BLBP-expression in astrocytes during experimental demyelination and in human multiple sclerosis lesions. *Brain Behav Immun*. 2011 Nov;25(8):1554-68.

Kleihues P and Ohgaki H. Primary and secondary glioblastomas: From concept to clinical diagnosis. *Neuro-Oncology*. 1999; Jan;1(1):44-51.

Kriegs M, Kasten-Pisula U, Rieckmann T, Holst K, Saker J, Dahm-Daphi J, Dikomey E. The epidermal growth factor receptor modulates DNA double-strand break repair by regulating non-homologous end-joining. *DNA Repair (Amst)*. 2010 Aug 5;9(8):889-97.

Kronenberg G, Reuter K, Steiner B, Brandt MD, Jessberger S, Yamaguchi M, Kempermann G. Subpopulations of proliferating cells of the adult hippocampus respond differently to physiologic neurogenic stimuli. *J Comp Neurol*. 2003 Dec 22;467(4):455-63.

Kurimasa A, Ouyang H, Dong LJ, Wang S, Li X, Cordon-Cardo C, Chen DJ, Li GC. Catalytic subunit of DNA-dependent protein kinase: impact on lymphocyte development and tumorigenesis. *Proc Natl Acad Sci U S A*. 1999 Feb 16;96(4):1403-8.

Kwon CH, Luikart BW, Powell CM, Zhou J, Matheny SA, Zhang W, Li Y, Baker SJ, Parada LF. Pten regulates neuronal arborization and social interaction in mice. *Neuron*. 2006 May 4;50(3):377-88.

Kwon CH, Zhao D, Chen J, Alcantara S, Li Y, Burns DK, Mason RP, Lee EY, Wu H, Parada LF. Pten haploinsufficiency accelerates formation of high-grade astrocytomas. *Cancer Res*. 2008 May 1;68(9):3286-94.

Lammering G, Hewit TH, Valerie K, Contessa JN, Amorino GP, Dent P, Schmidt-Ullrich RK. EGFRvIII-mediated radioresistance through a strong cytoprotective response. *Oncogene*. 2003 Aug 28;22(36):5545-53.

Lammering G, Valerie K, Lin PS, Mikkelsen RB, Contessa JN, Feden JP, Farnsworth J, Dent P, Schmidt-Ullrich RK. Radiosensitization of malignant glioma cells through overexpression of dominant-negative epidermal growth factor receptor. *Clin Cancer Res*. 2001 Mar;7(3):682-90.

Lapidot T, Sirard C, Vormoor J, Murdoch B, Hoang T, Caceres-Cortes J, Minden M, Paterson B, Caligiuri M, Dick JE. A cell initiating human acute myeloid leukaemia after transplantation into SCID mice. *Nature*. 1994 Feb 17;367(6464):645-8.

Lassman AB, Rossi MR, Raizer JJ, Abrey LE, Lieberman FS, Grefe CN, Lamborn K, Pao W, Shih AH, Kuhn JG, Wilson R, Nowak NJ, Cowell JK, DeAngelis LM, Wen P, Gilbert MR, Chang S, Yung WA, Prados M, Holland EC. Molecular study of malignant gliomas treated with epidermal growth factor receptor inhibitors: tissue analysis from North American Brain Tumor Consortium Trials 01-03 and 00-01. *Clin Cancer Res*. 2005 Nov 1;11(21):7841-50.

Learn CA, Hartzell TL, Wikstrand CJ, Archer GE, Rich JN, Friedman AH, Friedman HS, Bigner DD, Sampson JH. Resistance to tyrosine kinase inhibition by mutant epidermal growth factor receptor variant III contributes to the neoplastic phenotype of glioblastoma multiforme. *Clin Cancer Res*. 2004 May 1;10(9):3216-24.

Lees-Miller SP. PIKK-ing a new partner: a new role for PKB in the DNA damage response. *Cancer Cell*. 2008 May;13(5):379-80.

You MJ, Castrillon DH, Bastian BC, O'Hagan RC, Bosenberg MW, Parsons R, Chin L, DePinho RA. Genetic analysis of Pten and Ink4a/Arf interactions in the suppression of tumorigenesis in mice. *Proc Natl Acad Sci U S A*. 2002 Feb 5;99(3):1455-60.

Levine AJ, Hu W, Feng Z. The P53 pathway: what questions remain to be explored? *Cell Death Differ*. 2006 Jun;13(6):1027-36.

Li B, Yuan M, Kim IA, Chang CM, Bernhard EJ, Shu HK. Mutant epidermal growth factor receptor displays increased signaling through the phosphatidylinositol–3 kinase/AKT pathway and promotes radioresistance in cells of astrocytic origin. *Oncogene*. 2004 Jun 3;23(26):4594-602.

Li L, Liu F, Salmonsen RA, Turner TK, Litofsky NS, Di Cristofano A, Pandolfi PP, Jones SN, Recht LD, Ross AH. PTEN in neural precursor cells: regulation of migration, apoptosis, and proliferation. *Mol Cell Neurosci*. 2002 May;20(1):21-9.

Li, M., Luo, J., Brooks, C.L., and Gu, W. Acetylation of p53 inhibits its ubiquitination by Mdm2. *J Biol Chem*. 2002 Dec 27;277(52):50607-11.

Li YQ, Aubert I, Wong CS. Abrogation of early apoptosis does not alter late inhibition of hippocampal neurogenesis after irradiation. *Int J Radiat Oncol Biol Phys*. 2010 Jul 15;77(4):1213-22.

Lieber M. The Mechanism of Double-Strand DNA Break Repair by the Nonhomologous DNA End-Joining Pathway. *Annu. Rev. Biochem*. 2010. 79:181–211.

Ligon KL, Alberta JA, Kho AT, Weiss J, Kwaan MR, Nutt CL, Louis DN, Stiles CD, Rowitch DH. The oligodendroglial lineage marker OLIG2 is universally expressed in diffuse gliomas. *J Neuropathol Exp Neurol*. 2004 May;63(5):499-509.

Ligon KL, Kesari S, Kitada M, Sun T, Arnett HA, Alberta JA, Anderson DJ, Stiles CD, Rowitch DH. Development of NG2 neural progenitor cells requires Olig gene function. *Proc Natl Acad Sci U S A*. 2006 May 16;103(20):7853-8.

Liu X, Han EK, Anderson M, Shi Y, Semizarov D, Wang G, McGonigal T, Roberts L, Lasko L, Palma J, Zhu GD, Penning T, Rosenberg S, Giranda VL, Luo Y, Leverson J, Johnson EF, Shoemaker AR. Acquired resistance to combination treatment with temozolomide and ABT-888 is mediated by both base excision repair and homologous recombination DNA repair pathways. *Mol Cancer Res*. 2009 Oct;7(10):1686-92.

Lu C, Ward PS, Kapoor GS, Rohle D, Turcan S, Abdel-Wahab O, Edwards CR, Khanin R, Figueroa ME, Melnick A, Wellen KE, O'Rourke DM, Berger SL, Chan TA, Levine RL, Mellinghoff IK, Thompson CB. IDH mutation impairs histone demethylation and results in a block to cell differentiation. Nature. 2012 Feb 15;483(7390):474-8.

Lucassen PJ, Meerlo P, Naylor AS, van Dam AM, Dayer AG, Fuchs E, Oomen CA, Czéh B. Regulation of adult neurogenesis by stress, sleep disruption, exercise and inflammation: Implications for depression and antidepressant action. *Eur Neuropsychopharmacol*. 2010 Jan;20(1):1-17.

Ma HI, Chiou SH, Hueng DY, Tai LK, Huang PI, Kao CL, Chen YW, Sytwu HK. Celecoxib and radioresistant glioblastoma-derived CD133+ cells: improvement in radiotherapeutic effects. *J Neurosurg*. 2011 Mar;114(3):651-62.

Maher EA, Brennan C, Wen PY, Durso L, Ligon KL, Richardson A, Khatry D, Feng B, Sinha R, Louis DN, Quackenbush J, Black PM, Chin L, DePinho RA. Marked genomic differences characterize primary and secondary glioblastoma subtypes and identify two distinct molecular and clinical secondary glioblastoma entities. *Cancer Res*. 2006 Dec 1;66(23):11502-13.

Maher EA, Furnari FB, Bachoo RM, Rowitch DH, Louis DN, Cavenee WK, DePinho RA. Malignant glioma: genetics and biology of a grave matter. *Genes Dev*. 2001 Jun 1;15(11):1311-33.

McEllin B, Camacho CV, Mukherjee B, Hahm B, Tomimatsu N, Bachoo RM, Burma S. PTEN loss compromises homologous recombination repair in astrocytes: implications for glioblastoma therapy with Temozolomide or poly (ADP-ribose) polymerase inhibitors. *Cancer Research*. 2010 Jul 1;70(13):5457-64.

McLendon RE, Turner K, Perkinson K, Rich J. Second messenger systems in human gliomas. *Arch Pathol Lab Med*. 2007 Oct;131(10):1585-90.

Medrano S, Burns-Cusato M, Atienza MB, Rahimi D, Scrable H. Regenerative capacity of neural precursors in the adult mammalian brain is under the control of p53. *Neurobiol Aging*. 2009 Mar;30(3):483-97.

Mehta S, Huillard E, Kesari S, Maire CL, Golebiowski D, Harrington EP, Alberta JA, Kane MF, Theisen M, Ligon KL, Rowitch DH, Stiles CD. The central nervous system-restricted transcription factor Olig2 opposes p53 responses to genotoxic damage in neural progenitors and malignant glioma. *Cancer Cell*. 2011 Mar 8;19(3):359-71.

Mellert H, Sykes SM, Murphy ME, McMahon SB. The ARF/oncogene pathway activates p53 acetylation within the DNA binding domain. *Cell Cycle*. 2007 Jun 1;6(11):1304-6.

Mellinghoff IK, Wang MY, Vivanco I, Haas-Kogan DA, Zhu S, Dia EQ, Lu KV, Yoshimoto K, Huang JH, Chute DJ, Riggs BL, Horvath S, Liau LM, Cavenee WK, Rao PN, Beroukhim R, Peck TC, Lee JC, Sellers WR, Stokoe D, Prados M, Cloughesy TF, Sawyers CL, Mischel PS. Molecular determinants of the response of glioblastomas to EGFR kinase inhibitors. *N Engl J Med*. 2005 Nov 10;353(19):2012-24.

Mendes-Pereira AM, Martin SA, Brough R, McCarthy A, Taylor JR, Kim JS, Waldman T, Lord CJ, Ashworth A. Synthetic lethal targeting of PTEN mutant cells with PARP inhibitors. *EMBO Mol Med*. 2009 Sep;1(6-7):315-22.

Mizumatsu S, Monje ML, Morhardt DR, Rola R, Palmer TD, Fike JR. Extreme sensitivity of adult neurogenesis to low doses of X-irradiation. *Cancer Res*. 2003 Jul 15;63(14):4021-7.

Mochan TA, Venere M, DiTullio RA, Jr, Halazonetis TD. 53BP1, an activator of ATM in response to DNA damage. *DNA Repair (Amst)*. 2004 Aug-Sep;3(8-9):945-52.

Momand J, Zambetti GP, Olson DC, George D, Levine AJ. The mdm-2 oncogene product forms a complex with the p53 protein and inhibits p53-mediated transactivation. *Cell*. 1992 Jun 26;69(7):1237-45.

Monje ML, Mizumatsu S, Fike JR, Palmer TD. Irradiation induces neural precursor-cell dysfunction. *Nat Med*. 2002 Sep;8(9):955-62.

Mukherjee B, Camacho CV, Tomimatsu N, Miller J, Burma S. Modulation of the DNA-damage response to HZE particles by shielding. *DNA Repair (Amst)*. 2008 Oct 1;7(10):1717-30.

Mukherjee B, Kessinger C, Kobayashi J, Chen BP, Chen DJ, Chatterjee A, Burma S. DNA-PK phosphorylates histone H2AX during apoptotic DNA fragmentation in mammalian cells. *DNA Repair (Amst)*. 2006 May 10;5(5):575-90.

Mukherjee B, McEllin B, Camacho CV, Tomimatsu N, Sirasanagandala S, Nannepaga S, Hatanpaa KJ, Mickey B, Madden C, Maher E, Boothman DA, Furnari F, Cavenee WK, Bachoo RM, Burma S. EGFRvIII and DNA double-strand break repair: a molecular mechanism for radioresistance in glioblastoma. *Cancer Res*. 2009 May 15;69(10):4252-9.

Nagane M, Coufal F, Lin H, Bogler O, Cavenee WK, Huang HJ. A common mutant epidermal growth factor receptor confers enhanced tumorigenicity on human glioblastoma cells by increasing proliferation and reducing apoptosis. *Cancer Res*. 1996 Nov 1;56(21):5079-86.

Newcomb EW, Cohen H, Lee SR, Bhalla SK, Bloom J, Hayes RL, Miller DC. Survival of patients with glioblastoma multiforme is not influenced by altered expression of p16, p53, EGFR, MDM2 or Bcl-2 genes. *Brain Pathol*. 1998 Oct;8(4):655-67.

Nigro JM, Baker SJ, Preisinger AC, Jessup JM, Hostetter R, Cleary K, Bigner SH, Davidson N, Baylin S, Devilee P, Glover T, Collins FS, Weslon A, Modali R, Harris CC, Vogelstein B. Mutations in the p53 gene occur in diverse human tumour types. *Nature*. 1989 Dec 7;342(6250):705-8.

Nishikawa R, Ji XD, Harmon RC, Lazar CS, Gill GN, Cavenee WK, Huang HJ. A mutant epidermal growth factor receptor common in human glioma confers enhanced tumorigenicity. *Proc Natl Acad Sci U S A*. 1994 Aug 2;91(16):7727-31.

Nyati MK, Morgan MA, Feng FY, Lawrence TS. Integration of EGFR inhibitors with radiochemotherapy. *Nat Rev Cancer*. 2006 Nov;6(11):876-85.

O'Brien, C. A., Pollett, A., Gallinger, S. & Dick, J. E. A human colon cancer cell capable of initiating tumour growth in immunodeficient mice. *Nature*. 2007 Jan 4;445(7123):106-10.

O'Brien CA, Kreso A, Dick JE. Cancer stem cells in solid tumors: an overview. *Semin Radiat Oncol*. 2009 Apr;19(2):71-7.

Omar A and Mason P. Temozolomide: the evidence for its therapeutic efficacy in malignant astrocytomas. *Core Evid*. 2010 Jun 15;4:93-111.

O'Shaughnessy J, Osborne C, Pippen JE, Yoffe M, Patt D, Rocha C, Koo IC, Sherman BM, Bradley C. Iniparib plus chemotherapy in metastatic triple-negative breast cancer. *N Engl J Med*. 2011 Jan 20;364(3):205-14.

Parsons DW, Jones S, Zhang X, Lin JC, Leary RJ, Angenendt P, Mankoo P, Carter H, Siu IM, Gallia GL, Olivi A, McLendon R, Rasheed BA, Keir S, Nikolskaya T, Nikolsky Y, Busam DA, Tekleab H, Diaz LA Jr, Hartigan J, Smith DR, Strausberg RL, Marie SK, Shinjo SM, Yan H, Riggins GJ, Bigner DD, Karchin R, Papadopoulos N, Parmigiani G, Vogelstein B, Velculescu VE, Kinzler KW. An integrated genomic analysis of human glioblastoma multiforme. *Science*. 2008 Sep 26;321(5897):1807-12.

Piccirillo SG, Reynolds BA, Zanetti N, Lamorte G, Binda E, Broggi G, Brem H, Olivi A, Dimeco F, Vescovi AL. Bone morphogenetic proteins inhibit the tumorigenic potential of human brain tumour-initiating cells. *Nature*. 2006 Dec 7;444(7120):761-5.

Pidikiti R, Stojadinovic S, Speiser M, Song KH, Hager F, Saha D, Solberg TD. Dosimetric characterization of an image-guided stereotactic small animal irradiator. *Phys Med Biol*. 2011 Apr 21;56(8):2585-99.

Pietersen AM, Horlings HM, Hauptmann M, Langerød A, Ajouaou A, Cornelissen-Steijger P, Wessels LF, Jonkers J, van de Vijver MJ, van Lohuizen M. EZH2 and BMI1 inversely correlate with prognosis and TP53 mutation in breast cancer. *Breast Cancer Res*. 2008;10(6):R109.

Plummer ER. Inhibition of poly(ADP-ribose) polymerase in cancer. *Curr Opin Pharmacol*. 2006 Aug;6(4):364-8.

Prados MD, Chang SM, Butowski N, DeBoer R, Parvataneni R, Carliner H, Kabuubi P, Ayers-Ringler J, Rabbitt J, Page M, Fedoroff A, Sneed PK, Berger MS, McDermott MW, Parsa AT, Vandenberg S, James CD, Lamborn KR, Stokoe D, Haas-Kogan DA. Phase II study of erlotinib plus temozolomide during and after radiation therapy in patients with newly diagnosed glioblastoma multiforme or gliosarcoma. *J Clin Oncol*. 2009 Feb 1;27(4):579-84.

Prise KM, O'Sullivan JM. Radiation-induced bystander signalling in cancer therapy. *Nat Rev Cancer*. 2009 May;9(5):351-60.

Puc J, Keniry M, Li HS, Pandita TK, Choudhury AD, Memeo L, Mansukhani M, Murty VV, Gaciong Z, Meek SE, Piwnica-Worms H, Hibshoosh H, Parsons R. Lack of PTEN sequesters CHK1 and initiates genetic instability. *Cancer Cell*. 2005 Feb;7(2):193-204.

Puc J, Parsons R. PTEN loss inhibits CHK1 to cause double stranded-DNA breaks in cells. *Cell Cycle*. 2005 Jul;4(7):927-9.

Quintana E, Shackleton M, Sabel MS, Fullen DR, Johnson TM, Morrison SJ. Efficient tumour formation by single human melanoma cells. *Nature*. 2008 Dec 4;456(7222):593-8.

Quintana E, Shackleton M, Foster HR, Fullen DR, Sabel MS, Johnson TM, Morrison SJ. Phenotypic heterogeneity among tumorigenic melanoma cells from patients that is reversible and not hierarchically organized. *Cancer Cell*. 2010 Nov 16;18(5):510-23.

Raber J, Rola R, LeFevour A, Morhardt D, Curley J, Mizumatsu S, VandenBerg SR, Fike JR. Radiation-induced cognitive impairments are associated with changes in indicators of hippocampal neurogenesis. *Radiat Res*. 2004 Jul;162(1):39-47.

Raizer JJ, Abrey LE, Lassman AB, Chang SM, Lamborn KR, Kuhn JG, Yung WK, Gilbert MR, Aldape KA, Wen PY, Fine HA, MehtaM, DeAngelis LM, Lieberman F, Cloughesy TF, RobinsHI, Dancey J, Prados MD,North American Brain Tumor Consortium. A phase II trial of erlotinib in patients with recurrent malignant gliomas and nonprogressive glioblastoma multiforme postradiation therapy. *Neuro Oncol*. 2010 Jan;12(1):95-103.

Reitman ZJ, Jin G, Karoly ED, Spasojevic I, Yang J, Kinzler KW, He Y, Bigner DD, Vogelstein B, Yan H. Profiling the effects of isocitrate dehydrogenase 1 and 2 mutations on the cellular metabolome. *Proc Natl Acad Sci U S A*. 2011 Feb 22;108(8):3270-5.

Reya T, Morrison SJ, Clarke MF, Weissman IL. Stem cells, cancer, and cancer stem cells. *Nature*. 2001 Nov 1;414(6859):105-11.

Ricci-Vitiani L, Lombardi DG, Pilozzi E, Biffoni M, Todaro M, Peschle C, De Maria R. Identification and expansion of human colon-cancer-initiating cells. *Nature*. 2007 Jan 4;445(7123):111-5.

Rich JN, Reardon DA, Peery T, Dowell JM, Quinn JA, Penne KL, Wikstrand CJ, Van Duyn LB, Dancey JE, McLendon RE, Kao JC, Stenzel TT, Ahmed Rasheed BK, Tourt-Uhlig SE, Herndon JE 2nd, Vredenburgh JJ, Sampson JH, Friedman AH, Bigner DD, Friedman HS. Phase II trial of gefitinib in recurrent glioblastoma. *J Clin Oncol*. 2004 Jan 1;22(1):133-42.

Rola R, Raber J, Rizk A, Otsuka S, VandenBerg SR, Morhardt DR, Fike JR. Radiation-induced impairment of hippocampal neurogenesis is associated with cognitive deficits in young mice. *Exp Neurol*. 2004 Aug;188(2):316-30.

Roos W, Baumgartner M, Kaina B. Apoptosis triggered by DNA damage O6-methylguanine in human lymphocytes requires DNA replication and is mediated by p53 and Fas/CD95/Apo-1. *Oncogene*. 2004 Jan 15;23(2):359-67.

Roos WP, Nikolova T, Quiros S, Naumann SC, Kiedron O, Zdzienicka MZ, Kaina B. Brca2/Xrcc2 dependent HR, but not NHEJ, is required for protection against O(6)-methylguanine triggered apoptosis, DSBs and chromosomal aberrations by a process leading to SCEs. *DNA Repair (Amst)*. 2009 Jan 1;8(1):72-86.

Ross SE, Greenberg ME, Stiles CD. Basic helix-loop-helix factors in cortical development. *Neuron*. 2003 Jul 3;39(1):13-25.

Salazar OM, Rubin P, Feldstein ML, Pizzutiello R. High dose radiation therapy in the treatment of malignant gliomas: final report. *Int J Radiat Oncol Biol Phys*. 1979;5(10):1733–1740.

Salmena L, Carracedo A, Pandolfi PP. Tenets of PTEN tumor suppression. *Cell*. 2008 May 2;133(3):403-14.

San Filippo J, Sung P, Klein H. Mechanism of eukaryotic homologous recombination. *Annu Rev Biochem*. 2008;77:229–57.

Schlegel J, Stumm G, Brändle K, Merdes A, Mechtersheimer G, Hynes NE, Kiessling M. Amplification and differential expression of members of the erbB-gene family in human glioblastoma. *J Neurooncol*. 1994;22(33):201–7.

Sclafani AM, Skidmore JM, Ramaprakash H, Trumpp A, Gage PJ, Martin DM. Nestin-Cre Mediated Deletion of Pitx2 in the Mouse. *Genesis*. 2006 Jul;44(7):336-44.

Sergina NV, Moasser MM. The HER family and cancer: emerging molecular mechanisms and therapeutic targets. *Trends Mol Med*. 2007 Dec;13(12):527-34.

Serrano M, Lee H, Chin L, Cordon-Cardo C, Beach D, DePinho RA. Role of the INK4a locus in tumor suppression and cell mortality. *Cell*. 1996 Apr 5;85(1):27-37.

Shen WH, Balajee AS, Wang J, Wu H, Eng C, Pandolfi PP, Yin Y. Essential role for nuclear PTEN in maintaining chromosomal integrity. *Cell*. 2007 Jan 12;128(1):157-70.

Sherr CJ, McCormick F. The RB and p53 pathways in cancer. *Cancer Cell*. 2002 Aug;2(2):103-12.

Shvarts A, Steegenga WT, Riteco N, van Laar T, Dekker P, Bazuine M, van Ham RCA, van der Houven van Oordt W, Hateboer G, van der Eb AJ, Jochemsen AG. MDMX: a novel p53-binding protein with some functional properties of MDM2. *EMBO J*. 1996;15: 5349–5357.

Siliciano JD, Canman CE, Taya Y, Sakaguchi K, Appella E, Kastan MB. DNA damage induces phosphorylation of the amino terminus of p53. *Genes Dev*. 1997 Dec 15;11(24):3471-81.

Singh SK, Clarke ID, Terasaki M, Bonn VE, Hawkins C, Squire J, Dirks PB. Identification of a cancer stem cell in human brain tumors. *Cancer Res*. 2003 Sep 15;63(18):5821-8.

Singh SK, Hawkins C, Clarke ID, Squire JA, Bayani J, Hide T, Henkelman RM, Cusimano MD, Dirks PB. Identification of human brain tumour initiating cells. *Nature*. 2004 Nov 18;432(7015):396-401.

Song KH, Pidikiti R, Stojadinovic S, Speiser M, Seliounine S, Saha D, Solberg TD. An x-ray image guidance system for small animal stereotactic irradiation. *Phys Med Biol*. 2010 Dec 7;55(23):7345-62.

Sonoda E, Sasaki MS, Morrison C, Yamaguchi-Iwai Y, Takata M, Takeda S. Sister chromatid exchanges are mediated by homologous recombination in vertebrate cells. *Mol Cell Biol*. 1999 Jul;19(7):5166-9.

(a) Sonoda Y, Ozawa T, Aldape KD, Deen DF, Berger MS, Pieper RO. Akt pathway activation converts anaplastic astrocytoma to glioblastoma multiforme in a human astrocyte model of glioma. *Cancer Res*. 2001 Sep 15;61(18):6674-8.

(b) Sonoda Y, Ozawa T, Hirose Y, et al. Formation of intracranial tumors by genetically modified human astrocytes defines four pathways critical in the development of human anaplastic astrocytoma. *Cancer Res*. 2001 Jul 1;61(13):4956-60..

Srinivas S, Watanabe T, Lin CS, William CM, Tanabe Y, Jessell TM, Costantini F. Cre reporter strains produced by targeted insertion of EYFP and ECFP into the ROSA26 locus. *BMC Dev Biol*. 2001;1:4.

Stea B, Falsey R, Kislin K, Patel J, Glanzberg H, Carey S, Ambrad AA, Meuillet EJ, Martinez JD. Time and dose-dependent radiosensitization of the glioblastoma multiforme U251 cells by the EGF receptor tyrosine kinase inhibitor ZD1839 (‘Iressa’). *Cancer Lett*. 2003 Dec 8;202(1):43-51.

Steiner B, Klempin F, Wang L, Kott M, Kettenmann H, Kempermann G. Type-2 cells as link between glial and neuronal lineage in adult hippocampal neurogenesis. *Glia*. 2006 Dec;54(8):805-14.

Stojic L, Brun R, Jiricny J. Mismatch repair and DNA damage signalling. *DNA Repair (Amst)*. 2004 Aug-Sep;3(8-9):1091-101.

Stommel JM, Kimmelman AC, Ying H, Nabioullin R, Ponugoti AH, Wiedemeyer R, Stegh AH, Bradner JE, Ligon KL, Brennan C, Chin L, DePinho RA. Coactivation of receptor tyrosine kinases affects the response of tumor cells to targeted therapies. *Science.* 2007 Oct 12;318(5848):287-90.

Stupp R, Hegi ME, Mason WP, van den Bent MJ, Taphoorn MJ, Janzer RC, Ludwin SK, Allgeier A, Fisher B, Belanger K, Hau P, Brandes AA, Gijtenbeek J, Marosi C, Vecht CJ, Mokhtari K, Wesseling P, Villa S, Eisenhauer E, Gorlia T, Weller M, Lacombe D, Cairncross JG, Mirimanoff RO; European Organisation for Research and Treatment of Cancer Brain Tumour and Radiation Oncology Groups; National Cancer Institute of Canada Clinical Trials Group. Effects of radiotherapy with concomitant and adjuvant temozolomide versus radiotherapy alone on survival in glioblastoma in a randomised phase III study: 5-year analysis of the EORTC-NCIC trial. *Lancet Oncol*. 2009 May;10(5):459-66.

Stupp R, Mason WP, van den Bent MJ, Weller M, Fisher B, Taphoorn MJ, Belanger K, Brandes AA, Marosi C, Bogdahn U, Curschmann J, Janzer RC, Ludwin SK, Gorlia T, Allgeier A, Lacombe D, Cairncross JG, Eisenhauer E, Mirimanoff RO; European Organisation for Research and Treatment of Cancer Brain Tumor and Radiotherapy Groups; National Cancer Institute of Canada Clinical Trials Group. Radiotherapy plus concomitant and adjuvant temozolomide for glioblastoma. *N Engl J Med*. 2005 Mar 10;352(10):987-96.

Suh H, Deng, W, Gage F. Signaling in adult neurogenesis. *Annu Rev Cell Dev Biol*. 2009;25:253-75

Symington L and Gautier J. Double-Strand Break End Resection and Repair Pathway Choice. *Annu Rev Genet*. 2011;45:247-71.

Tada E, Parent JM, Lowenstein DH, Fike JR. X-irradiation causes a prolonged reduction in cell proliferation in the dentate gyrus of adult rats. *Neuroscience*. 2000;99(1):33-41.

Tada E, Yang C, Gobbel GT, Lamborn KR, Fike JR. Long-term impairment of subependymal repopulation following damage by ionizing irradiation. *Exp Neurol*. 1999 Nov;160(1):66-77.

Takahashi K, Yamanaka S. Induction of pluripotent stem cells from mouse embryonic and adult fibroblast cultures by defined factors. *Cell*. 2006 Aug 25;126(4):663-76.

Tanaka T, Munshi A, Brooks C, Liu J, Hobbs ML, Meyn RE. Gefitinib radiosensitizes non-small cell lung cancer cells by suppressing cellular DNA repair capacity. *Clin Cancer Res*. 2008 Feb 15;14(4):1266-73.

Taupin P. BrdU immunohistochemistry for studying adult neurogenesis: Paradigms, pitfalls, limitations, and validation. *Brain Res Rev*. 2007 Jan;53(1):198-214.

Tomimatsu N, Mukherjee B, Burma S. Distinct roles of ATR and DNA-PKcs in triggering DNA damage responses in ATM-deficient cells. *EMBO Rep*. 2009 Jun;10(6):629-35.

Toulany M, Kasten-Pisula U, Brammer I, Wang S, Chen J, Dittmann K, Baumann M, Dikomey E, Rodemann HP. Blockage of epidermal growth factor receptor-phosphatidylinositol 3-kinase-AKT signaling increases radiosensitivity of K-RAS mutated human tumor cells in vitro by affecting DNA repair. *Clin Cancer Res*. 2006 Jul 1;12(13):4119-26.

Toulany M, Kehlbach R, Florczak U, Sak A, Wang S, Chen J, Lobrich M, Rodemann HP. Targeting of AKT1 enhances radiation toxicity of human tumor cells by inhibiting DNA-PKcs-dependent DNA double-strand break repair. *Mol Cancer Ther*. 2008 Jul;7(7):1772-81..

Tutt A, Robson M, Garber JE, Domchek SM, Audeh MW, Weitzel JN, Friedlander M, Arun B, Loman N, Schmutzler RK, Wardley A, Mitchell G, Earl H, Wickens M, Carmichael J. Oral poly(ADP-ribose) polymerase inhibitor olaparib in patients with BRCA1 or BRCA2 mutations and advanced breast cancer: a proof-of-concept trial. *Lancet*. 2010 Jul 24;376(9737):235-44.

Tsuzuki T, Izumoto S, Ohnishi T, Hiraga S, Arita N, Hayakawa T. Neural cell adhesion molecule L1 in gliomas: correlation with TGF-beta and p53. *J Clin Pathol*. 1998 Jan;51(1):13-7.

Turcan S, Rohle D, Goenka A, Walsh LA, Fang F, Yilmaz E, Campos C, Fabius AW, Lu C, Ward PS, Thompson CB, Kaufman A, Guryanova O, Levine R, Heguy A, Viale A, Morris LG, Huse JT, Mellinghoff IK, Chan TA. IDH1 mutation is sufficient to establish the glioma hypermethylator phenotype. *Nature*. 2012 Feb 15;483(7390):479-83.

Uberti D, Piccioni L, Cadei M, Grigolato P, Rotter V, Memo M. p53 is dispensable for apoptosis but controls neurogenesis of mouse dentate gyrus cells following gamma-irradiation. *Brain Res Mol Brain Res*. 2001 Sep 10;93(1):81-9.

Uhrbom L, Dai C, Celestino JC, Rosenblum MK, Fuller GN, Holland EC. Ink4a-Arf loss cooperates with KRas activation in astrocytes and neural progenitors to generate glioblastomas of various morphologies depending on activated Akt. *Cancer Res*. 2002 Oct 1;62(19):5551-8.

van den Bent MJ, Brandes AA, Rampling R, Kouwenhoven MC, Kros JM, Carpentier AF, Clement PM, Frenay M, Campone M, Baurain JF, Armand JP, Taphoorn MJ, Tosoni A, Kletzl H, Klughammer B, Lacombe D, Gorlia T. Randomized phase II trial of erlotinib versus temozolomide or carmustine in recurrent glioblastoma: EORTC brain tumor group study 26034. *J Clin Oncol*. 2009 Mar 10;27(8):1268-74.

Venkitaraman AR. Linking the cellular functions of BRCA genes to cancer pathogenesis and treatment. *Annu Rev Pathol*. 2009;4:461–87.

Verhaak RG, Hoadley KA, Purdom E, Wang V, Qi Y, Wilkerson MD, Miller CR, Ding L, Golub T, Mesirov JP, Alexe G, Lawrence M, O'Kelly M, Tamayo P, Weir BA, Gabriel S, Winckler W, Gupta S, Jakkula L, Feiler HS, Hodgson JG, James CD, Sarkaria JN, Brennan C, Kahn A, Spellman PT, Wilson RK, Speed TP, Gray JW, Meyerson M, Getz G, Perou CM, Hayes DN; Cancer Genome Atlas Research Network. Integrated genomic analysis identifies clinically relevant subtypes of glioblastoma characterized by abnormalities in PDGFRA, IDH1, EGFR, and NF1. *Cancer Cell*. 2010 Jan 19;17(1):98-110.

Veuger SJ, Curtin NJ, Richardson CJ, Smith GC, Durkacz BW. Radiosensitization and DNA repair inhibition by the combined use of novel inhibitors of DNA-dependent protein kinase and poly(ADP-ribose) polymerase-1. *Cancer Res*. 2003 Sep 15;63(18):6008-15.

von Bohlen und Halbach, O. Immunohistological markers for proliferative events, gliogenesis, and neurogenesis within the adult hippocampus. *Cell Tissue Res*. 2011 Jul;345(1):1-19.

Walker MD, Green SB, Byar DP, Alexander E Jr, Batzdorf U, Brooks WH, Hunt WE, MacCarty CS, Mahaley MS Jr, Mealey J Jr, Owens G, Ransohoff J 2nd, Robertson JT, Shapiro WR, Smith KR Jr, Wilson CB, Strike TA. Randomized comparisons ofradiotherapy and nitrosoureas for the treatment of malignant glioma after surgery. *N Engl J Med*. 1980 Dec 4;303(23):1323-9.

Walker MD, Strike TA, Sheline GE. An analysis of dose-effect relationship in the radiotherapy of malignant gliomas. *Int J Radiat Oncol Biol Phys*. 1979 Oct;5(10):1725-31.

Wang J, Sakariassen PØ, Tsinkalovsky O, Immervoll H, Bøe SO, Svendsen A, Prestegarden L, Røsland G, Thorsen F, Stuhr L, Molven A, Bjerkvig R, Enger PØ. CD133 negative glioma cells form tumors in nude rats and give rise to CD133 positive cells. *Int J Cancer*. 2008 Feb 15;122(4):761-8.

Wang J, Wakeman TP, Lathia JD, Hjelmeland AB, Wang XF, White RR, Rich JN, Sullenger BA. Notch promotes radioresistance of glioma stem cells. *Stem Cells*. 2010 Jan;28(1):17-28.

Wang JY, Edelmann W. Mismatch repair proteins as sensors of alkylation DNA damage. *Cancer Cell*. 2006 Jun;9(6):417-8.

Wang Y, Yang J, Zheng H, Tomasek GJ, Zhang P, McKeever PE, Lee EY, Zhu Y. Expression of mutant p53 proteins implicates a lineage relationship between neural stem cells and malignant astrocytic glioma in a murine model. *Cancer Cell*. 2009 Jun 2;15(6):514-26.

Ward RJ, Dirks PB. Cancer stem cells: at the headwaters of tumor development. *Annu Rev Pathol*. 2007;2:175-89.

Watanabe K, Tachibana O, Sata K, Yonekawa Y, Kleihues P, Ohgaki H. Overexpression of the EGF receptor and p53 mutations are mutually exclusive in the evolution of primary and secondary glioblastomas. *Brain Pathol*. 1996 Jul;6(3):217-23.

Watanabe K, Sato K, Biernat W, Tachibana O, von Ammon K, Ogata N, Yonekawa Y, Kleihues P, Ohgaki H. Incidence and timing of p53 mutations during astrocytoma progression in patients with multiple biopsies. *Clin Cancer Res*. 1997 Apr;3(4):523-30.

Weterings E and Chen D. The endless tale of non-homologous end-joining. *Cell Res*. 2008 Jan;18(1):114-24

Wick W, Furnari FB, Naumann U, Cavenee WK, Weller M. PTEN gene transfer in human malignant glioma: sensitization to irradiation and CD95L-induced apoptosis. *Oncogene*. 1999 Jul 8;18(27):3936-43.

Wilson DM 3rd, Thompson LH. Molecular mechanisms of sister-chromatid exchange. *Mutat Res*. 2007 Mar 1;616(1-2):11-23.

Wong AJ, Bigner SH, Bigner DD, Kinzler KW, Hamilton SR, Vogelstein B. Increased expression of the epidermal growth factor receptor gene in malignant gliomas is invariably associated with gene amplification. *Proc Natl Acad Sci U S A*. 1987 Oct;84(19):6899-903.

Xiao A, Wu H, Pandolfi PP, Louis DN, Van Dyke T. Astrocyte inactivation of the pRb pathway predisposes mice to malignant astrocytoma development that is accelerated by PTEN mutation. *Cancer Cell*. 2002 Mar;1(2):157-68.

Xiao A, Yin C, Yang C, Di Cristofano A, Pandolfi PP, Van Dyke T. Somatic induction of Pten loss in a preclinical astrocytoma model reveals major roles in disease progression and avenues for target discovery and validation. *Cancer Res*. 2005 Jun 15;65(12):5172-80.

Xu N, Hegarat N, Black EJ, Scott MT, Hochegger H, Gillespie DA. Akt/PKB suppresses DNA damage processing and checkpoint activation in late G2. *J Cell Biol*. 2010 Aug 9;190(3):297-305.

Xu W, Yang H, Liu Y, Yang Y, Wang P, Kim SH, Ito S, Yang C, Wang P, Xiao MT, Liu LX, Jiang WQ, Liu J, Zhang JY, Wang B, Frye S, Zhang Y, Xu YH, Lei QY, Guan KL, Zhao SM, Xiong Y. Oncometabolite 2-hydroxyglutarate is a competitive inhibitor of α-ketoglutarate-dependent dioxygenases. *Cancer Cell*. 2011 Jan 18;19(1):17-30.

Yin Y, Shen WH. PTEN: a new guardian of the genome. *Oncogene*. 2008 Sep 18;27(41):5443-53.

Zhang Y, Xiong Y, Yarbrough WG. ARF promotes MDM2 degradation and stabilizes p53: ARF-INK4a locus deletion impairs both the Rb and p53 tumor suppression pathways. *Cell*. 1998 Mar 20;92(6):725-34..

Zheng H, Ying H, Yan H, Kimmelman AC, Hiller DJ, Chen AJ, Perry SR, Tonon G, Chu GC, Ding Z, Stommel JM, Dunn KL, Wiedemeyer R, You MJ, Brennan C, Wang YA, Ligon KL, Wong WH, Chin L, DePinho RA. p53 and Pten control neural and glioma stem/progenitor cell renewal and differentiation. *Nature*. 2008 Oct 23;455(7216):1129-33.

Zheng X, Shen G, Yang X, Liu W. Most C6 cells are cancer stem cells: evidence from clonal and population analyses. *Cancer Res*. 2007 Apr 15;67(8):3691-7.

Zhu H, Acquaviva J, Ramachandran P, Boskovitz A, Woolfenden S, Pfannl R, Bronson RT, Chen JW, Weissleder R, Housman DE, Charest A. Oncogenic EGFR signaling cooperates with loss of tumor suppressor gene functions in gliomagenesis. *Proc Natl Acad Sci U S A*. 2009 Feb 24;106(8):2712-6.

Zhu Y, Guignard F, Zhao D, Liu L, Burns DK, Mason RP, Messing A, Parada LF. Early inactivation of p53 tumor suppressor gene cooperating with NF1 loss induces malignant astrocytoma. *Cancer Cell*. 2005 Aug;8(2):119-30.

Zhuo L, Theis M, Alvarez-Maya I, Brenner M, Willecke K, Messing A. hGFAP-cre transgenic mice for manipulation of glial and neuronal function in vivo. *Genesis*. 2001 Oct;31(2):85-94